Modeling the Time-to-Corrosion Cracking of the Cover Concrete in Chloride Contaminated Reinforced Concrete Structures

by

Youping Liu

Dissertation submitted to the Faculty of the

Virginia Polytechnic Institute and State University

in partial fulfillment of the requirements for the degree of

Doctor of Philosophy

in

Civil Engineering

APPROVED:

_____

Richard E. Weyers, Chair

_____	_____
Imad L. Al-Qadi	Richard M. Barker
_____	_____
Jesse J. Brown, Jr.	Richard D. Walker

October 21, 1996

Blacksburg, Virginia

Keywords: Chloride, Corrosion, Cracking, Deterioration, Model

Modeling the Time-to-Corrosion Cracking of the Cover Concrete in Chloride Contaminated Reinforced Concrete Structures

Youping Liu

Richard E. Weyers, Committee Chairman

Department of Civil Engineering

(Abstract)

Significant factors on steel corrosion in chloride contaminated reinforced concrete and time-to-corrosion cracking were investigated in this study. Sixty specimens were designed with seven admixed chloride contents, three concrete cover depths, two reinforcing steel bar diameters, two exposure conditions, and a typical concrete with water to cement ratio of 0.45. Corrosion current density (corrosion rate), corrosion potential, ohmic resistance of concrete and temperature were measured monthly on these specimens using both the 3LP and Gecor devices. Metal loss measurements were performed in accordance with ASTM G1-90, method C3.5, after specimens cracked. The actual corrosion weight loss of the steel reinforcing bars was then compared to the result obtained from the corrosion rate measurement devices.

An interaction model for characterizing the dynamic corrosion process was developed based on the five-year corrosion database. The model demonstrates that the corrosion rate is a function of chloride content, temperature at reinforcement depth, ohmic resistance of concrete, and corrosion time after initiation. A time-to-corrosion cracking model was suggested based on a corrosion-cracking conceptual model and critical mass of corrosion products. The model predicted times to corrosion cracking are in good agreement with the observed times to corrosion cracking of the cover concrete.

Acknowledgments

I am extremely grateful to Dr. Weyers, who gave me the opportunity to work on this research project, for his guidance, support and patience throughout my studies at Virginia Tech. I would like to extend my sincere gratitude to other committee members, Dr. Al-Qadi, Dr. Barker, Dr. Brown and Dr. Walker, for their valuable comments and advice.

I would like to thank the sponsors of this research project: Strategic Highway Research Program (SHRP), Federal Highway Administration (FHWA) and Center for Infrastructure Assessment and Management (CIAM) at Virginia Tech.

Thanks are also due to the former graduate students, Peterson and Newhouse, for their work and contributions on this research project.

I would like to recognize my colleagues, especially Agata, Jerzy, John and Jon, for their help and friendliness. Also, thanks goes to Bret Farmer, Clark Brown and Dennis Huffman, for their assistance with laboratory work.

I am grateful to my parents and brothers for their constant support and continuous encouragement. Their belief in me and their pride in my accomplishments were the motivation and reward for all the hard work I did.

Finally, a special thanks goes to my wife, Yanjun, for her love and quiet support.

Table of Contents

Abstract ii
Acknowledgments iii
List of Figures vii
List of Tables x
Notations xi

1.0 Introduction 1

1.1 Background 1
1.2 Deterioration Models 1
1.3 Scope of Study 3

2.0 Review of Corrosion of Steel in Concrete

2.1 Background 5
2.1.1 Mechanism of Electrochemical Corrosion 5
2.1.2 Pourbaix Diagrams 7
2.1.3 Polarization 8
2.1.4 Passivity 11
2.1.5 Growth of Rust Film 11
2.2 Corrosion of Steel in Concrete 12
2.2.1 Concrete as an Electrolyte 12
2.2.2 Principles of Steel Corrosion in Concrete 16
2.2.3 Initiation of Steel Corrosion in Concrete 19
2.2.4 Corrosive Activity of Concrete 21
2.3 Corrosion Monitoring Techniques 25
2.3.1 Half-cell Potential 25
2.3.2 Linear Polarization Technique 26
2.3.3 AC Impedance 28
2.3.4 Gravimetric Technique (Weight Loss Method) 28
2.3.5 Techniques for Determining the Chloride Content 29
2.4 Summary 29

3.0 Review of Time to Cracking Models 32

3.1 Cady-Weyers' Deterioration Model 32
3.2 Bazant's Mathematical Models of Time to Cracking 32
3.3 Morinaga's Empirical Equation of Time to Cracking 34
3.4 Other Metal Loss Criteria to Cracking 35
3.5 Some Comments on Existing Models 36

4.0 Experimental Design 38

4.1 Materials 38
4.2 Design Variables 40
4.3 Corrosion Cell Design 42
4.3.1 Slab Series Design 42
4.3.2 Block Series Design 45
4.4 Test Methods 45
4.4.1 Corrosion Rate Measurement 45
4.4.2 Chloride Content Analysis 47
4.3.3 Temperature Measurement 47
4.3.4 Relative Humidity Measurement 48

5.0 Results and Discussions 49

5.1 Visual Observations 49
5.2 Measured Corrosion Data 49
5.2.1 Monthly Corrosion Potentials 49
5.2.2 Measured Corrosion Rate, Temperature and ohmic Concrete Resistance Versus Time 58
5.2.3 Chloride Content Analysis 78
5.2.4 Ohmic Resistance of Concrete and Chloride Content 80
5.2.5 Relative Humidity in Concrete 80
5.3 Weight Loss Measurements 82
5.4 Comparison of Corrosion Rates by Linear Polarization Method and Weight Loss Methods 83
5.5 Modeling the Dynamic Corrosion Rate 84
5.5.1 Model Development 84
5.5.2 Model Interpretations 90
5.5.3 Model Applications 94
5.6 Modeling the Time to Cracking 95
5.6.1 Corrosion-Cracking Model 95
5.6.2 Growth of Rust Products 100
5.6.3 Time to Cracking 101
5.6.4 Applications of the Proposed Models 103

6.0 Conclusions 105

7.0 Recommendations for Further Research 107

References 108

Appendix A Conversion of Corrosion Rate 115
Appendix B Climate Data in Blacksburg, Virginia, USA 116
Vita 117

List of Figures

Figure 1. 1	A schematic sketch of steel corrosion sequence in concrete	2
Figure 1. 2	Chloride corrosion deterioration process for a concrete element with a mean cover depth of 2 in.	3
Figure 2.1	Pourbaix diagram for the FeO-H_2O system at 25°F for 10^{-6} M, activities of all metal ions	7
Figure 2.2	A schematic Evans diagram	8
Figure 2.3	Potential versus current plot illustrating cathodic diffusion polarization	9
Figure 2.4	Potential versus current plot illustrating resistance polarization	10
Figure 2.5	Dimensional ranges of solids and pores in a hydrated cement paste	14
Figure 2.6	Pore size distribution in hydrated cement paste	15
Figure 2.7	Mechanism of corrosion of steel in concrete	17
Figure 2.8	The relative volumes of iron and its corrosion reaction products	18
Figure 2.9	The degree of carbonation as a function of relative humidity	19
Figure 2.10	The critical chloride content according to CEB recommendations	22
Figure 2.11	Copper-copper sulfate half cell circuitry	26
Figure 4.1	A schematic diagram of the slab design	43
Figure 4.2	A schematic diagram of the two additional slabs design with two different concrete layers	44
Figure 4.3	A schematic diagram of the block design	46
Figure 4.4	Test setup for relative humidity measurement	48
Figure 5.1	Corrosion cracks on the surface of in the outdoor test specimens	50
Figure 5.2	Corrosion potentials versus time for different admixed chloride series, 3LP measurements for indoor specimens	51
Figure 5.3	Corrosion potentials versus time for different admixed chloride series, Gecor measurements for indoor specimen	52
Figure 5.4	Corrosion potentials versus time for different admixed chloride series, 3LP measurements for outdoor specimens, 2 in. cover depth	53
Figure 5.5	Corrosion potentials versus time for different admixed chloride series, Gecor measurements for outdoor specimens, 2 in. cover depth	54
Figure 5.6	Corrosion potentials versus time for different admixed chloride series, 3LP measurements for outdoor specimens, 3 in. cover depth	55
Figure 5.7	Corrosion potentials versus time for different admixed chloride series, Gecor measurements for outdoor specimens, 3 in. cover depth	56
Figure 5.8	Corrosion potentials versus time for four additional slabs, outdoor specimens, 1 in. cover depth	57
Figure 5.9	Corrosion rates, concrete ohmic resistances and temperatures over time, 0.0 lb/yd^3 admixed chloride, indoor specimens	59
Figure 5.10	Corrosion rates, concrete ohmic resistances and temperatures over time, 0.6 lb/yd^3 admixed chloride, indoor specimens	60

Figure 5.11 Corrosion rates, concrete ohmic resistances and temperatures over time, 1.2 lb/yd^3 admixed chloride, indoor specimens 61
Figure 5.12 Corrosion rates, concrete ohmic resistances and temperatures over time, 2.4 lb/yd^3 admixed chloride, indoor specimens 62
Figure 5.13 Corrosion rates, concrete ohmic resistances and temperatures over time, 4.8 lb/yd^3 admixed chloride, indoor specimens 63
Figure 5.14 Corrosion rates, concrete ohmic resistances and temperatures over time, 9.6 lb/yd^3 admixed chloride, indoor specimens 64
Figure 5.15 Corrosion rates, concrete ohmic resistances and temperatures over time, 0.0 lb/yd^3 admixed chloride, outdoor specimens, 2 in. cover 65
Figure 5.16 Corrosion rates, concrete ohmic resistances and temperatures over time, 0.6 lb/yd^3 admixed chloride, outdoor specimens, 2 in. cover 66
Figure 5.17 Corrosion rates, concrete ohmic resistances and temperatures over time, 1.2 lb/yd^3 admixed chloride, outdoor specimens, 2 in. cover 67
Figure 5.18 Corrosion rates, concrete ohmic resistances and temperatures over time, 2.4 lb/yd^3 admixed chloride, outdoor specimens, 2 in. cover 68
Figure 5.19 Corrosion rates, concrete ohmic resistances and temperatures over time, 4.8 lb/yd^3 admixed chloride, outdoor specimens, 2 in. cover 69
Figure 5.20 Corrosion rates, concrete ohmic resistances and temperatures over time, 9.6 lb/yd^3 admixed chloride, outdoor specimens, 2 in. cover 70
Figure 5.21 Corrosion rates, concrete ohmic resistances and temperatures over time, 0.0 lb/yd^3 admixed chloride, outdoor specimens, 3 in. cover 71
Figure 5.22 Corrosion rates, concrete ohmic resistances and temperatures over time, 0.6 lb/yd^3 admixed chloride, outdoor specimens, 3 in. cover 72
Figure 5.23 Corrosion rates, concrete ohmic resistances and temperatures over time, 1.2 lb/yd^3 admixed chloride, outdoor specimens, 3 in. cover 73
Figure 5.24 Corrosion rates, concrete ohmic resistances and temperatures over time, 2.4 lb/yd^3 admixed chloride, outdoor specimens, 3 in. cover 74
Figure 5.25 Corrosion rates, concrete ohmic resistances and temperatures over time, 4.8 lb/yd^3 admixed chloride, outdoor specimens, 3 in. cover 75
Figure 5.26 Corrosion rates, concrete ohmic resistances and temperatures over time, 9.6 lb/yd^3 admixed chloride, outdoor specimens, 3 in. cover 76
Figure 5.27 Corrosion rates, concrete ohmic resistances and temperatures over time, 12.0 lb/yd^3 admixed chloride, outdoor specimens, 1 in. cover 77
Figure 5.28 Relationships between acid soluble and water soluble chloride content analysis 79
Figure 5.29 Relationship between ohmic resistance of concrete and acid soluble chloride content for outdoor specimens 81
Figure 5.30 Changes of relative humidity in air and concrete at 2 inch depth during a daytime (from 9:00 am to 7:00 pm, Oct. 11, 1995) 81
Figure 5.31 Changes of relative humidity in air and concrete at 2 in. depth over time 82
Figure 5.32 The measured corrosion rates versus model predicted values 86

Figure 5.33	Measured corrosion rates and predicted values over time, admixed chloride 2.4 lb/yd^3, 2 in. cover, outdoor specimens	87
Figure 5.34	Measured corrosion rates and predicted values over time, admixed chloride 2.4 lb/yd^3, 3 in. cover, outdoor specimens	87
Figure 5.35	Measured corrosion rates and predicted values over time, admixed chloride 4.8 lb/yd^3, 2 in. cover, outdoor specimens	88
Figure 5.36	Measured corrosion rates and predicted values over time, admixed chloride 4.8 lb/yd^3, 3 in. cover, outdoor specimens	88
Figure 5.37	Measured corrosion rates and predicted values over time, admixed chloride 9.6 lb/yd^3, 2 in. cover, outdoor specimens	89
Figure 5.38	Measured corrosion rates and predicted values over time, admixed chloride 9.6 lb/yd^3, 3 in. cover, outdoor specimens	89
Figure 5.39	Effects of temperature on the corrosion rate	91
Figure 5.40	Effects of ohmic resistance of concrete on the corrosion rate	91
Figure 5.41	Effects of chloride content on the corrosion rate	92
Figure 5.42	Effects of corrosion time on the corrosion rate	93
Figure 5.43	Changes of temperatures at different cover depths during daytime	94
Figure 5.44	A schematic diagram of the corrosion-cracking	96
Figure 5.45	Expansive pressure on surrounding concrete due to formation of rust products	99
Figure 5.46	Effects of tensile strength of concrete and type of corrosion products on the time to cracking (2 in. cover depth and corrosion rate 2 mA/ft^2)	102
Figure 5.47	Effects of corrosion rates and cover depths on the time to cracking (f'_t = 472 psi, E = 3,900,000 psi, and α =0.57)	102
Figure 5.48	Critical mass of rust products versus concrete cover depth	103

List of Tables

Table 2.1	Guidance on interpretation of results from half-cell surveys (according to ASTM C 876 -91)	25
Table 2.2	3LP and Gecor guidelines	28
Table 3.1	Existing criteria for metal loss	35
Table 4.1	Aggregate properties	39
Table 4.2	Mechanical and chemical tests of steel	39
Table 4.3	Test variables	40
Table 4.4	Mixture proportions	41
Table 4.5	Compressive strength of concrete	41
Table 4.6	Slab matrix	42
Table 4.7	Block matrix	45
Table 5.1	Observed times to cracking for outdoor specimens	49
Table 5.2	Results of chloride content analysis after four-year outdoor exposure	78
Table 5.3	Mean ohmic resistance of concrete up to five years at different exposure conditions	80
Table 5.4	Measured weight loss and calculated average corrosion over time	82
Table 5.5	Corrosion rates from different test methods	83
Table 5.6	Adjusted measured corrosion rates by the model	95
Table 5.7	Model predicted times to cracking and observed times to cracking	104
Table 5.8	Model predicted times to cracking for other two series specimens	104

Notations

α	constant related to corrosion product, equals molecular weight of steel divided by the molecular weight of corrosion products
ρ_{st}	density of steel
ρ_{rust}	density of corrosion products (rust)
ν_c	Poisson's ratio
C	concrete cover depth
D	diameter of steel reinforcement
E	potential
E_c	elastic modulus of concrete
F	Faraday's constant = 96,494 coulombs per mole
f_c	compressive strength of concrete
f_t'	tensile strength of concrete
I	current
i_{cor}	corrosion current density
P	pressure at concrete/corrosion products interface
R	gas constant
R_c	ohmic resistance of concrete
T	temperature in degree K
t	time
t_{cr}	time to corrosion cracking
W_{crit}	critical mass of corrosion products to induce cracking of the concrete cover
W_p	the required amount of corrosion products to fill the porous area around steel/concrete interface
W_S	the amount of corrosion products to generate the tensile stress
W_{st}	the amount of steel corroded

1.0 Introduction

1.1 Background

Chloride-induced steel corrosion is one of the major worldwide deterioration problems for steel reinforced concrete structures. The high alkaline environment of good quality concrete forms a passive film on the surface of the embedded steel which normally prevents the steel from further corroding [1]. However, under chloride attack, the passive film is disrupted or destroyed, and the steel spontaneously corrodes [2-3]. The volume of rust products is about four to six times larger than that of iron. This volume increase induces internal tensile stresses in the cover concrete, and when these stresses exceed the tensile strength of the concrete, the cover concrete is damaged by cracking, delamination and spalling. In addition to loss of cover concrete, a reinforced-concrete member may suffer structural damage due to loss of bond between steel and concrete and loss of rebar cross-sectional area [4].

Since the later 1960's, chloride de-icing salts used on roadways in the United States have been increased greatly; currently about 10 millions tons of salts are used annually [5]. It has been reported [6] that more than 40 percent of total highway bridges in the United States are structurally deficient or functionally obsolete. The cost of repairing and replacing these bridges is estimated at $70 billion. Approximately 20 percent of total estimated cost is due to the corrosion deterioration of concrete bridges. There are insufficient funds to address all the present repair, rehabilitation and replacement needs. However, through the use of deterioration models, cost-effective decisions concerning the time to repair or rehabilitate or replace existing structures can be made as well as predicting future maintenance and replacement needs and the selection of the most effective corrosion abatement systems.

1.2 Deterioration Models

Tuutti [7] suggested a model for predicting the service lives of reinforced concrete structures (see Figure 1.1). The maximum acceptable corrosion level is related to the appearance of cracks. The deterioration process consists of two periods: initiation and propagation. The length of the initiation period can be estimated from the time required for aggressive species to reach reinforcement surfaces and trigger active corrosion, while that of the propagation period can be taken as the time elapse until repair becomes mandatory.

One model which can be used to estimate the remaining life of concrete bridge components in corrosive environments is the deterioration model developed by Cady and Weyers [8], which is based on the premise that salt-induced corrosion of the steel is the

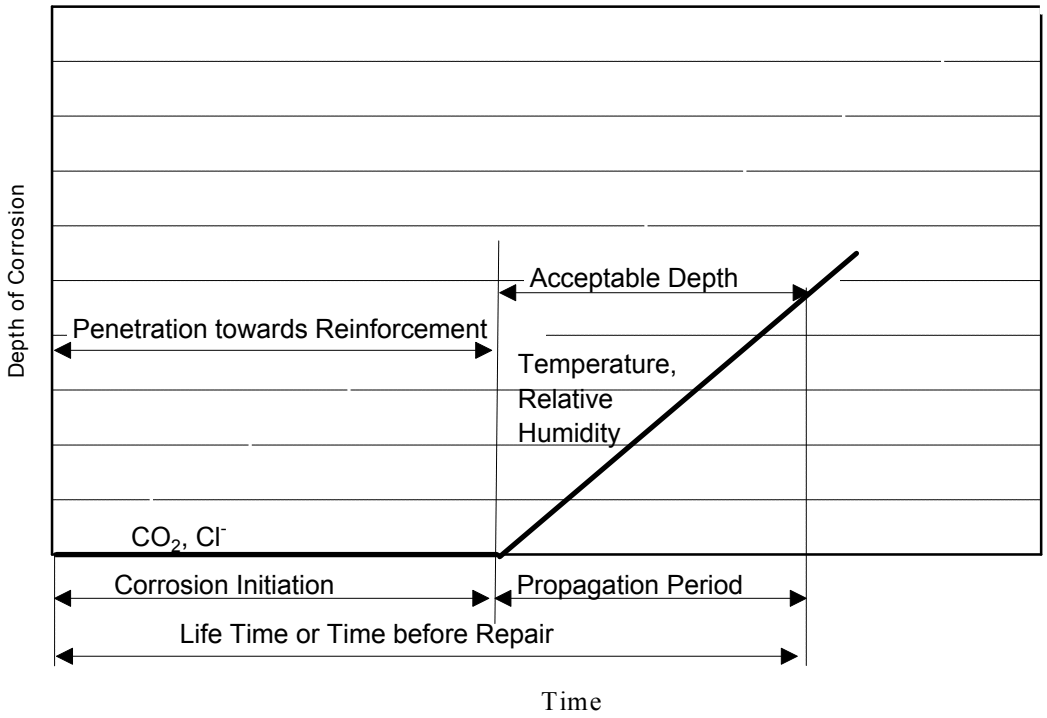

Figure 1.1. A schematic sketch of steel corrosion sequence in concrete [7].

main cause of deck deterioration. The model predicts deck deterioration as measured in an area percentage of the entire deck. The total area of spalls, delaminations, asphalt patches, and crack lengths multiplied by a tributary width combine to produce the total damage.

The model has three distinct phases: diffusion, corrosion and deterioration (see Figure 1.2). The first phase, diffusion, is defined as the time for chloride ions to penetrate the concrete cover and reach the corrosion threshold limit on steel surfaces at a cover depth equal to 2.5% of the cover depth distribution. The diffusion time usually can be determined empirically using Fick's second law [9]. The second phase, corrosion, is defined as a period of time from initiation of corrosion to first cracking of the 2.5% cover concrete. The third phase, deterioration, describes the time to reach a damage level of a percent which is deemed as the time to rehabilitation. During this phase, from the cracking of the concrete cover at 2.5% cover depth to the time for rehabilitation, it has been shown empirically that the deck will continue to deteriorate at a relatively uniform rate [10].

Bazant developed physical-mathematical models to determine the time to cracking for chloride induced corrosion of steel in concrete based on steady-state corrosion [11-12]. In his model, the time to cracking is a function of corrosion rate, cover depth, spacing, and certain mechanical properties of concrete such as tensile strength, modulus of elasticity, Poisson's ratio and creep

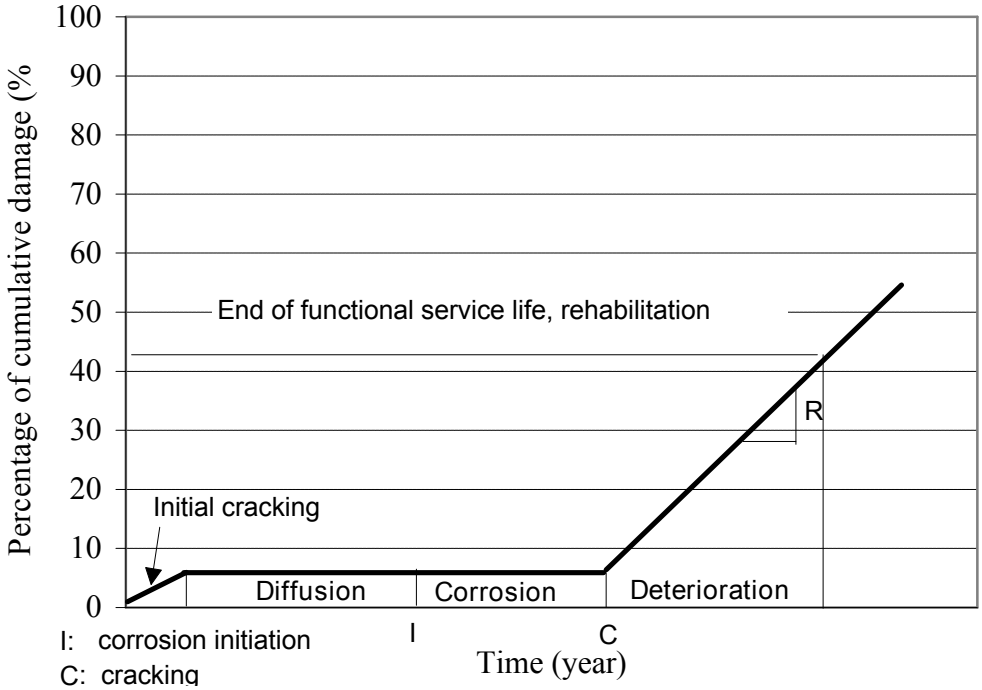

Figure 1.2. Chloride corrosion deterioration process for a concrete element with a mean cover depth of 2 in. (50 mm) [8].

coefficient. A sensitivity analysis of Bazant's theoretical equations demonstrates that for the parameters of concrete strength, cover depth, reinforcing size, horizontal spacing and corrosion rate, corrosion rate is the most significant parameter in determining the time to cracking of the cover concrete. Unfortunately, Bazant's model has never been validated experimentally.

1.3 Scope of Study

This study was initiated to validate or modify a set of theoretical equations to predict the time to cracking for field linear polarization measurements using K. C. Clear's 3LP and the Geocisa Gecor devices [13-16]. The experiment was designed to simulate typical bridge deck construction conditions and investigate the influences of significant factors on the corrosion process in chloride contaminated reinforcement structures based on sensitivity analysis of Bazant's model [17-18].

In August, 1991, a total of 56 specimens were constructed with six series of admixed chloride contents, 0.0, 0.6, 1.2, 2.4, 4.8 and 9.6 lb/yd^3 (0.0, 0.36, 0.71, 1.42, 2.85, and 5.69 kg/m^3), two concrete cover depths of 2 and 3 in. (50 and 76 mm), two reinforcing steel diameters of 0.63 and 75 in. (16 and 19 mm), two reinforcing spacings of 6 and 8 in (152 and 203 mm). In late June, 1995, four additional slabs were designed with a higher admixed chloride, 12.0 lb/yd^3 (7.2 kg/m^3), and thinner cover depth, 1 in. (25 mm), which were expected to crack at a very short time. Forty-four specimens were outdoors and the others indoors in order to maintain a near constant concrete moisture and temperature.

The 3LP and Gecor devices were used to measure the corrosion current density. Measurements were performed once a month, and concrete temperatures at the bar depth and ohmic resistances were also recorded. Metal loss measurements were performed in accordance with ASTM G1-90, Method C3.5 and compared with the measured corrosion rates for specimens which cracked. Statistical analysis of the initial corrosion measurements demonstrated that the variability for each experimental cell along a reinforcing bar and within a specimen is small with the largest variability being between specimens within corrosion cells. Thus, the number of monthly measurements with an experimental cell was reduced to 7 or 8 for each device.
The objectives of this research are:

1. Investigate the factors which affect the corrosion rate in chloride induced corrosion of steel in reinforced concrete structures.

2. Develop a model to characterize the corrosion process and predict the corrosion rate of steel in chloride contaminated reinforced concrete structures.

3. Suggest a modified model for predicting the time to corrosion cracking in chloride- induced corrosion of steel in reinforced concrete structures.

2.0 Review of Corrosion of Steel in Concrete

2.1 Background

Corrosion is defined as the degradation of a metal by an electrochemical reaction with its environment [19-21]. According to the thermodynamic laws, there is a strong tendency for high energy states to transform into low energy states. It is this tendency of metals to recombine with elements present in the environment that leads to the phenomenon known as corrosion. All interactions between elements and compounds are governed by the free energy changes (ΔG) available to them. For a spontaneous reaction to occur, ΔG must be negative. At room temperature most chemical compounds of metals have lower values (more negative) of ΔG than the uncombined metals; therefore, most metals have an inherent tendency to corrode.

2.1.1 Mechanism of Electrochemical Corrosion

Basic Corrosion Cell

In electrochemical corrosion, there are two reactions which occur at the metal/liquid interface: the electron producing reaction which is an anodic reaction (oxidation) and the electron consuming reaction which is a cathodic reaction (reduction). For a basic corrosion cell, there are four essential components involved:

a. The anode. The anode usually corrodes by loss of electrons from electrically neutral metal atoms to form discrete ions. These ions may remain in solution or react to form insoluble corrosion products. The corrosion reaction of a metal, M, is usually expressed by the simplified equation:

$$M \rightarrow M^{z+} + ze^- \qquad (2.1)$$

in which the number of electrons taken from each atom is governed by the valency of the metal. For iron, z equals two.

b. The cathode. The cathode reaction must consume the electrons produced by the anode process. There are two basic reactions which occur at the cathode depending on the pH of the solution:

$$(a) \quad pH < 7: \quad 2H^+ + 2e^- \rightarrow H_2 \qquad (2.2)$$

$$(b) \quad pH > 7: \quad 2H_2O + O_2 + 4e^- \rightarrow OH^- \qquad (2.3)$$

c. An electrolyte. This is the name given to the solution, which must, of necessity, conduct electricity. In the solution cations can move from anodic to cathodic regions and anions move in opposite direction.

d. Electrical connection. The anode and cathode must be in electrical contact for a current to flow in the corrosion cell.

The removal of any one of the four components of the simple corrosion cell will stop the corrosion reaction.

Faraday's Law

The free energy change of the corrosion process in terms of the potential difference and the charge transported is known as Faraday's Law:

$$\Delta G = z E F \qquad (2.4)$$

where E is the measured potential (volts) and z is the number of electrons transferred in the corrosion reaction. F represents the charge transported by one mole of electrons and has the value of 96,494 coulombs per mole.

Nernst Equation

For a reaction: $A + B \rightarrow C + D$,

$$\Delta G = \Delta G^{o} + RT \ln \frac{[C][D]}{[A][B]} \qquad (2.5)$$

where R is a gas constant which equals to 8.3143 J $mol^{-1}K^{-1}$, T is temperature (in degree K). Symbol (^{o}) represents standard state parameters at 298 K and 1 atmosphere pressure. The terms in the square brackets represent the concentrations of the species in the solution which are expressed in moralities (moles per liter). The Nernst equation is obtained from this reaction of change in free energy, equation 2.5,

$$E = E^{o} - \frac{RT}{zF} \ln \frac{[products]}{[reactants]} \qquad (2.6)$$

The Nernst equation describes how the electrode potential varies with the concentrations of participating substances.

2.1.2 Pourbaix Diagrams

Based on thermodynamic data on reactions between metal and water, Pourbaix [22] developed potential versus pH diagrams which indicate thermodynamically stable phases as a function of electrode potential and pH. The Pourbaix diagram for iron is shown in Figure 2.1.

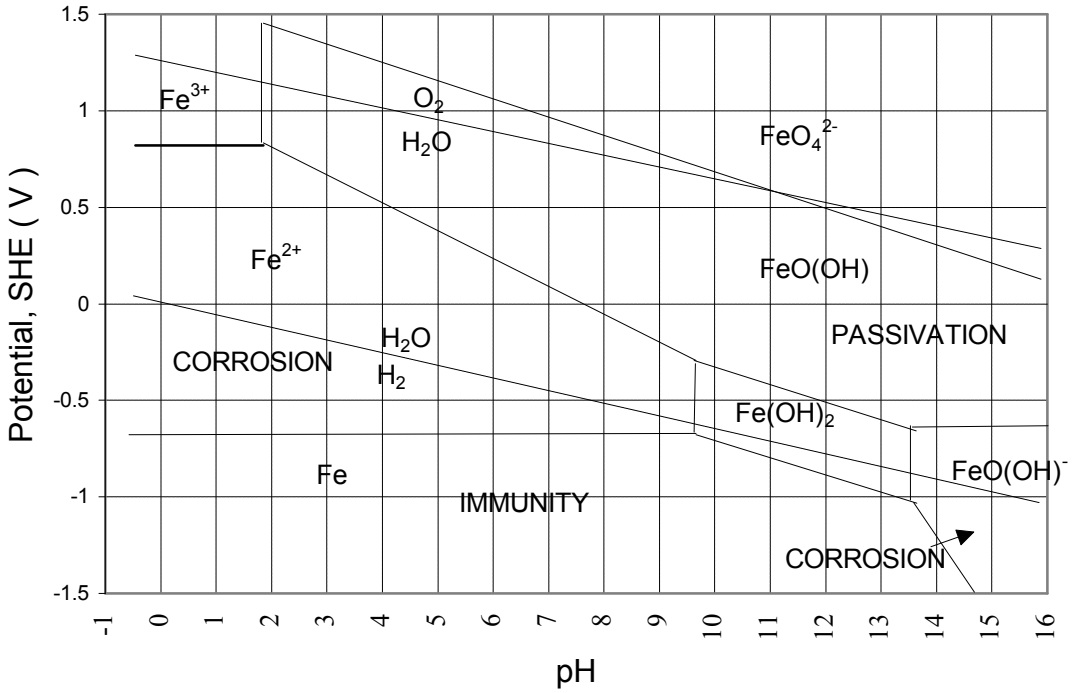

Figure 2.1. Pourbaix diagram for the FeO-H_2O system at 77°F (25°C) for 10^{-6}M, activities of all metal ions [22].

There are three general regions described as regions of corrosion, passivity and immunity. A soluble product is formed under a range of acidic conditions and under a narrow range of vary alkaline conditions. These are regions of corrosion. Between these two regions an insoluble film is formed, and that region is referred as passive region. The third region, immunity, shows that metal is thermodynamically stable and no corrosion will occur. Pourbaix diagrams provide a strong thermodynamic basis for understanding corrosion reactions. There are two main limitations on use of the diagrams. One arises from lack of kinetic data and the other comes from the purity of environment. In practice, corrosion processes are involved in contaminated environments.

2.1.3 Polarization

The difference between the potentials of an electrode with and without current is called electrochemical polarization. This polarization represents an overpotential defined as:

$$h_a = E_{corr} - E_a \tag{2.7}$$

$$h_c = E_c - E_{corr} \tag{2.8}$$

where h_a, h_c are the overpotentials and E_a, E_c are the equilibrium potentials for anode and cathode, respectively. E_{corr} is a corrosion potential.

Evans [23] introduced a simplified graphic method of representing the relationship between current I and potential E. Figure 2.2 illustrates the simplest example of an Evans diagram. The abscissa may represent the total current or its logarithm. The intersection of two curves represents the conditions at which the anodic and cathodic currents are equal and no net external current flows and, thus, defines the corrosion potential, E_{corr}, and corrosion current, I_{corr}.

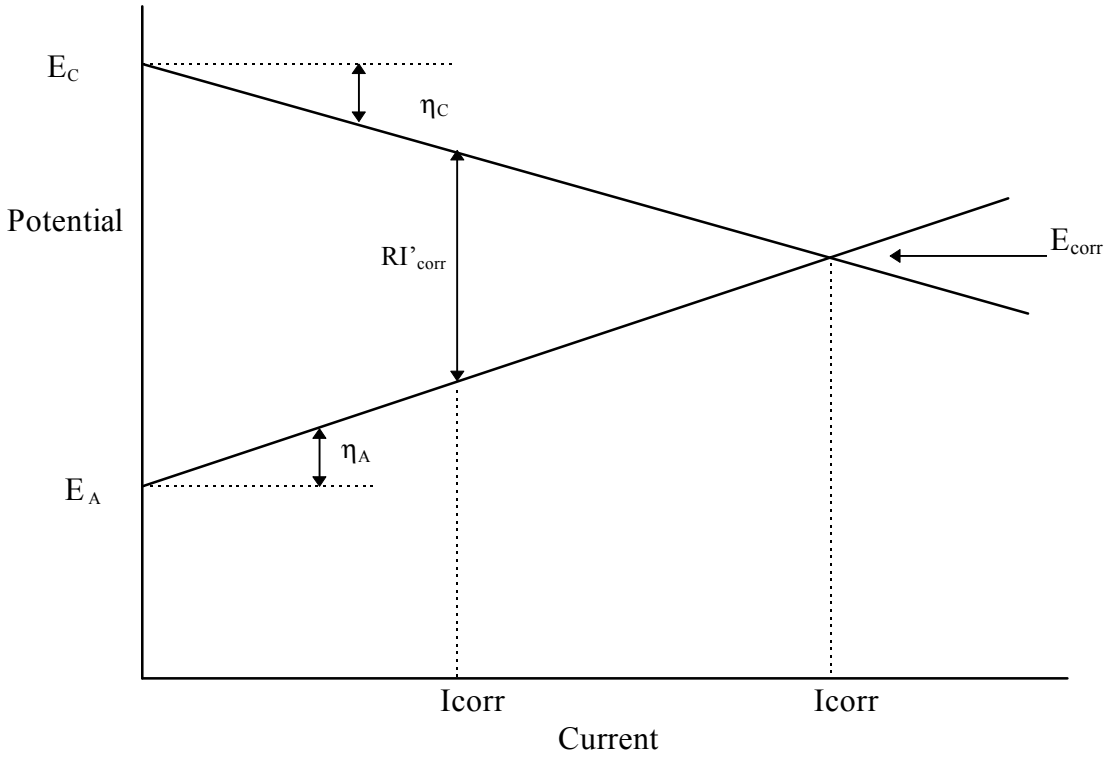

Figure 2.2. A schematic of Evans diagram [23].

There are three kinds of polarizations which may act separately or simultaneously, namely concentration, resistance (ohmic) and activation polarization.

Concentration Polarization Concentration polarization is caused by the concentration on the electrode surface from that of the bulk solution. An example of this would be depletion of oxygen at cathode. The rate of oxygen diffusion through the concrete to the reinforcement determines the rate of corrosion. This is illustrated in Figure 2.3 for two different rates of oxygen diffusion.

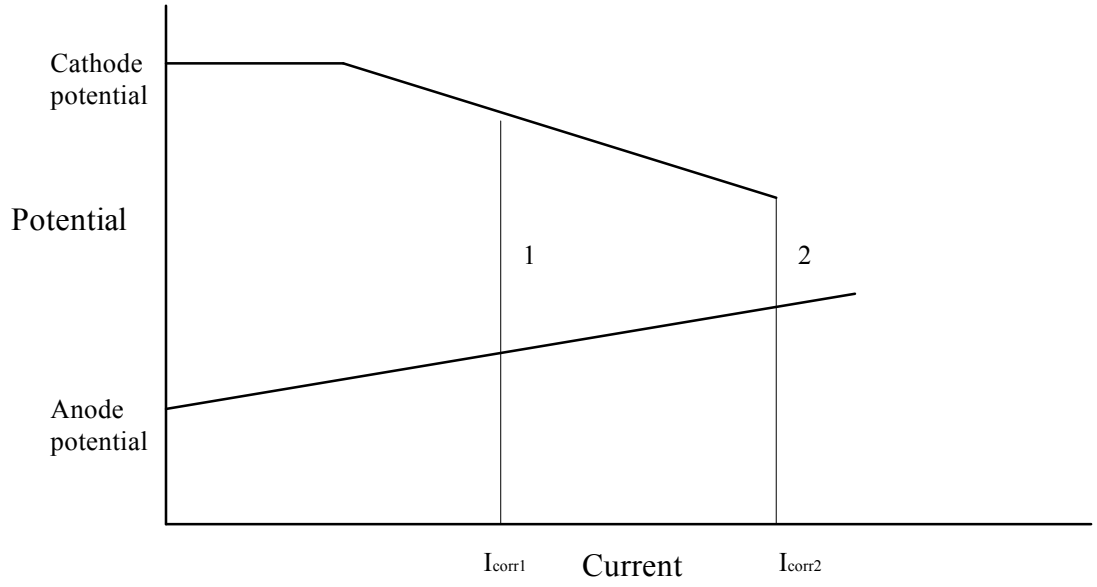

Figure 2.3. Potential versus current plot illustrating cathodic diffusion polarization.

The limiting current density, i_L (the highest current density possible for a given electrode reaction due to the limitation imposed by the diffusion velocity of the reaction particles), is an important quantity related to concentration polarization. The limiting current density is inversely proportional to the thickness of the diffusion boundary layer d_N [24], that is

$$i_L \, d_N = \text{constant} \tag{2.9}$$

For a cathode process, the concentration polarization is given by [25]

$$h_C = \frac{0.059}{z} \log\frac{C_e}{C_0} = \frac{0.059}{z} \log\left(1 - \frac{i}{i_L}\right) \tag{2.10}$$

where C_e is concentration on an electrode;

C_0 is bulk concentration;
i is an applied current density;
i_L is a limiting current density;
z is change of ionic charge in an electrode process; and
h_C is concentration polarization.

Resistance Polarization. Resistance (Ohmic) polarization is due to an ohmic resistance in a film, e.g. an oxide film on the electrode surface, causing an ohmic potential drop, which may be written as:

$$h_R = R\,I \tag{2.11}$$

where R is the film resistance for all the electrode surfaces, I is the current. Figure 2.4 illustrates two cases of resistance control, where the potential available for corrosion is the difference in potential between anode and cathode minus the relevant IR drop.

Activation Polarization. Activation polarization occurs due to a certain slow step in the electrode process requiring an activation energy for overcoming the reaction hindrance.

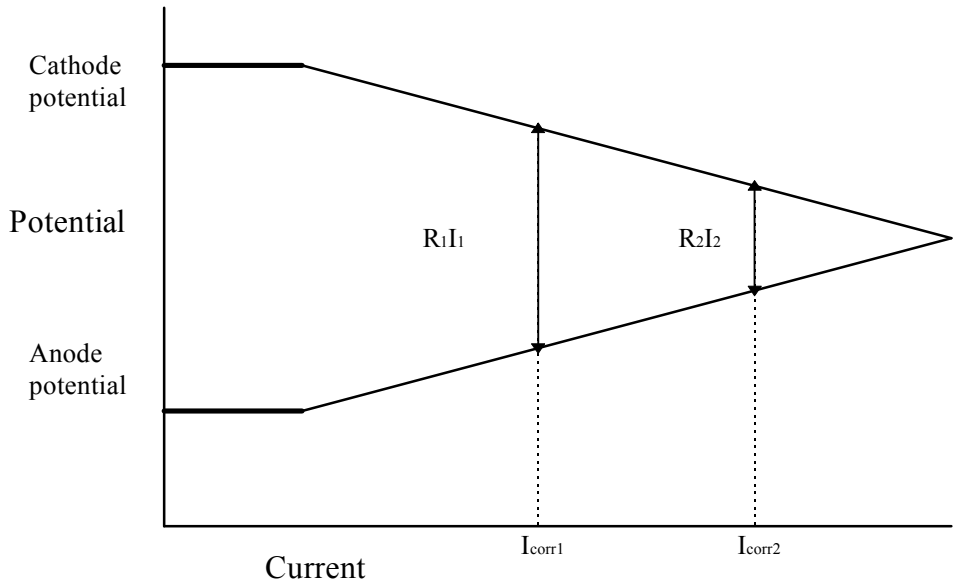

Figure 2.4. Potential versus current plot illustrating resistance polarization.

A logarithmic relationship is obtained based on the well-known Tafel's equation [26] (for $I_a > 10I_0$):

$$\eta_A = b \log \frac{I_a}{I_0} = a + b \log I_a \qquad (2.12)$$

where a and b are constants known as the Tafel intercept and Tafel slope parameters, respectively, and can be determined empirically. I_a is the applied current, and I_0 exchange current. The parameter a is related to the exchange current I_0, which is the equilibrium current flowing back and forth through the electrode-electrolyte interface at equilibrium and is a measure of the reversibility of the reaction. The parameter b, on the other hand, gives an insight into mechanism of the electrode reaction [27]. The activation polarization is strongly dependent on the composition of the solution, particularly its content of anions and inhibitors.

2.1.4 Passivity

Passivity occurs when the corrosion product is insoluble and adherent and results in the formation of an ultra-thin protective film on the surface of the metal. Passivity is of two kinds, chemical and mechanical passivity.

Chemical Passivity. This type of passivity is due to an invisible thin but dense and semiconducting oxide film on the metal surface, displacing the electrode potential of the metal strongly in the positive direction.

Mechanical Passivity. Mechanical passivity is due to the precipitation of solid salts on the metal surface. The cause of strongly reduced corrosion rate in this case is a thick but more or less porous salt layer, usually non-conducting in itself.

The maintenance of passivity needs certain electrochemical environmental conditions. The breakdown of passive film is usually brought about by changes of the electrochemical environmental conditions or mechanical forces.

2.1.5 Growth of Rust Film

The growth of corrosion products may follow linear or parabolic law depending on the properties of rust oxides [28-29].

For a metal that does not form protective oxide film, the rate of growth of oxide film remains constant, that is,

$$y = kt \qquad (2.13)$$

where k is a constant, y is the film thickness and t is the corrosion time.

For a metal that forms protective oxide film, the rate of corrosion process will be retarded by diffusion of corrodant through the film. This results in a thickening of the film, the rate of which continuously decreases with time, that is,

$$y^2 = Kt \tag{2.14}$$

where K is a constant related to the diffusion coefficient and concentration of corrodant, y and t are film thickness and corrosion time, respectively.

However, the relationship between corrosion rate and time is not so simple as described above. It is more proper to express the deterioration rate with time by the more general relationship [30],

$$y^n = kt \tag{2.15}$$

where y is the overall corrosion expressed in term of penetration or weight loss, t is the corrosion time; k is a coefficient depending on the metal and external corrosion conditions; n is a constant which is related to the degree of retardation of diffusion. A decrease in the diffusion coefficient with the film growth results in an increase in n .

2.2 Corrosion of Steel in Concrete

In general, good quality concrete of appropriate mix proportion, compacting, and curing provides an excellent protective environment for steel. The physical protection is afforded by the cover concrete acting as a physical barrier to the access of aggressive species. Chemical protection is provided by concrete's high alkalinity solution within the pore structure of cement paste matrix due to the presence of sodium and potassium oxides in the cement, as well as calcium hydroxide produced in the hydration reactions of cement components [1,4,31]. The range of high pH values of typical concrete (12.5-13.5) is within the pH domain in which insoluble oxides of iron are thermodynamically stable (see Figure 2.1). This gives rise to passivation of the metal surface in which significant corrosion is hindered due to the anodic formation of a protective surface film.

Unfortunately, the physical barrier of the cover concrete is not perfect, because the porous structure of concrete and existing microcracks allow the ingress of aggressive species which cause the breakdown of the passive film. The most common causes of passive film breakdown are incorporation of chloride ions in the film and neutralization of the pore solution by atmospheric carbonation (CO_2).

2.2.1 Concrete as An Electrolyte

The process of corrosion of steel in concrete is generally considered as being electrochemical in nature, and the basic mechanisms of electrochemical theory of corrosion developed for liquid

electrolytesapply [32-35]. However, electrochemical corrosion of iron in concrete has a number of characteristic differences that are determined by the peculiarities of electrochemical processes in the complex "concrete electrolyte", the properties of which are affected by the microporous structure of the concrete and service exposure conditions.

Structure of Concrete

Concrete is a highly heterogeneous and complex structure, which contains a heterogeneous distribution of different types and amounts of solid phases, pores, and microcracks [4]. In addition, the structure of concrete is also subject to change with time, environmental humidity and temperature. A large amount of water can exist in the hydrated cement paste, depending on the environmental humidity, porosity and pore size distribution of the hydrated cement paste. The presence and transport of the corrosion reactants (water, oxygen and various ions), the corrosion products, and the passage of the ionic current necessary to support corrosion are normally confined to the cement paste phase—cement paste pore solution and the structure and distribution of pores.

Cement paste pore solution. The composition of the pore solution is the decisive factor in determining whether embedded steel will be passivated or whether it will actively corrode. Researchers on the influence of a number of factors on the composition of pore solution [36-38] have shown that the presence of sodium and potassium oxides in the cement, as well as calcium hydroxide produced in the hydration reactions of cement components can give the pore solution of ordinary portland cement a pH of about 13 while the pH of blended cement is somewhat lower. The range of high pH values of typical concrete is within the pH domain in which insoluble oxides of iron are thermodynamically stable to maintain a passive film on steel surface. Unfortunately, the pH value of concrete can be reduced by carbonation and by leaching.

The Structure and Distribution of Pores The structure, pore size distribution and pore connectivity in the cement phase determine the availability of oxygen and moisture at the steel surface, both of which are necessary for the maintenance of a passive film. They also determine the penetration or diffusion rate of chloride ion and carbon dioxide which, as mentioned above, are the two most common causes in the corrosion of embedded steel in concrete.

The typical sizes of both the solid phase and the voids in hydrated cement paste are shown in Figure 2.5 [4]. Pore size distributions are mainly affected by the water/cement ratio, and the degree of hydration.

The typical pore size distribution plots of several hydrated cement paste specimens tested by the mercury intrusion technique are shown in Figure 2.6 [39]. The size of interlayer space (gel pore) is too small to have an adverse affect on the permeability of the hydrated cement paste, and water in these small voids are held by hydrogen bonding. It is the capillary pore system which is responsible for diffusion and permeation processes and, therefore, of importance for corrosion.

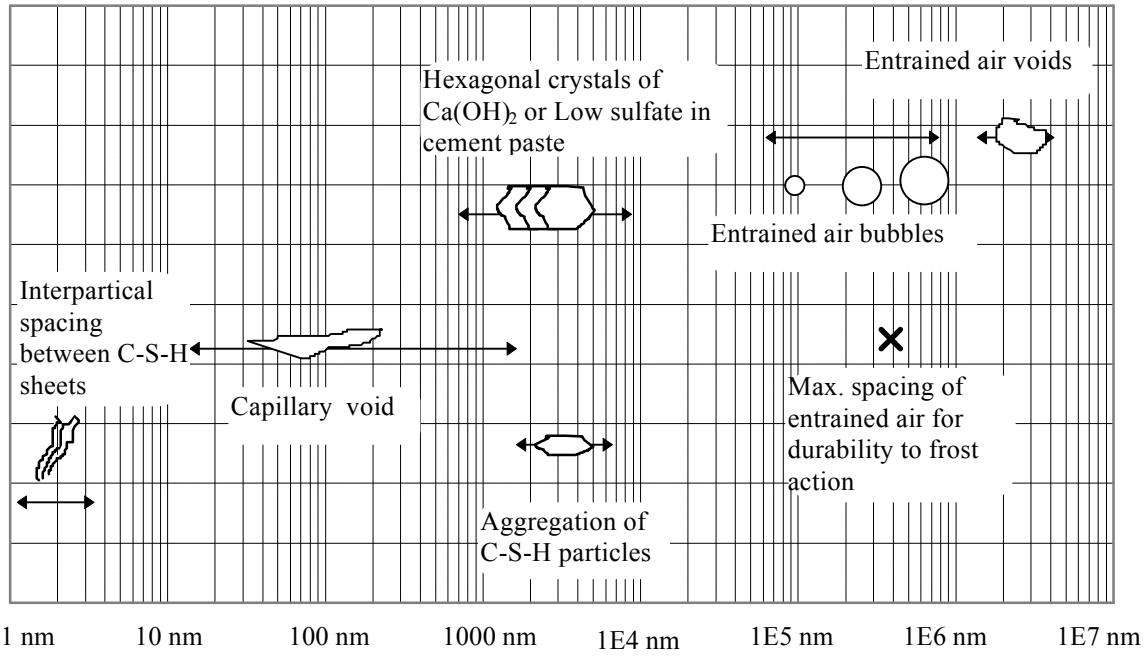

Figure 2.5. Dimensional range of solids and pores in a hydrated cement paste [4].

Concrete Electrolyte

The concrete pore system filled with pore water and air provides a path for corrosive elements and the electrolyte. The following properties are characteristic for concrete as a medium of corrosion.

The presence of the different types of water in the concreteIn addition to vapor empty or partially water-filled voids, water can exist in the hydrated cement paste in several forms as the following states.

a. Capillary water. This is the water present in voids larger than about 50 Å.

b. Adsorbed water. This is the water that is close to the solid surface; that is, under the influence of attraction forces, water molecules are physically adsorbed onto the surface of solid in the hydrated cement paste. A major portion of the adsorbed water can be lost by drying the hydrated cement paste to 30 percent relative humidity.

c. Interlayer water. This is the water associated with the C-S-H structure which is strongly hold by hydrogen bonding. The interlayer water is lost on strong drying (i.e., below 11 percent relative humidity).

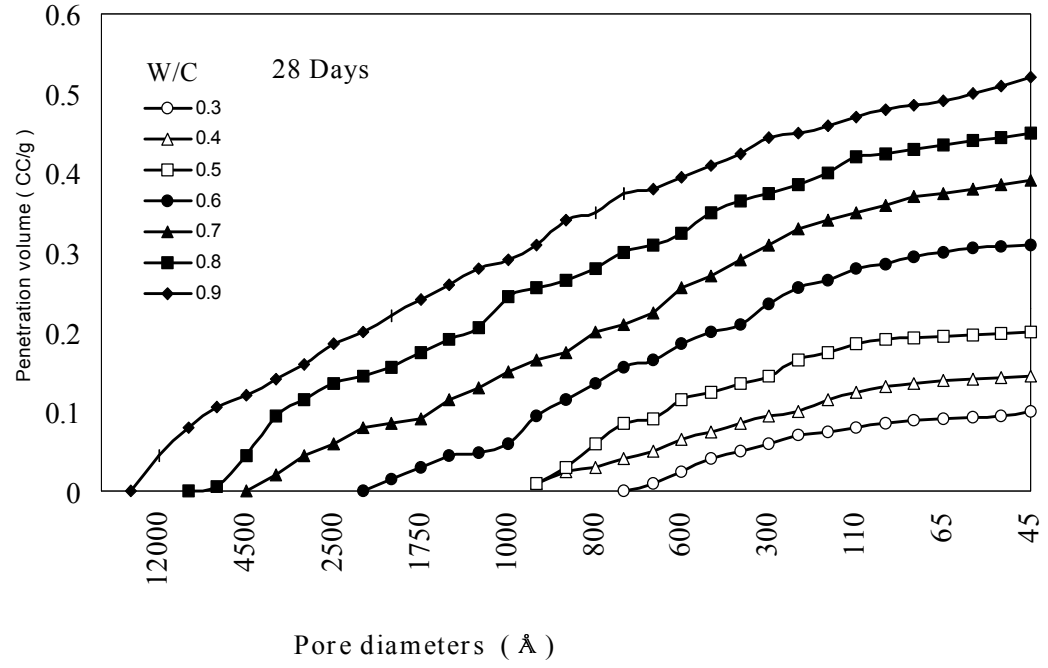

a. Different water cement ratios.

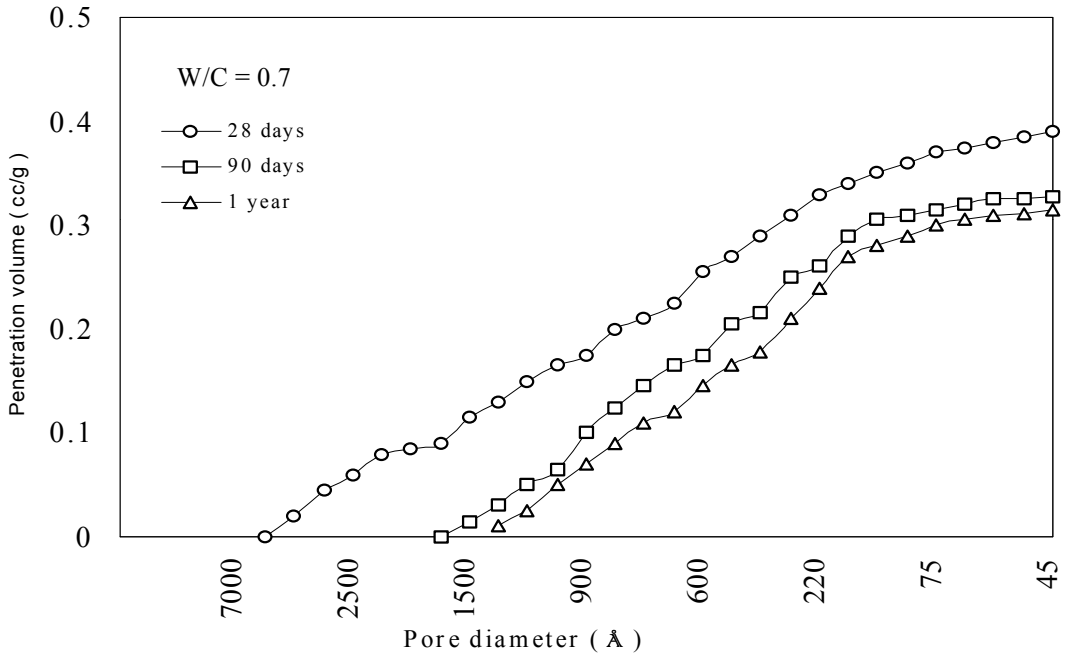

b. Different ages with W/C=0.7.

Figure 2.6. Pore size distribution in hydrated cement pastes [39].

d. Chemically combined water. This is the water that is an internal part of the structure of various cement hydration products which is not lost on drying.

It is important to note that the concrete is an ionic conductor of electric current with the exception of its very dry condition, and it can be considered as a corrosive electrolyte. However, it is quite different from the usual liquid electrolyte, because of its physicochemical properties.

The highly heterogeneous and dynamic nature of the structure of concrete. The electrochemical properties of the concrete vary within very wide limits, depending not only on its internal structure but also on its location, and seasonal weather condition. Therefore, concrete can vary considerably in electrical conductivity during its service life.

These properties of concrete as an electrolyte will influence the character of the electrochemical reactions significantly by changing the conditions required for cathodic and anodic processes. The most fundamental characteristic is the difference in mechanism and the rate of oxygen supply under different corrosion conditions: through the liquid electrolyte (corrosion of metal in solution), through a thin film of electrolyte (such as atmospheric corrosion), or through a solid microporous electrolyte (such as steel corrosion in concrete). In solution, access of oxygen to the corroding surface of the metal is dependent primarily on diffusion; in the atmosphere, on the moisture thickness; and in concrete, on its structure (pore size distribution, porosity and pore connectivity), degree of saturation and cover depth. The corrosion process (or rate of corrosion) in concrete also is dependent on the conductivity of concrete electrolyte.

2.2.2 Principles of Steel Corrosion in Concrete

Corrosion of steel in concrete is an electrochemical process. The corroding system consists of an anode in which steel is corroded, a cathode, an electrical conductor, and an electrolyte (concrete pore solution). The potential difference between anode and cathode is the driving electrical force for steel corrosion.

Usually, the process can be divided into primary electrochemical processes and secondary processes.

Primary Electrochemical Processes

For steel in concrete, as the passive film is degraded by chloride ions or the pH reduced by carbonation, the metallic Fe at the anode is oxidized to form ferrous ions (Fe^{2+}):

$$Fe \rightarrow Fe^{2+} + 2e^{-} \qquad (2.16)$$

The electrons released at the anode flow through the steel to the cathodic areas, as illustrated in Figure 2.7 [4]. The above reaction is initially balanced by a cathodic reaction of dissolved oxygen (O_2) to hydroxyl ions (OH^-):

$$O_2 + 2\ H_2O + 4\ e^- \rightarrow 4\ OH^- \qquad (2.17)$$

The anodic product Fe^{2+} reacts with the cathodically formed hydroxyl ions to produce a ring of a white precipitate of ferrous hydroxide ($Fe(OH)_2$):

$$Fe^{2+} + 2OH^- \rightarrow Fe(OH)_2 \qquad (2.18)$$

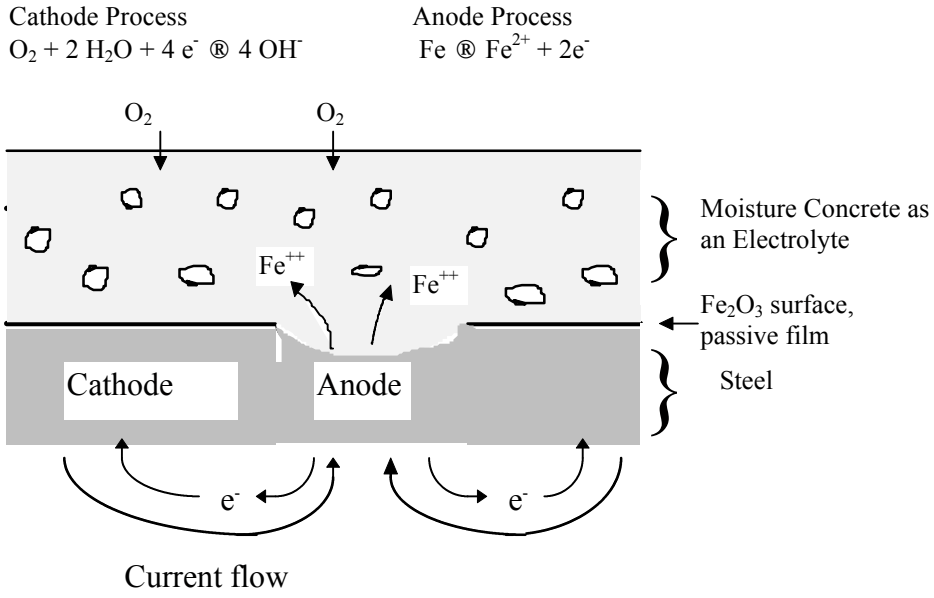

Figure 2.7. Mechanism of corrosion of steel in concrete [4].

Secondary Processes

The $Fe(OH)_2$ can be further converted to hydrated ferric oxide ($Fe_2O_3 \times H_2O$), also known as ordinary red-brown rust, and black magnetite (Fe_3O_4) preceded by the formation of green hydrated magnetite ($Fe_3O_4 \times H_2O$):

$$4\ Fe(OH)_2 + O_2 \rightarrow Fe_2O_3 \times H_2O + 2H_2O \qquad (2.19)$$

$$6\,Fe(OH)_2 + O_2 \rightarrow 2\,Fe_3O_4 \cdot H_2O + 4\,H_2O \quad (2.20)$$

$$Fe_3O_4 \cdot H_2O \rightarrow Fe_3O_4 + H_2O \quad (2.21)$$

The composition of rust on iron may be expressed as a general formula:

$$m \cdot Fe(OH)_2 + n \cdot Fe(OH)_3 + p \cdot H_2O \quad (2.22)$$

where the values ofm, n and p vary considerably, depending on conditions such as pH of the solution, the oxygen supply and moisture content.

Since the volume of rust products is much higher (about 4 to 6 times) than that of the iron as shown in Figure 2.8 [40], the formation of rust products will lead to cracking and spalling of the cover concrete when expansive stress exceeds the tensile strength of the concrete, and reduction of steel reinforcing cross section may lead to structure failure.

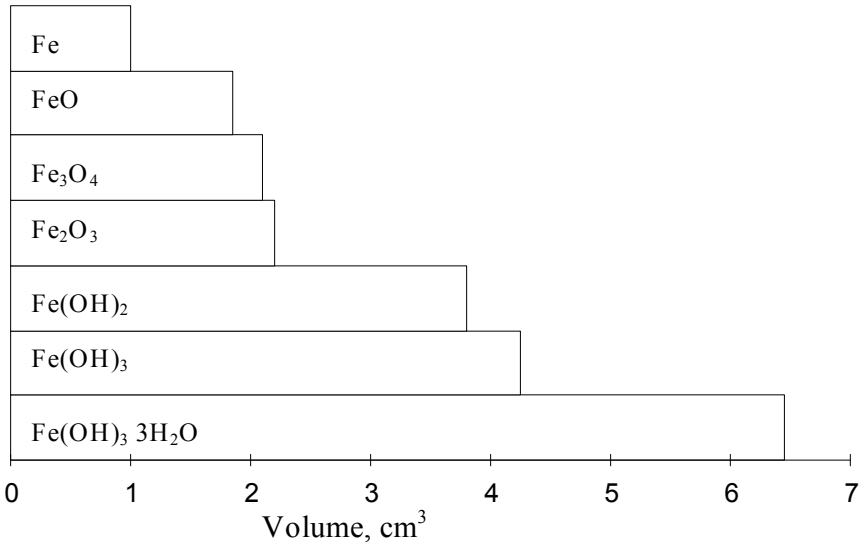

Figure 2.8. The relative volumes of iron and its corrosion reaction products [40].

2.2.3 Initiation of Steel Corrosion in Concrete

The high alkaline environment of good quality concrete forms a passive film on the surface of the embedded steel which normally prevents the steel from further corroding. The maintenance of passivity of steel in concrete requires a high pH and presence of both water and oxygen. Two major causes of steel corrosion in reinforced concrete and consequent initiation of active corrosion are carbonation induced corrosion and chloride induced corrosion.

Carbonation Induced Corrosion

Concrete structures are constantly affected by CO_2 in the atmosphere. In the presence of CO_2 which in aqueous solution is a weak acid, the different hydrates in cement paste such as portlandite ($Ca(OH)_2$) and CSH, can react with CO_2 and become carbonated.

$$Ca(OH)_2 + CO_2 \rightarrow CaCO_3 + H_2O \quad (2.23)$$

$$2NaOH + CO_2 \rightarrow Na_2CO_3 + H_2O \quad (2.24)$$

The results of carbonation lowers the pH value [41-42], and the protective film covering the steel surface which is maintained in a high pH environment is dissolved and it causes corrosion of steel.

The carbonation rate is mainly determined by quality of concrete which is a function of cement type, water/cement ratio and proportion of cement. The degree of saturation of the concrete is also a decisive factor in determining the carbonation rate because the CO_2 permeates the concrete most rapidly in the gas phase but the carbonation reaction takes place in the liquid phase. In a completely dry concrete or a completely saturated concrete, the carbonation reaction rate is very slow. When the pores have a layer of moisture on the walls but not completely saturated (50 to 80 percent relative humidity), the CO_2 can rapidly reach the vicinity of the pore walls and have enough water to be able to react. Figure 2.9 [43] illustrates the effect of the relative humidity on the degree of carbonation.

Chloride Induced Corrosion

It is well documented [1,4,7,11,44-51] that the presence of chloride ions in reinforced concrete can cause the steel to corrode if sufficient oxygen and moisture are present to sustain the reaction. The chloride-induced corrosion is the most prevalent and damaging cause of corrosion of steel in concrete.

Source of Chloride in Concrete There are two means by which chloride ions may be introduced into concrete:

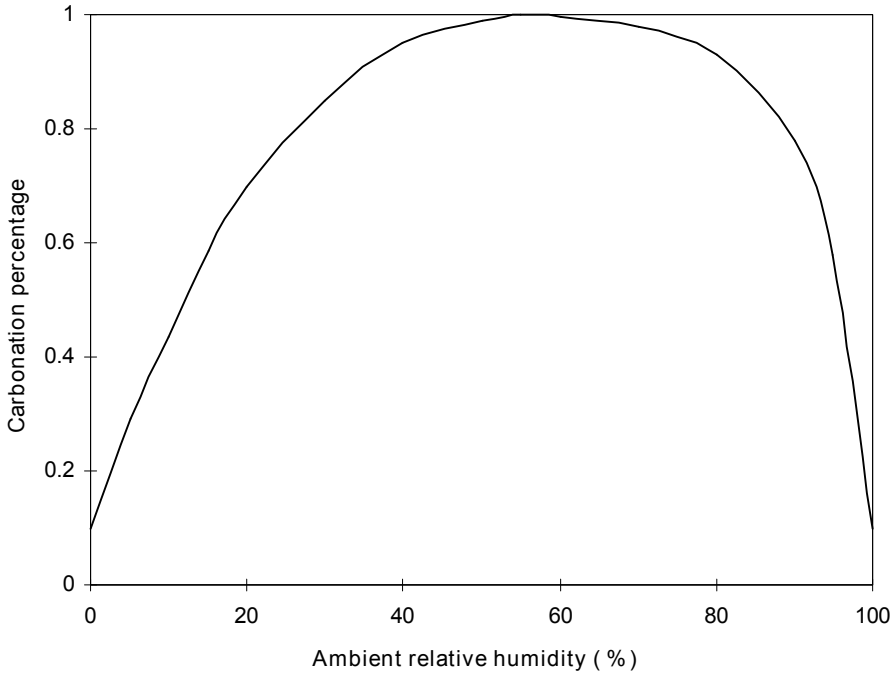

Figure 2.9. The degree of carbonation as a function of the relative humidity [43].

a. Internal source–from concrete-making materials. Chloride ions may be introduced in the fresh concrete mix if the concrete-making materials (water, cement and aggregate) are contaminated with chlorides. Some concrete admixtures such as calcium chlorides also contain chloride ions.

b. External source–from de-icing salts orseawater. De-icing salts are widely used in the areas of the world where the pavement and bridge decks are kept clean and bare in the winter. This is the most common source of chloride ions. Chloride ions are also prevalent inseawater so that the structures exposed to theseawater are also contaminated. The penetration of chloride ions from external sources to the steel surface is mainly through capillary attraction and ionic diffusion.

Mechanism of Chloride Attack The mechanism of chloride induced corrosion of steel is not yet fully understood. It is generally believed [52-57] that the chloride ions become incorporated in the passive film, replacing some of the oxygen and increasing both its conductivity and its solubility.

It has been suggested that chloride ions can complex with the ferrous ions produced by corrosion to form soluble complexes of iron (II) chloride. The resulting iron chloride complex ion then

combines with hydroxyl ions to form $Fe(OH)_2$ in solution and releases the chloride ions back to solution to complex more iron and thus essentially acts as a catalyst in corrosion reactions.

Threshold Chloride Concentrations To initiate corrosion, a threshold concentration of chloride (minimum concentration of chloride necessary to destroy the passive film) is required in excess of the amount immobilized by reaction with tricalcium aluminate in cement. It is generally believed that only freely dissolved chloride ions in the concrete pore water can be involved in the corrosion reactions.

This threshold concentration of chloride ions to initiate corrosion is controversial, because it is dependent on so many factors including quality of concrete (W/C ratio, mixture proportions, type of cement), relative humidity and temperature of the concrete, the pH of the pore solution and sulfated content [58-61].

Figure 2.10 illustrates the relation between some factors and the threshold chloride concentration given by CEB (Comité Euro-International d'Beton) [62]. The value of 0.4 % of chloride ion by weight of the cement suggested in Figure 2.10 is also considered by RILEM [63] as an appropriate threshold. For the typical concrete mixtures normally used in practice, the threshold chloride content is reported to be in the range of 0.60 to 0.83 kg of chloride ions per cubic meter of concrete (1.0 -1.4 lb/yd^3).

2.2.4 Corrosion Activity of Concrete

It is well known that the rate of corrosion of steel in concrete at different situations can vary widely, ranging from tens and even hundreds of times. The rate of corrosion of steel in concrete is mainly dependent on ionic conductivity of concrete electrolyte, its humidity and temperature, and the quality of cover concrete as related to the transport of the corrosive species from external environment to the steel surface.

Conductivity of Concrete

Generally the best measure of corrosivity of concrete is its conductivity, usually expressed as the reciprocal, the resistivity. A low concrete resistivity indicates a high corrosive activity. The resistivity of the concrete is mainly determined by the salt content in the pore water, degree of saturation and temperature. The resistivity of the concrete can vary widely for different conditions [64-67].

Gjorv [65] has reported resistivity values of 7,000 and 6,000,000 Ω-cm for 100 % and 20 % saturated concrete, respectively, which are possible in natural environments. High water/cement ratio, chloride bearing, saturated concrete provide the lowest resistivity, while low water/cement ratio, well cured, dry concrete provides the highest.

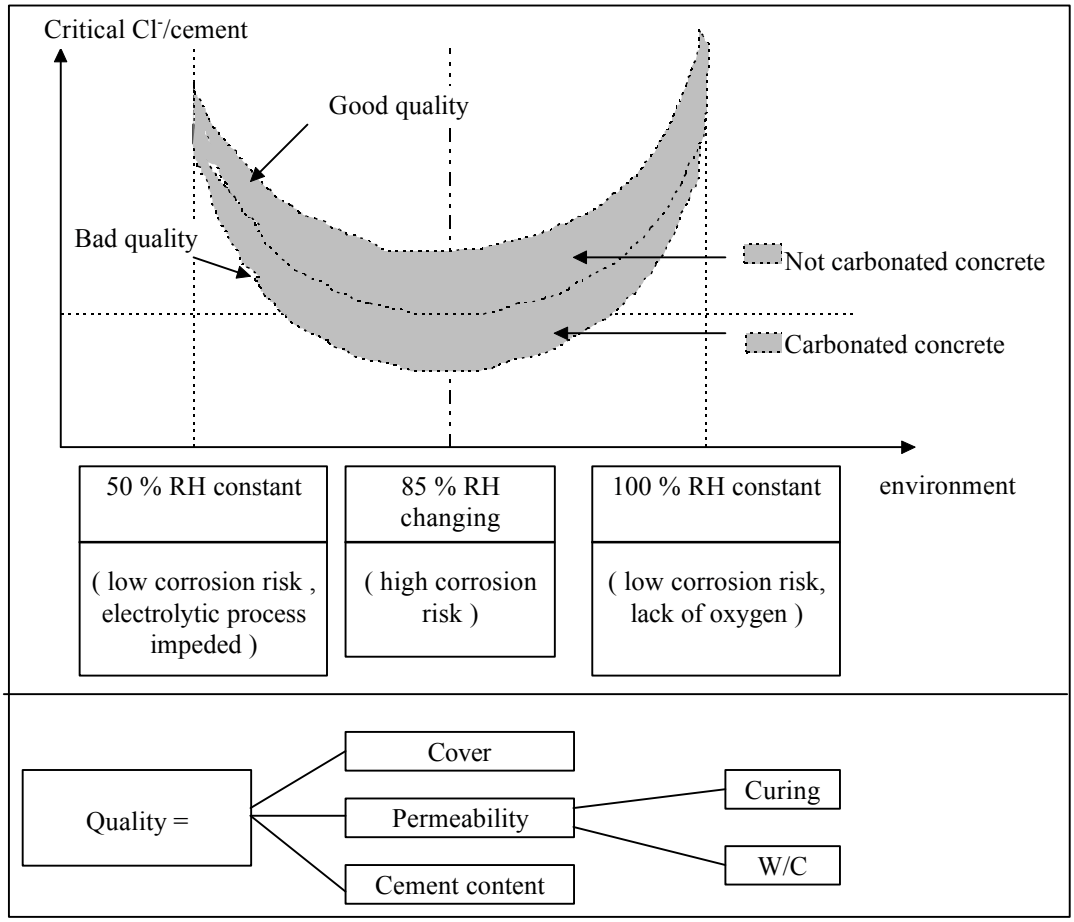

Figure 2.10. The critical chloride content according to CEB recommendations [62].

There is an absence of complete correlation between electrical resistivity and concrete corrosivity. Because the corrosion process in concrete is a complex process, oxygen availability at cathode area is also a controlling factor for the rate of corrosion of steel in concrete. The relationship between moisture and oxygen in concrete is presented below.

Water-Air Relationship in Concrete

The concrete capillary-pore system filled with water and air acts as the corrosive electrolyte. Apart from the pore structure, porosity and pore size distribution of the concrete, water content in the concrete is dependent on the local amount and time of rainfall, and external relative humidity and temperature.

A certain water content in concrete is an essential requirement for corrosion to take place. As a rule, the presence of oxygen is also necessary for cathodic reaction process. If a pore volume of the concrete is only partly filled with water, transfer of oxygen will be easy to the steel surface by means of diffusion in the gas phase. Whereas, when a pore volume of the concrete is completely filled with water, then oxygen can reach the steel surface only by diffusion through the pore water, and the diffusivity of oxygen in water is about four powers lower than that in air [30]. Kobayashi [68] has reported that when moisture content of concrete is lowered from 80 % to 40 %; the value of oxygen diffusion coefficient becomes approximately 15 times higher.

With an increase in the water content in concrete, the corrosion rate will first increase due to an improved conductivity. When the water content approaches to a degree of complete filling of the concrete pores, the corrosion rate rapidly decreases to a low value due to the strongly obstructed supply of oxygen.
The importance of water content for oxygen transport explains why the corrosion rate is considerably higher in the structure located within the tidal and splash zone than below the tidal zone, corrosion is very rapid in the splash zone.

Penetration of Corrosion Species in Concrete

Usually, penetration of a particular substance such as chloride ions into concrete can be in two forms: capillary attraction and ionic diffusion, depending on the degree of saturation in the concrete [69-70]. The content of chloride ions (not total chloride content, only soluble one) at steel surface has a great effect on the corrosivity of steel in concrete. The quality of cover concrete (permeability) and cover depth are the key to determine the ease of chloride ions reaching the steel surface.

Capillary Attraction. While in dry to semi-dry concrete, ions can migrate along with water under the influence of capillary attraction. The rate of penetration of chloride ions under capillary attraction is much faster than that of ionic diffusion.

Ionic Diffusion. When concrete is in semi-wet to near-saturation, ionic migration occurs primarily through the diffusion process. The diffusion generally follows the Fick's second law. A solution to Fick's second law based on initial and boundary conditions is as following:

$$\frac{(C_s - C_x)}{(C_s - C_0)} = \text{erf}\left[\frac{X}{\sqrt{(4 D_e t)}}\right] \qquad (2.25)$$

where C_s is diffusant concentration of sample at the surface;
C_x is diffusant concentration of sample at the depth x;
C_0 is initial diffusant concentration of sample at the surface;
D_e is effective diffusivity; and
t is the time in service.

The effective diffusion coefficient, D_e in concrete is a function of porosity, inter-connectivity, tortuosity and ionic mobility. Temperature also has a strong influence on the ionic mobility.

Therefore, the time to initiate corrosion (the time required for the chloride concentration at depth of reinforcement to reach its corrosion threshold value) can be determined using equation 2.25 for uniform temperature conditions.

Temperature Factor

Temperature of concrete can vary widely, depending on the geographic latitude and climatic conditions and also on the time of year and day.

The temperature dependence of the kinetics of electrode processes and processes of diffusion that take place in the concrete can be a certain degree expressed by the Arrehenius equation [30]:

$$U = A\, e^{\frac{-Q}{RT}} \qquad (2.26)$$

where U is the speed of process (rate of corrosion); A and Q are constants; e is the base of the natural logarithm; T is the absolute temperature; and R is the gas constant.

The process of steel corrosion in concrete, the rate of which is usually determined by the kinetics of diffusion or by the kinetics of electrode process, will generally rise exponentially with a rise in temperature, in accordance with the above equation.

However, because of the complexity of the corrosion process in the concrete, there can be quite a significant deviation from this dependence [71-72]. For example, if a high temperature is associated with more rapid drying or lower oxygen solubility in the concrete moisture, the temperature dependence of corrosion in concrete will usually be quite different. Clear [73] suggested that the corrosion current density measured at given field temperature can be adjusted to another temperature using the formula:

$$i_1 = i_2\, e^{2283\left(\frac{1}{T_2}-\frac{1}{T_1}\right)} \qquad (2.27)$$

where i_1 is the corrosion current density at temperature T_1;
i_2 is the corrosion current density at temperature T_2;
T_1 is the temperature of the concrete at measurement (in degrees K);
T_2 is the temperature that one desires to know the corrosion current density (in degrees K).

The influence of temperature on corrosion in concrete has not been sufficiently investigated. As is known, the corrosion activity of different concrete structures under the conditions of constant

temperature can vary widely. It is better to investigate the influence of temperature on corrosion in concrete together with other factors such as conductivity and relative humidity.

2.3 Corrosion Monitoring Techniques

Corrosion of steel embedded in concrete is not visually evident until the damage reaches to the external signs of deterioration as rust spots, cracks or spalling. In order to predict the corrosion service life of reinforced concrete structures and to determine the need of repair or rehabilitation, it is necessary to use non-destructive techniques for assessing the corrosion activity and measuring the corrosion rate of the reinforcements.

Due to the special electrolytic characteristics of the concrete structures, it is difficult to develop accurate corrosion monitoring devices applied to the reinforced structures. However, several electrochemical techniques are successfully used for monitoring corrosion of steel in concrete such as half-cell potential, linear polarization techniques and AC impedance

2.3.1 Half-cell Potential

Corrosion is an electrochemical process as described in previous sections. The process of corrosion causes electrical potentials to be generated and the half-cell provides a method of detecting and categorizing these electrical potentials. The method and equipment are presented in ASTM C 876 [74]. The measurement of the free corrosion potential of the reinforcement consists of determination of the voltage difference between the steel and reference electrode in contact with the concrete (see Figure 2.11).

A good contact between the reference electrode and the concrete must be ensured in order to minimize the ohmic drops and avoid errors [75]. The more negative the reading, the greater the probability of corrosion. The significance of half-cell readings and their relationship to potential for corrosion is well documented [76-77]. The guidance on interpretation of results from half-cell surveys given in ASTM C 876 is summarized in Table 2.1, in this case, the reference electrode is a copper/copper sulfate half-cell.

Table 2.1. Guidance on interpretation of results from half-cell surveys (according to ASTM C 876-91) [74].

E_{corr} ($Cu/CuSO_4$)	Probability of Corrosion
> -0.20 V	greater than 90% probability of no corrosion
-0.35 to -0.20 V	corrosion activity uncertain
< -0.35 V	greater than 90% probability of active corrosion

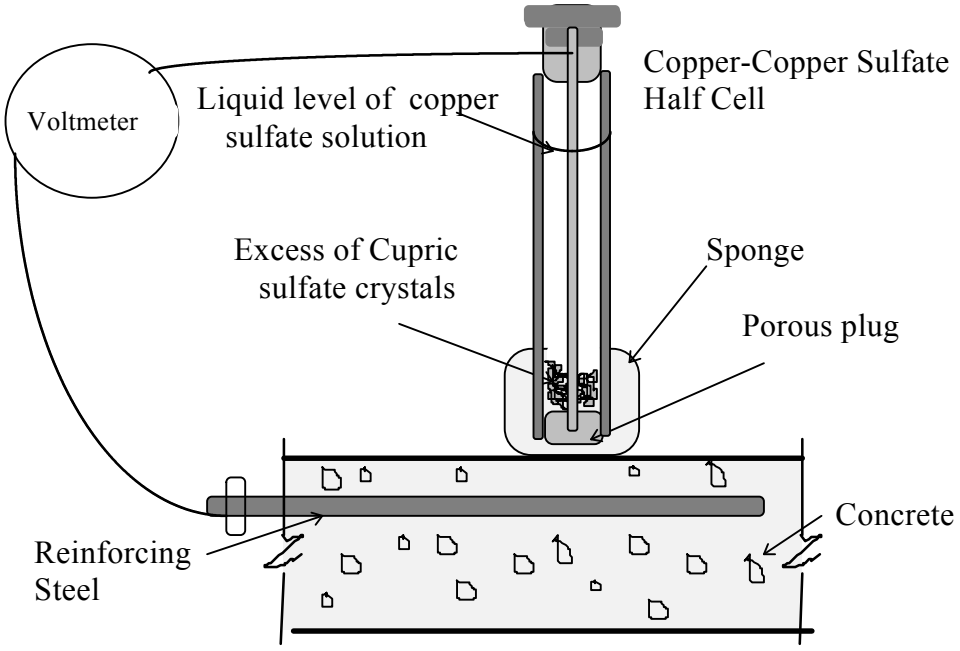

Figure 2.11. Copper-copper sulfate half cell circuitry [74].

Since the potential of any metal in contact with concrete is a function of a large number of variables related to composition of pore solution, degree of polarization, temperature, and cover depth, no quantitative (corrosion rate) conclusion can be drawn from it. Potentials do not provide information on the amount of corrosion. The validity of these interpretations has been questioned in some situations such as saturated structures, or when carbonation is the cause of the corrosion orcathodic processes are modified. However, half-cell potential technique is still a useful tool widely used for the on-site testing of the corrosion state of the reinforcement [78-80].

2.3.2 Linear Polarization Technique

The term linear polarization refers to the linear regions of the polarization curve, in which slight changes in current applied to corroding metal in an ionic solution cause corresponding changes in the potential of the metal. Stern et al. [27]showed that for a simple corroding system, the polarization curve for a fewmillivolts around the corrosion potential obeys a quasi-linear relationship. The slope of this relationship is called "Polarization Resistance" [27,81]:

$$R_p = (\Delta E/\Delta I)_{\Delta E \to 0} \qquad (2.28)$$

This slope is related to the instantaneous corrosion rate through the Stern-Geary equation:

$$I_{corr} = \frac{(\beta_a \beta_c)}{2.3\ R_p\ (\beta_a + \beta_c)} = \frac{B}{R_p} \qquad (2.29)$$

where b_a: the anodic Tafel slope ;
b_c: the cathodic Tafel slope;
R_p: the polarization resistance;
B: Stern-Geary constant.

The value of B is determined from the particular electrochemical cell and generally ranges from 13 to 52 mV depending on the system [82]. For measuring it, a potentiostat is necessary.

Based on the theories of polarization resistance to obtain evidence of corrosion activity, two devices which are currently used for measuring the corrosion rate (corrosion current density) both in laboratory and in the field are K. C. Clear's 3LP [13] and Geocisa Gecor device [15].

The term "3LP" represents the "three electrode linear polarization" technique. This technique uses a counter electrode to apply a cathodic current to the steel reinforcement, called the working electrode. A third electrode, the reference electrode, monitors the corresponding change in potential of the steel/concrete interface. By knowing the Tafel slopes and using the Stern-Geary relationship, a corrosion current can be determined. This current can then be converted to a corrosion current density by knowing the area of the steel which is polarized.

The Gecor device uses the same linear polarization technique as 3LP. A difference between the 3LP and Gecor devices is that the Gecor device has a guard ring electrode which is used to confine the influence area of the counter electrode by actively confining the polarization current during the measurement process. Another significant difference is the polarization rate. The Gecor polarization rate is device controlled based on the rate of corrosion, whereas the 3LP device is operator dependent within a set of guidelines. In addition, the devices use different Tafel slope values in calculating the corrosion current density. The result of these differences is approximately an order of magnitude difference in the measured corrosion current density between the instruments. The general guidelines for interpreting the results of the 3LP [14] and Gecor [16] as supplied by the instrument manufacturers are summarized in Table 2.2.

The linear polarization techniques have been widely used to measure the corrosion current density both in laboratory and in the field [14,83-86]. The main difficulty involved in applying polarization resistance on-site is the definition of area over which the applied potential (or current) is going to act.

Table 2.2. Guidance on interpretation of results of 3LP and Gecor.

i_{corr} (mA/ft^2)	Gecor Device Corrosion State	i_{corr} (mA/ft^2)	3LP Device Expectation
<0.1	Passive	< 0.2	No damage expected
0.1-0.5	Low corrosion	0.2-1.0	Damage possible 10-15 years
0.5-1.0	Moderate	1.0-10.0	Damage possible 2-10 years
> 1.0	High corrosion	> 10.0	Damage possible < 2 years

2.3.3 AC Impedance

AC impedance technique is the application to the working electrode maintained at its corrosion potential by potentiostat of a small amplitude (a few millivolts, ΔE peak to peak) sinusoidal voltage in an extensive frequency range [83,87-88]. The response at every frequency is sinusoidal signal with a different amplitude (measured as ΔI in response to the sinusoidal voltage) and a phase shift relative to the input signal.

The ratio of $\Delta E/\Delta I = Z$ (impedance) is a sinusoidal function that can be decomposed in resistive term in phase with the input signal and in a capacitive term with a phase shift of 90°,

$$Z = R_e + [\, R_T / (\, 1 + j\omega C R_T \,) \,] \qquad (2.30)$$

where R_e is the electrolyte ohmic resistance, C is the capacitance of the electrode, ω is the angular frequency ($\omega = 2\pi f$), j is the imaginary unit of $\sqrt{-1}$, and R_T is the transfer resistance assumed to be equivalent to the polarization resistance R_p obtained through the linear polarization method. Electrolyte ohmic resistance R_e value is attained at high frequency range while at low frequency limit the $R_e + R_T$ is obtained. Through Stern-Geary formula, the corrosion intensity may be calculated from R_T value.

Impedance data are obtained in concrete over a range of frequencies which depend on the size of the specimen and the actual corrosion rate.

2.3.4 Gravimetric Technique (Weight Loss Method)

This technique is a destructive method, which consists in weighing the specimens' bars before and after being introduced in the concrete to be tested. The detail test procedures for preparing, cleaning, and evaluating corrosion test specimens are described in ASTM G1 [89]. The

difference in weight (gravimetric loss) is a quantitative average of the attack. he average corrosion rate may be obtained as follows:

$$\text{corrosion rate} = (K \times W) / (A \times T \times D) \qquad (2.31)$$

where K is a constant, T is the exposure time, A is the surface area, W is the mass loss, and D is the density of the corroding metal. No instantaneous corrosion rates can be measured in this technique, but only a mean during the period of test. Obviously, the gravimetric method is the most accurate method to quantify corrosion attack in laboratory experiments.

Although this method is very time-consuming and only applicable to the laboratory studies, it is a useful tool to check the accuracy of the electrochemical techniques that are able to measure the corrosion rate quantitatively, such as the Linear Polarization and AC Impedance techniques.

2.3.5 Techniques for Determining the Chloride Content

One method to estimate the potential for chloride induced corrosion damage is to measure the chloride content of the concrete at depth of reinforcement. There are several analytical values considered to designate the chloride content such as acid-soluble content and water soluble content. Acid soluble is the most widely used measurement and indicates the proportion of chloride which is soluble in nitric acid. The water soluble chloride is that extractable in water in defined conditions.

Many test procedures have been published [90-94] to measure these different values of chloride content. The ASTM C 1218 [92] describes a standard test method for water-soluble chloride in mortar and concrete. The ASTM C 1152 [93] presents a standard test method for acid-soluble chloride in mortar and concrete. A rapid analysis proposed by Henry [94] can also be used to test the acid-soluble chloride content.

The chloride content can be expressed in terms of percent chloride by the mass of cement (% in weight of cement) or in terms of pounds of chloride per cubic yard of concrete (kilogram of chloride per cubic meter of concrete). The results of chloride content may be used to determine if a site has a high enough level of chloride ions to initiate corrosion. Note that the threshold level of chloride concentration to initiate corrosion differs for the different conditions pre0 sented in section 2.2.3.

2.4 Summary

1. Concrete is a heterogeneous, capillary-porous dynamic system possessing ionic conductivity. The corrosion processes of steel in concrete can be considered primarily electrochemical.

However, electrochemical corrosion of steel in concrete has its own peculiarities, determined largely by the characteristic properties of the concrete as a corrosion electrolyte.

2. Due to the presence of sodium and potassium oxides in the cement, as well as calcium hydroxide produced in the hydration reactions of cement components, concrete's high alkalinity solution within the pore structure of cement paste matrix provides a good environment to form a passive film on the steel surface to protect it from further corroding. This passive film will be destroyed or dissolved either by chloride ions attack or by decrease in pH value due to carbonation.

3. The chloride-induced corrosion is the most prevalent and damaging cause of corrosion of steel in concrete. However, the mechanism of chloride-induced corrosion of steel is not yet fully understood. It is generally believed that the chloride ions become incorporated in the passive film, replacing some of the oxygen and increasing both its conductivity and its solubility.
4. To initiate corrosion, a threshold concentration of chloride is required in excess of the amount of immobilized chloride by reaction with tricalcium aluminate in cement. The threshold concentration of chloride ions to initiate corrosion is dependent on many factors including quality of concrete (W/C ratio, mixture proportions and type of cement), relative humidity and temperature of the concrete, and pH value of pore solution.

5. The penetration of chloride ions into concrete takes place in two forms, capillary attraction and ionic diffusion, depending on the degree of saturation in the concrete. The time to initiation of corrosion of steel in concrete is dependent on quality of cover concrete, cover depth and exposure conditions.

6. The transport of oxygen in concrete to the steel surface is mainly by diffusion process. The rate of diffusion of oxygen is determined by the pore structure, pore size distribution of concrete and its moisture content. It decreases sharply with the increase in moisture content because the diffusivity of oxygen in water is about four powers lower than that in air.

7. Ohmic resistivity of the concrete can fluctuate within wide limits, determined by the salt content in the pore water, degree of saturation and concrete temperature.

8. Temperature at depth of concrete/steel interface can also fluctuate within wide limits depending on the geographic latitude and climatic conditions and also on the time of year and day. Temperature has a significant effect on the corrosion rate, because temperature changes can influence the diffusion of reactants, electrochemical and chemical reactions, conductivity of the concrete and solubility of oxygen.

9. The corrosivity of steel in concrete depends on many factors: ohmic resistivity, moisture content, salts content, air penetration and temperature. However, until recently, the relationship between the corrosivity of steel in concrete and its physicochemical properties

has not been fully established. The basic reason for this is that the corrosion process of steel in concrete is a dynamic process due to the dynamic nature of concrete structure and seasonal or daily changes of exposure conditions such as temperature and relative humidity.

10. Electrochemical techniques have been successfully used for monitoring the corrosion state of reinforced concrete structures. Because of the special electrolytic characteristic of the concrete structure and complexities of the corrosion process in concrete, much research work is still needed on direct corrosion test for the different concretes and different exposure conditions.

3.0 Review of Time to Cracking Models

There are several ways of predicting service life due to the corrosion damage of reinforcement in concrete using different deterioration models [7,8,12,95-98]. A deterioration model developed by Cady and Weyers [8] based on field and laboratory data has been used to estimate the time to rehabilitate concrete bridge decks. The quantitative prediction of the time to cracking is useful for establishing the overall deterioration model to predict the service life. Mathematics models [12] or empirical equations [95] for predicting the time to cracking have been suggested. Due to the complexity of the corrosion process in concrete, the observed data from the field and laboratory deviate significantly from existing models. It is necessary to establish the quantitative relationships among those factors that control the time to cracking, and thus the time to corrosion cracking of the cover concrete in reinforced concrete can be better predicted.

3.1 Cady-Weyers' Deterioration Model

Based on the premise that salt-induced corrosion of the steel is the main cause of deck deterioration, a deterioration model developed by Cady and Weyers has been used to estimate the remaining life of concrete bridge components in corrosive environments [8]. The model predicts deck deterioration as measured in an area percentage of the entire deck. The total area of spalls, delaminations, asphalt patches, and crack lengths multiplied by a tributary width combine to produce the total damage.

There are three distinct phases in the model: diffusion, corrosion and deterioration (see Figure 1.2). The first phase, diffusion, is defined as the time for chloride ions to penetrate the concrete cover and to initiate corrosion. The diffusion time usually can be determined empirically using Fick's Second Law [9,99-101]. The second phase, corrosion, is defined as a period of time from initiation of corrosion to first cracking of concrete cover, the time to cracking ranges between 2 to 5 years [10]. The third phase, deterioration, describes the time for damage to reach a level of percent damage which is deemed as the right time for repair or rehabilitation.

According to Cady-Weyers' model, the corrosion rate is the key to predicting the time to cracking. The corrosion rate is largely controlled by the rate of oxygen diffusion to the cathode, resistivity of the pore solution, and temperature. The quantitative prediction of the time to cracking using corrosion rate from the currently corrosion rate devices (3LP and Gecor) is the task of this study.

3.2 Bazant's Mathematical Models for Time to Cracking

Based on theoretical physical models [11] for corrosion of steel in concrete exposed to seawater, Bazant suggested a simplified mathematical model to calculate the time to corrosion cracking of concrete cover. The basic assumptions of Bazant's models are as following:

a. Oxygen and chloride ion transport through concrete cover are quasi-stationary and one dimensional.

b. A steady-state of corrosion producing expansive rust layer begins at depassivation time.

c. The model is based on red rust which is more dangerous for cracking concrete and assumes $r_r = r_{rt}/4$, where r_r and r_{rt} are the density of rust products and steel, respectively.

The time of corrosion to cracking, t_{cr}, follows [12]:

$$t_{cr} = \rho_{cor} \frac{D \Delta D}{S j_r} \qquad (3.1)$$

where S is the bar spacing, D is the diameter of the bar, ΔD is the change in diameter of the bar, j_r is the rate of rust production, and r_{cor} is a function of the mass densities of steel and rust, $r_{cor} = [(1/r_r) - (0.523/r_{st})]^{-1} p/2$.

Stress and cracking caused in concrete cover by this increase in diameter can be routinely solved by a finite element method. Considering concrete to be a homogenous elastic material, ΔD is calculated according to the different failure mode depending on the cover depth and spacing of the reinforcement. If the spacing, S, is less than 6D, then the following formula governs ΔD [12]:

$$\Delta D = 2 f_t \frac{L}{D} \delta_{pp} \qquad (3.2)$$

where f_t is the tensile strength of the concrete and δ_{pp} is the bar hole flexibility. For this condition, the expected mode of failure is inclined cracking. The bar hole flexibility is taken as the average of the following bar hole flexibilities, the first being for the case of concrete acting as a thick-walled cylinder and the second being for the case of the concrete acting as an infinite medium:

$$\delta^{o}_{pp} = \frac{D}{E_{ef}} (1 + \nu) + \frac{2 D^3}{S^2 E_{ef}} \qquad (3.3)$$

$$\delta'_{pp} = \frac{D}{E_{ef}} \left[1 + \nu + \frac{D^2}{2L(L+D)}\right] + \frac{2D^3}{S^2 E_{ef}} \qquad (3.4)$$

The average of the above two equations, the bar hole flexibility, δ_{pp}, becomes:

$$\delta_{pp} = \left(\frac{D(1+\varphi_{cr})}{E}\right)\left\{(1+\nu)+D^2\left[\frac{2}{S^2}+\frac{1}{4L(L+D)}\right]\right\} \qquad (3.5)$$

where φ_{cr} is the creep coefficient of the concrete, ν is the Poisson's ratio of the concrete, and E is the elastic modulus of the concrete.

If $L > (S - D)/2$, then another failure mode (cover peeling) governs ΔD [12]:

$$\Delta D = f_t\left(\frac{S}{D} - 1\right)\delta_{pp} \qquad (3.6)$$

The time to cracking t_{cr} may be solved from equation 3.1 if ΔD is estimated from equation 3.2 or 3.6.

According to Bazant's models, the time to cracking is a function of corrosion rate, cover depth, spacing, and certain mechanical properties of concrete such as tensile strength, modulus of elasticity, Poisson's ratio and creep coefficient. A sensitivity analysis of Bazant's theoretical equations demonstrates that for these parameters, corrosion rate is the most significant parameter in determining the time to cracking of the cover concrete. Unfortunately, Bazant's model has never been validated experimentally.

To predict the time to cracking of chloride contaminated concrete, using corrosion rate data measured from currently corrosion rate devices (3LP and Gecor), Peterson [17] and Newhouse [18] have reported that the predicted time to cracking calculated from Bazant's model is much shorter than the observed one.

3.3 Morinaga's Empirical Equations

Based on field and laboratory data, the empirical equations suggested by Morinaga [95] can be used for predicting the time to cracking. It is assumed that cracking of concrete will first occur when there is a certain quantity of corrosion products forming on the reinforcement. The amount is given by:

$$Q_{cr} = 0.602d\left(1 + \frac{2c}{d}\right)^{0.85} \qquad (3.7)$$

where Q_{cr} is the critical mass of corrosion products (10^{-4} g/cm^2);
c is the cover to the reinforcement (mm);

d is the diameter of reinforcing bars (mm).

The time for cracking to take place is given by:

$$t_{cr} = \frac{Q_{cr}}{i_{cor}} \qquad (3.8)$$

where i_{cor} is the corrosion rate in gram per day, t_{cr} is the time to cracking in days. The corrosion rate i_{cor} can be either measured or estimated statistically from the existing data. According to Morinaga's equations, the time to cracking is a function of the corrosion rate, concrete cover depth and reinforcing size. Therefore, the time to cracking can be easily predicted.

In a previous study [17], the observed time to cracking was 671 days for outdoor exposure, 2 in (50 mm) of cover depth, 8 in (203 mm) of spacing, # 5 reinforcing steel bar (16 mm in diameter), measured corrosion rate of 2.185 mA/ft^2 per year (5.88×10^{-5} g/cm^2 days) from weight loss method (ASTM G1-90, method C3.5). Based on equations 3.7 and 3.8, the predicted time to cracking is about 88 days, which is also much shorter than the observed one.

3.4 Other Criteria on Time to Cracking

The actual metal loss required to cause cracking of concrete has been a subject of disagreement among the researchers for years. A wide range of cracking criteria has been presented for different situations and conditions. The metal loss required for cracking from different researchers has been summarized and is presented as Table 3.1 [17].

Table 3.1. Existing criteria for metal loss.

Existing Information of Metal Loss Required for Cracking	
Spellman and Stratfull (1968) [102], Laboratory experiment	0.1 mils (2.54 μm)
Spellman and Stratfull (1968) [102], Field Experiment	up to 29 mils (734 μm)
Kenneth Clear (1989) [14], Interpretation of Results	3.7 mils (94 μm)
Zdenek Bazant (1979) [12], Interpretation of Equations	0.3 mils (7.87 μm)
Clementa et al. [103], interpretation of Results	600 to 1200 mils (15240 to 30480 μm)
Hladky et al. [105], Interpretation of Results	0.63 to 1.26 mils (16 to 32 μm)

However, the amount of metal loss or in terms of weight of rust products to induce concrete cracking may have a wide range, because concrete itself is a highly heterogeneous structure both in macro-structure and micro-structure, and corrosion of steel in concrete is also not uniform; some of the corrosion products may fill the voids or some of them may migrate away from the steel/concrete interface. The amount of metal loss or rust product is largely dependent on parameters such as concrete cover depth, properties of rust products and concrete properties.

3.5 Some Comments on Existing Models

It is well recognized that both the corrosion rate and cover depth have a large effect on the time to cracking as shown in Bazant's and Morinaga's equations. As described above, the estimated times to cracking from the existing models are significantly shorter than the observed data from field and laboratory. This may be related to the complexity of compositions and properties of corrosion products and corrosion processes.

Compositions and Properties of Corrosion Products

As mentioned in section 2.2.2, the final corrosion products may be expressed as follows,

$$m \cdot Fe(OH)_2 + n \cdot Fe(OH)_3 + p \cdot H_2O \qquad (3.9)$$

where the values of m, n and p vary considerably, depending on conditions such as pH of the solution, the oxygen supply, and moisture content. The volumes of different iron oxidations are shown in Figure 2.8. It is obvious that different kinds of rust products have different density and volume expansion, which may have a large influence on the time to cracking.

It has been reported [57] that the density of rust products ranges from 150-221 lb/ft^3 (2440-3600 kg/m^3). According to a recent study [105], the corrosion products are assumed to be made of crystalline components (magnetite, goethite and lepidocrocite), amorphous components ($Fe(OH)_3$ and FeOOH) and others (e.g., water etc.). The corrosion products of steel in concrete are made up to 30 % of crystalline components, 55-65 % of amorphous components. The densities of magnetite, goethite and lepidocrocite are about 325, 206-269, and 256 lb/ft^3 (5200, 3300-4300 and 4100 kg/m^3), respectively; density of amorphous component ($Fe(OH)_3$ and FeOOH) is about 187-250 lb/ft^3 (3000-4000 kg/m^3).

According to Bazant's model, the density of red rust is one-fourth that of steel, 122 lb/ft^3 (1960 kg/m^3). This value is relatively low compared to other researchers. This is one of the possible reasons that the existing models underestimate the time to cracking of corrosion of steel in concrete.

Growth of Rust Products

Both of Bazant's mathematical models [12] and Morinaga's empirical equations [95] are based on the steady state corrosion process to calculate the time to cracking. It is noted that the corrosion process is a dynamic process. The growth of rust products may not be taken as a simple linear function as in equation 3.2 and equation 3.8. The growth of rust products may follow equation 2.15,

$$y^n = kt \qquad (2.15)$$

where the value of n is usually larger than one. In case of atmospheric corrosion or soil corrosion, n has values between 1 to 3 depending on the suppression of diffusion [30]. In case of corrosion of steel in concrete, n value may reach a value of about 2 [106]. This indicates that the rate of diffusion process decreases in proportion to the amount (thickness) of rust products.

Therefore, use of a simple linear function to describe the relationship between growth of rust products and time may underestimate the time to cracking of corrosion of steel in the concrete.

Complexity of Corrosion Process

Corrosion is an electrochemical process, and strongly dependent on environmental factors (temperature, relative humidity, rainfall) and properties of concrete structure. These factors act simultaneously on the corrosion process in the service conditions. The influences of these factors on the corrosion process should be considered as an interaction among them. The interaction model for corrosion has not been sufficiently studied due to the lack of the long term corrosion data in the field. Most of the research work in accelerated corrosion tests is limited to the effects of the individual variable. In fact, these factors can not be separated or isolated from each other in the service conditions.

It is necessary to develop an interaction model to characterize the corrosion process based on long term corrosion tests. Therefore, the service life of a reinforced concrete structure in different environmental conditions can be better predicted.

These three limitations may be the reasons that there is a large deviation between the predicted time to cracking using existing models and the observed data from the field and laboratory. The existing models for predicting time to cracking need to be modified.

4.0 Experimental Design

In order to investigate the effects of significant variables on the corrosion phase, one of three phases in the deterioration model for predicting the remaining life of a typical bridge deck developed by Cady and Weyers, and to modify the existing models for predicting the time to cracking of the cover concrete in chloride-induced corrosion of reinforcement, an experimental test was designed to simulate a typical bridge deck, based on sensitivity analysis of Bazant's theoretical equations.

This experiment included test variables of different admixed chloride contents (corrosion rates), concrete cover depths, reinforcing sizes and spacings, and exposure conditions. The different admixed chloride contents were designed to simulate the different corrosion rates which affect on the time to cracking of the concrete cover.

Both 3LP and Gecor devices were used to measure the corrosion current density. The corrosion measurements were performed once a month, and concrete temperatures at the bar depth and resistances of concrete were also taken at each measurement. Metal loss measurements were performed accordance with ASTM G1-90, Method C.3.5 when specimens cracked; the results were compared with the measured corrosion rates by 3LP and Gecor devices. Both water soluble (ASTM C-1218) and acid soluble (ASTM C-1152) chloride content analysis for the different series of specimens were also performed.

4.1 Materials

Cement

Type I Portland cement from Tarmac Cement Co. in Roanoke, Virginia, was used. The tri-calcium aluminate content obtained from the manufacturer was in the range of 9.5% to 11.0 %.

Aggregate

The coarse aggregate used in this study was a #57 crushed limestone quarried by Acco Stone Co. in Blacksburg, Virginia. The fine aggregate used was a siliceous natural sand processed at Acco Stone Co. as well. The physical characteristics of both aggregates are outlined in Table 4.1.

Steel

The steel reinforcing bars used for this study were Grade 60, #4, #5, and #6 bars manufactured at Roanoke Electric Steel Co. in Roanoke, Virginia. Batch testing results of mechanical and chemical properties are presented in Table 4.2.

Table 4.1. Aggregate properties.

Course Aggregate: #57 Crushed Limestone		Fine Aggregate: Siliceous Natural Sand	
Dry Unit Weight	96.4 lb/ft^3 (1544 kg/m^3)	Bulk Specific Gravity (Dry)	2.60
Voids in Dry Agg.	44.2%	Bulk Specific Gravity (SSD)	2.66
Bulk Specific Gravity (Dry)	2.77	Apparent Specific Gravity	2.66
Bulk Specific Gravity (SSD)	2.78	Absorption	0.35%
Apparent Specific Gravity	2.81	Fineness Modulus	2.8
Absorption	0.62%		

Table 4.2. Mechanical and chemical tests of steel.

Yield and Tensile Strength of Steel					Chemical Properties	
Size	Grade	Batch	Yield psi (MPa)	Tensile psi (MPa)	Chemical Component	%
#6	60	1	75285 (527)	119035 (837)	C	0.41 - 0.42
	60	2	63070 (441)	98010 (686)	Mn	0.90 - 0.96
	60	3	73295 (513)	110795 (775)	P	0.012 - 0.032
#5	60	1	60160 (421)	92100 (645)		
	60	2	65000 (455)	99920 (699)	S	0.030 - 0.043
#4	60	1	65000 (455)	104000 (725)		

Composite Reinforcing Bar

The composite reinforcing bars were used as temperature bars, which were purchased from International Grating in Houston, Texas.

Sodium Chloride

Granular sodium chloride, from Fisher Scientific Co., was used to incorporate the chloride ions for the initiation of the corrosion process.

Air Entrainment

A commercial air entraining admixture, Daravair from W. R. Grace & Co., was used to improve the frost resistance of the concrete.

4.2 Design Variables

An experimental test was designed and constructed in Summer, 1991, to achieve six different corrosion rates, two concrete cover depths, reinforcing sizes and spacings, and exposure conditions. A total of 56 specimens were constructed with six admixed chloride contents, 0.0, 0.6, 1.2, 2.4, 4.8, and 9.6 lb/yd^3 (0.0, 0.36, 0.71, 1.42, 2.85, and 5.69 kg/m^3); concrete cover depths of 2 and 3 inches (51 and 76 mm); reinforcing diameters of 5/8 and 3/4 inch (16 and 19 mm); spacings of 6 and 8 inches (152 and 203 mm); and exposure conditions of indoor and outdoor sites. Four additional specimens with 12.0 lb/yd^3 (7.20 kg/m^3) and 1 inch (25 mm) cover depth were constructed in June, 1995. Table 4.3 illustrates the experimental design.

Table 4.3. Test variables.

Factors	Series
Admixed Chloride	0.0, 0.6, 1.2, 2.4, 4.8, 9.6 and 12.0 lb/yd^3 (0.0, 0.36, 0.71, 1.42, 2.85, 5.69 and 7.20 kg/m^3)
Cover Depth	1, 2 and 3 inch (25, 51 and 76 mm)
Exposure Condition	indoor and outdoor
Reinforcing bar Spacing	6 and 8 inch (152 and 203 mm)
Steel Size	diameters of 5/8 and 6/8 inch (16 and 19 mm)

The concrete batches were proportioned to meet specifications for a typical bridge deck concrete. The concrete mixture proportions are shown in Table 4.4. Compressive strength tests were conducted on each batch at 3, 7 and 28 days. The results are summarized in Table 4.5.

Forty of the original 56 specimens and the four additional specimens were placed outdoors and the others indoors in order to maintain a near constant concrete moisture content and temperature. Indoor specimen surfaces were wetted with water once a week and covered with a loose fitting sheet of clear plastic. The measured temperature of indoor specimens varied from a low of 50 °F (10 °C) in the winter to a high of 80 °F (5 °C) in the summer. The measured temperature of outdoor specimens varied from a low of -4 °F (-20 °C) in the cold winter to a high of 116 °F (45 °C) in the hot summer.

Table 4.4. Mixture proportions.

Chloride Series lb/yd^3 (kg/m^3)	0.0 (0.0)	0.6 (0.36)	1.2 (0.71)	2.4 (1.42)	4.8 (2.85)	9.6 (5.69)	12.0 (7.2)
Cement, lb/yd^3 (kg/m^3)	635 (381)	635 (381)	632 (379)	632 (379)	632 (379)	628 (337)	635 (382)
Water, gal/yd^3 (kg/m^3)	34.3 (173)	32.3 (160)	32.2 (159)	31.2 (155)	33.2 (167)	32.7 (162)	34.2 (172)
W/C Ratio	0.45	0.42	0.42	0.41	0.44	0.43	0.45
Coarse Agg., lb/yd^3 (kg/m^3)	1780 (1068)	1780 (1068)	1728 (1037)	1798 (1079)	1779 (1067)	1797 (1078)	1780 (1068)
Fine Agg., lb/yd^3 (kg/m^3)	1197 (718)	1197 (718)	1197 (718)	1177 (706)	1187 (712)	1189 (713)	1197 (718)
Daravair oz/yd^3 (g/m^3)	9.8 (367)	8.5 (319)	8.5 (319)	9.8 (367)	9.7 (363)	11.1 (416)	9.75 (367)
Salt, NaCl, lb/yd^3 (kg/m^3)	0.0 0.0	1.2 (0.6)	2.0 (1.2)	4.0 (2.4)	8.0 (4.8)	16.0 (9.6)	20.0 (12.0)
Chloride, lb/yd^3(kg/m^3)	0.0 (0.0)	0.6 (0.36)	1.2 (0.71)	2.4 (1.42)	4.8 (2.85)	9.6 (5.69)	12.0 (7.2)
Slump, in (mm)	6 (150)	4 (100)	6.75 (170)	3.25 (80)	4 (100)	4 (100)	5 (125)
Unit Wt. lb/yd^3 (kg/m^3)	148.8 (2232)	146.4 (2196)	143.2 (2148)	149.1 (2232)	149.1 (2232)	142.6 (2139)	145.0 (2197)
Air Content, %	3.2	5	5.4	4.2	4.7	6.7	5.9

Table 4.5. Compressive strength of concrete.

Admixed Chloride Series (lb/yd^3)	0.0	0.6	1.2	2.4	4.8	9.6	12.0
3 Day, psi (MPa)	3040 (21.3)	3740 (26.2)	3380 (23.6)	3820 (26.7)	3820 (26.7)	3660 (25.6)	3283 (23.0)
7 Day, psi (MPa)	3680 (25.8)	4400 (30.8)	4120 (28.8)	4580 (32.0)	4400 (30.8)	4100 (28.7)	3899 (27.4)
28 Day, psi (MPa)	4420 (30.9)	5590 (39.1)	4990 (34.9)	5660 (39.6)	5130 (35.9)	4560 (31.9)	5053 (35.6)

4.3 Corrosion Cell Design

4.3.1 Slab Series Design

The 60 slabs were designed to simulate a section of a bridge deck structure (see Table 4.6). Figure 4.1 illustrates a schematic diagram of the slab design. Each specimen was a 46.5 × 46.5 in (1180 ×1180 mm) square slab, 8.5 in (216 mm) thick. The top mat of the slab contained five electrically isolated steel reinforcing bars in the longitudinal direction and three #4 fiberglass bars in the transverse, while the bottom mat had three #4 fiberglass bars in both directions. The bars were tied to each other by means of plastic ties instead of wire ties to insure that the steel bars would be electrically isolated from each other and no other metal was corroding besides the bars. The steel bars were cleaned with hexane and covered with electroplating tape to a known length of 42 in (1070 mm). This configuration of reinforcement was selected because 90 percent of all corrosion occurs as microcell corrosion in the top layer of steel bars, and since the fiberglass reinforcement is impervious to corrosion, the corrosion would be isolated in the steel bars of the top mat. Type T thermocouples were placed at the bar level to determine the temperature at depth of the reinforcement. A low modulus epoxy, Epon 828 produced by Shell, was used to coat the sides of the slabs in order to simulate a continuous structure. Two of the four additional slabs (OF series, with admixed chlorides of 12.0 lb/yd^3 (7.2 kg/m^3)) were designed with two different concrete layers, and the steel bars in two layers were connected with a resistor of 100 ohms. The bottom layer was 6 in. thick concrete without admixed chloride and the top layer was 3 in. concrete with admixed chlorides of 12.0 lb/yd^3 as shown in Figure 4.2.

Table 4.6. Slab matrix.

Admixed Chloride Series (lb/yd^3)	Outdoor Slabs			Indoor Slabs
	1 in Cover	2 in Cover	3 in Cover	2 in Cover
0.0		2	2	2
0.6		3	3	3
1.2		9	3	3
2.4		3	3	3
4.8		3	3	3
9.6		3	3	2
12.0	4			

All the slabs were coded to allow easy identification of the design and chloride concentration. The code consists of two capitalized letters which indicate the exposure condition and series, respectively, followed with values of cover depth (in inch), reinforcing spacing (in inch),

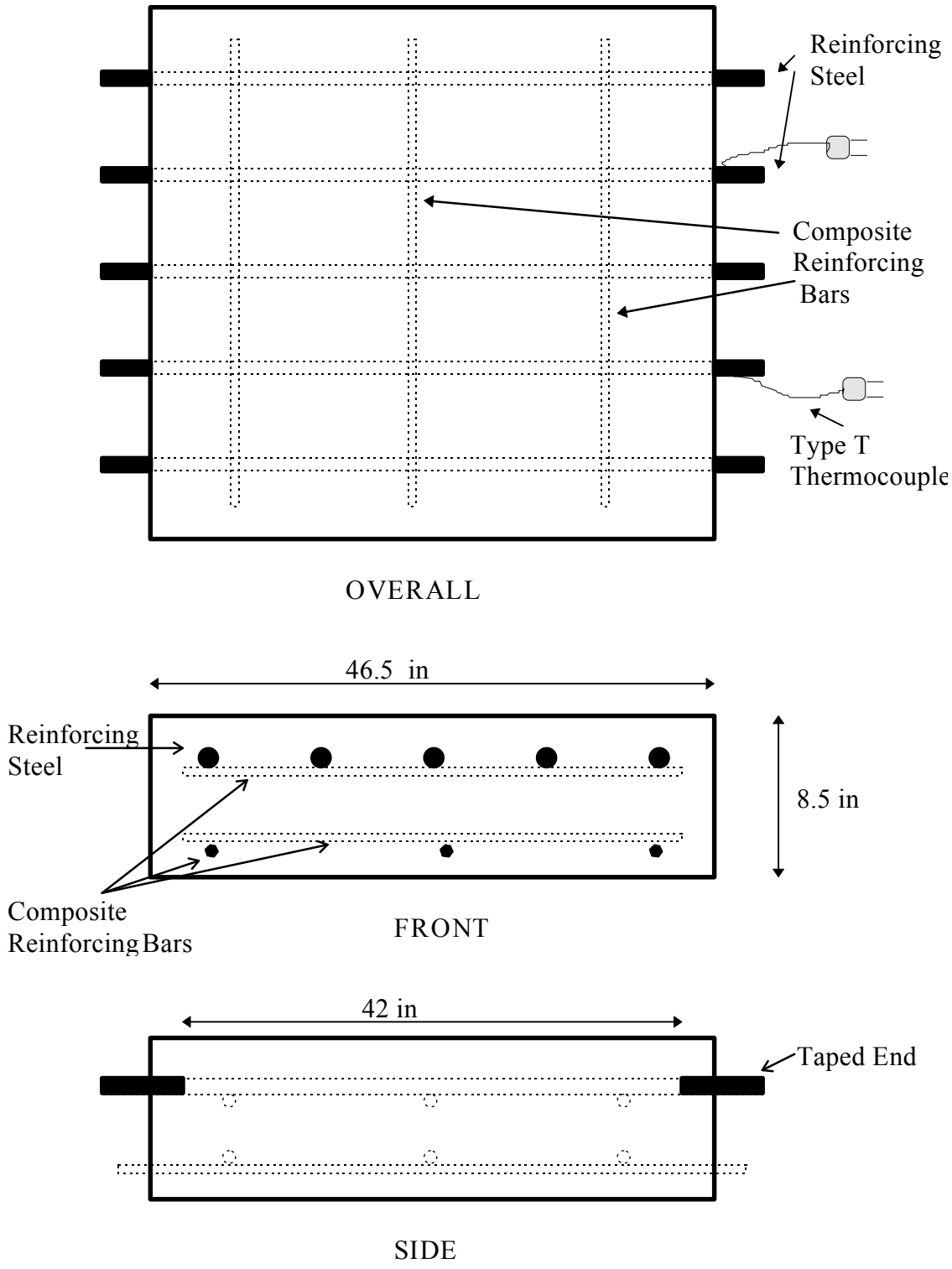

Figure 4.1. A schematic diagram of the slab design.

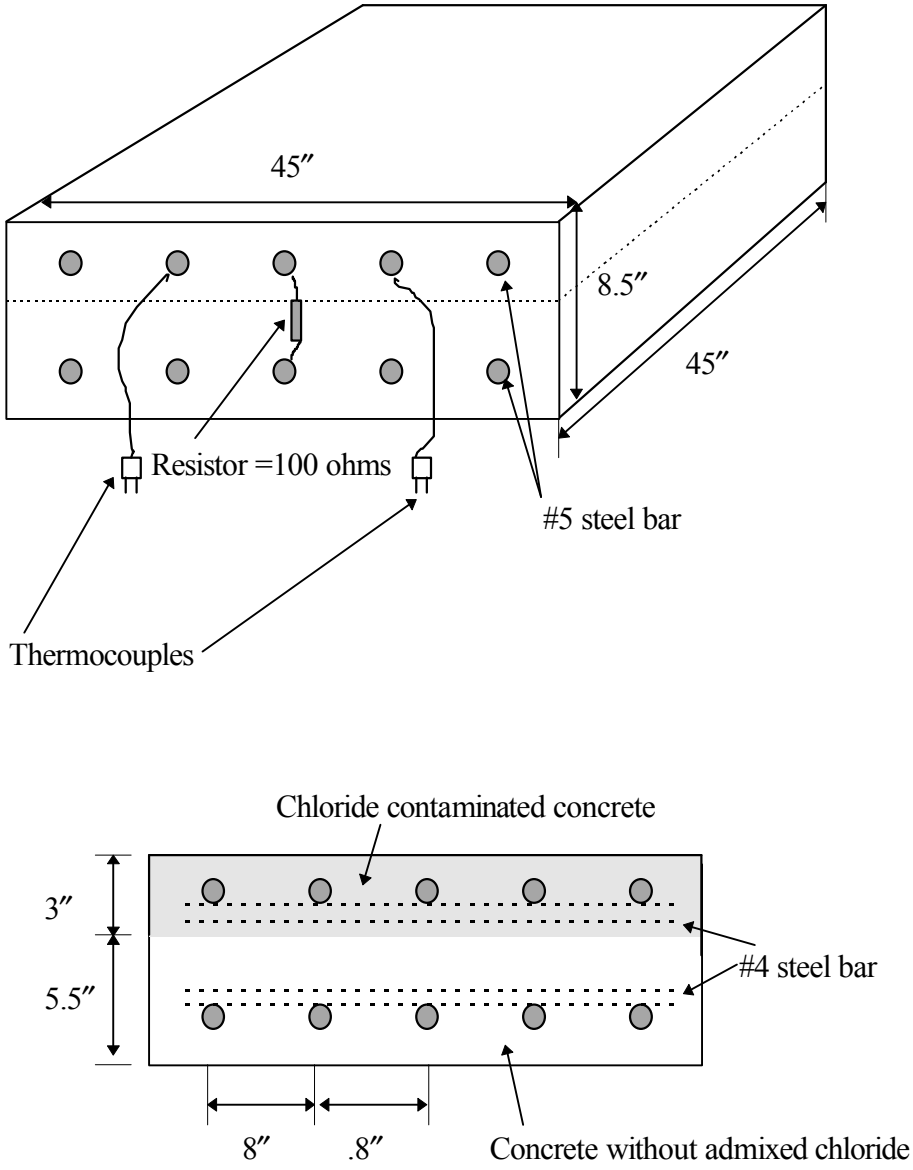

Figure 4.2. A schematic diagram of the two additional slabs design with two different concrete layers.

reinforcing size (number of bar size), admixed chloride content (in lb/yd^3) and specimen number. For example, OB3859.6-1 means outdoor specimens, B series with 3 inch cover depth, 8 inch reinforcing spacing, #5 reinforcing steel, 9.6 lb/yd^3 admixed chloride, No. 1 specimen; IA2854.8-2 means indoor specimen, A series with 2 inch cover depth, 8 inch reinforcing spacing, #5 reinforcing steel, 4.8 lb/yd^3 admixed chloride, No. 2 specimen.

4.3.2 Block Series Design

In addition to the large scale slab specimens, smaller test blocks were cast along with the slabs. Three test blocks were cast at each of the six different chloride contents, making a total of 18 blocks (see table 4.7).

Table 4.7. Block matrix.

Admixed Chloride Series (lb/yd^3)	0	0.6	1.2	2.4	4.8	9.6
Outdoor Blocks	2	2	2	2	2	2
Indoor Blocks	1	1	1	1	1	1

All of the blocks were cast with a single #4 bar with a 2 in. (50 mm) cover depth. The blocks were 11.5 $\times$ 13 in. (288$\times$375 mm) and 7 in. (175 mm) thick. The specimens also contained a type T thermocouple located at the bar level. The sides of the blocks were coated with the same low modulus epoxy used in the large slab specimens in order to simulate a continuous structure. Figure 4.3 shows the diagram of the blocks.

4.1 Test Methods

4.4.1 Corrosion Rate Measurement

Two devices 3LP (K.C. Clear, Inc., Sterling, Virginia) and Gecor (GEOCISA, Madrid, Spain) devices were used to measure the corrosion rate in this study.

The four-point polarization sequence (0, 4, 8 and 12 mV) was used in 3LP method. Because in 3LP the polarization rate is controlled by operator, the following procedures were followed:

a) Set up equipment by wetting sponge, positioning the counter electrode over the rebar to be tested, connecting the rebar ground lead, and confirming that the half-cell potential is stable and nulling to zero.

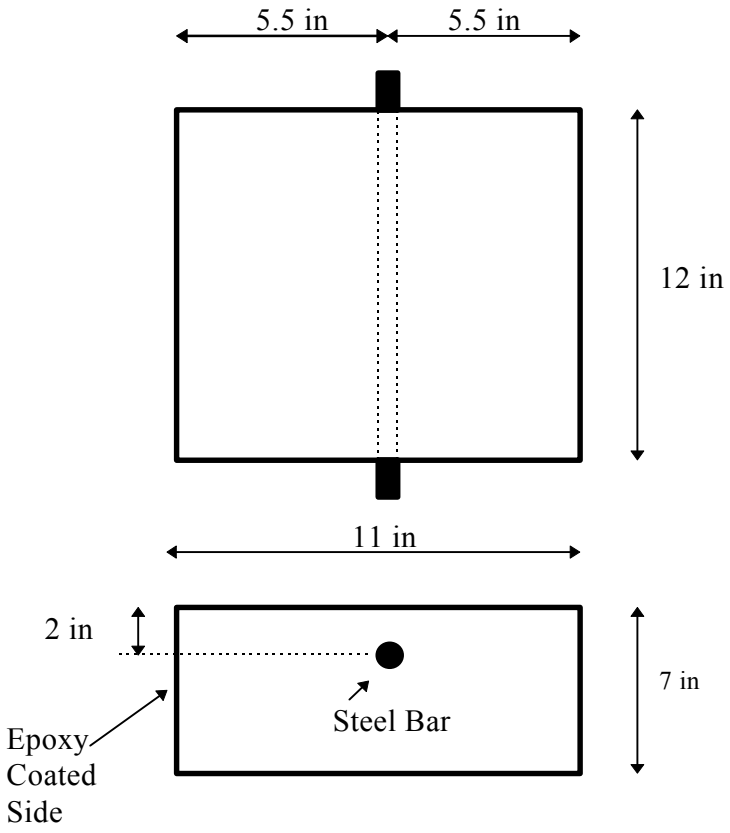

Figure 4.3. A schematic diagram of the block design.

b) Slowly increase the current to the counter electrode until the half-cell potential meter reads 4.0 mV, read and record the current on the digital meter to the nearest 0.0001 mA.
c) Continue to increase the current, read and record the corresponding current reading at the half-cell shift of 8, and 12 mV.
d) Reduce the current to zero, confirm that the potential returns to between -2 and 2 mV within two minutes.
e) Input the data into 3LP program and calculate the corrosion current density.

The Gecor corrosion-rate-meter (LG-ECM-03) is a fully automatic device. The parameters which need to be introduced are: the reference (location), the calculated rebar area under the sensor (LG -ECS-04), which should be keyed in square centimeters (cm^2), and the test date. The polarization rate is device controlled based on the rate of corrosion. The duration of a single measurement lasts about 2 to 5 minutes depending on the state of the reinforcement. The results obtained from the Gecor device are:

a) Corrosion potential, E_{corr}, related to Ag/AgCl electrode, measured in mV.
b) Corrosion intensity, I_{corr}, measured in $\mu A/cm^2$.
c) Concrete ohmic resistance, R_{ohm}, measured in Kohm.

The results can be stored in the device and transferred to the computer by designed software for further corrosion data analysis.

Gravimetric technique (weight loss method) was used measure the mean corrosion rate at the time of specimen cracking to assess the results of 3LP and Gecor devices. The detailed test procedures is presented in ASTM G1-90 [89], method C 3.5. The chemical cleaning solution was made of 500 ml hydrochloric acid (HCl, specific gravity 1.19), 3.5g hexamethylene tetramine and 500 ml reagent water. The corrosion products were removed after 5 to 6 cleaning cycles. The average corrosion rate can be obtained according to equation 2.31.

4.4.2 Chloride Content Analysis

In this investigation, both acid-soluble and water-soluble chloride content analysis methods were used to determine the chloride content. The concrete cores were taken from the specimens at the depth of the reinforcement after a certain period of exposure. The acid-soluble method and water-soluble method follow procedures specified as ASTM C 1152 and ASTM C 1218, respectively.

The acid-soluble method sequentially involves weighing a 5 to 10 mg finely pulverized sample, adding 75 ml distilled water and 25 ml nitric acid (1: 1), bringing to a boil, filtering , adding 2 ml sodium chloride (0.05 N) to the filtrate, cooling to room temperature and measuring the chloride content by an Orion microprocessor ion analyzer (Model 960) which is programmed to provide chloride content directly.

For the water-soluble method, the acid extraction used for acid-soluble method was replaced by water extraction. The water extraction includes adding 50 ml distilled water to the sample and bringing to a boil for 5 minutes, standing for 24 hours, then filtering, and adding 3 ml nitric acid (1:1) to the filtrate, bringing to a boil, and then following the same filtration procedures as the acid soluble method.

4.4.3 Temperature Measurement

Type T thermocouples were placed at the depth of reinforcement to determine the temperature at that depth during each corrosion measurement. A microprocessor thermometer (Model HH21, Omega Engineering, Inc.) was used to measure the temperature.

4.4.4 Relative Humidity Measurement

A cylinder specimen (4×4×8 in. (102×102×203 mm)) was designed to measure the internal relative humidity of concrete at depth of 2 in. (51 mm) cover concrete as shown in Figure 4.4. The side of the specimen was coated with a low modulus epoxy (Epon 828), then wrapped with aluminum foil, and coated with the same epoxy again. This would simulate a continuous structure. A Model RH-30 hand held temperature/humidity indicator with RH-30-1 probe (Omega Engineering, Inc.) was used to measure the relative humidity.

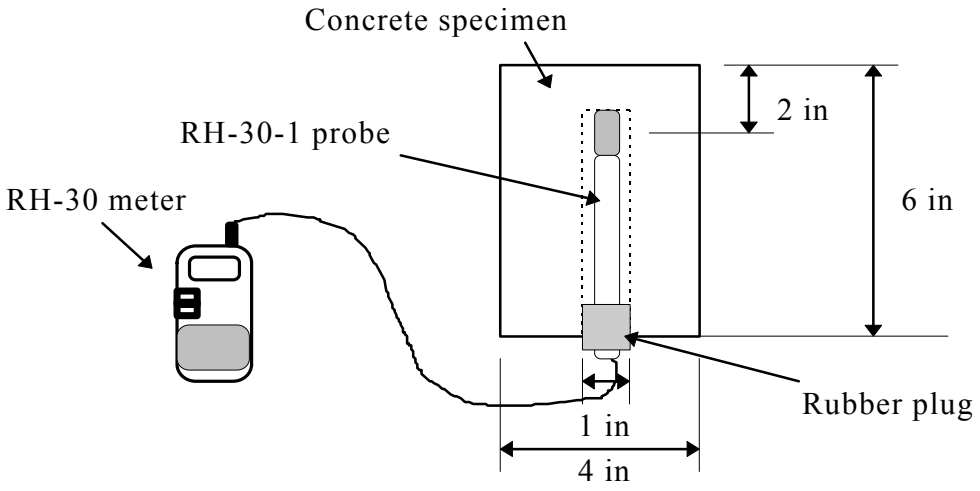

Figure 4.4. Test setup for relative humidity measurement.

5.0 Results and Discussions

5.1 Visual Observations

Up to five years of experimental testing, only outdoor test specimens with the highest admixed chloride series have cracked. The observed times to cracking for these specimens are listed in Table 5.1. In the cracked specimens, it was found that most of the cracks were located right above the reinforcing steel and parallel with reinforcing steel (see Figure 5.1).

Table 5.1. Observed times to cracking for outdoor specimens.

Admixed chloride content (lb/yd^3)	Cover depth (in.)	Rebar diameter (in.)	Observed time to cracking (year)
9.6	2	5/8″	1.84
9.6	3	5/8″	3.54
9.6 (Block)	2	1/2″	2.38
12.0	1	5/8″	0.72

When the specimens cracked, three 4 in. diameter cores were taken from each slab. It was observed that localized corrosion occurred at the rebar surface and most of the corrosion area was located on the upper part of the steel surface. This was due to the highly heterogeneous structure of the concrete and the presence of chloride ions, which results in the oxygen-rich area acting as the cathode site and the wetted area at steel/concrete interface acting as the anode.

5.2 Measured Corrosion Data

5.2.1 Monthly Corrosion Potentials

For indoor specimens, the monthly mean measured corrosion potentials from 3LP (mV, Cu-$CuSO_4$) and Gecor (mV,Ag-AgCl) devices for six series of admixed chloride are presented in Figures 5.2 and 5.3. As shown from these figures, the corrosion potentials become more positive with exposure time and also show a slight seasonal change. The decrease of potentials (more positive) may be related to a reduced corrosion activity between measurements. The seasonal change of potentials is due to small changes of moisture and temperature at different times.

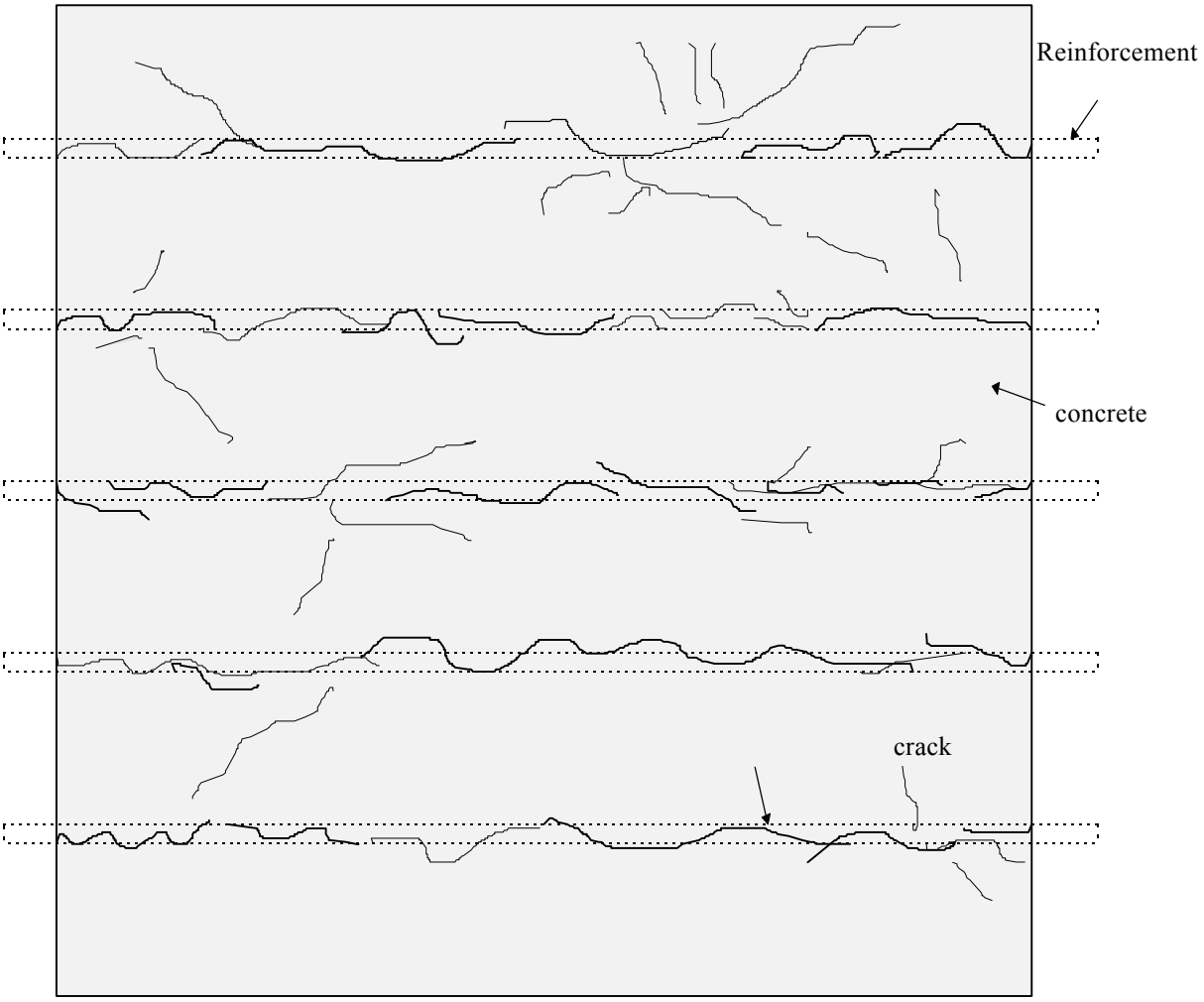

Figure 5.1. Corrosion cracking on the surface of the outdoor test specimens.

Among different admixed chloride series, only 9.6 lb/yd^3 series has more negative potential than that of other series, which indicates that this series has a high probability of active corrosion.

For outdoor specimens, Figures 5.4 and 5.5 present the monthly mean measured corrosion potentials from 3LP (mV, Cu-$CuSO_4$) and Gecor (mV,Ag-AgCl) for six series of admixed chloride with 2 inches cover depth; while Figures 5.6 and 5.7 illustrate the measured corrosion potentials for 3 inches cover depth series, and Figure 5.8 is for the four additional specimens with 1 inch cover depth. From these figures, it can be seen that within the admixed chloride series, there is no significant difference in measured corrosion potentials between 2 and 3 in. cover

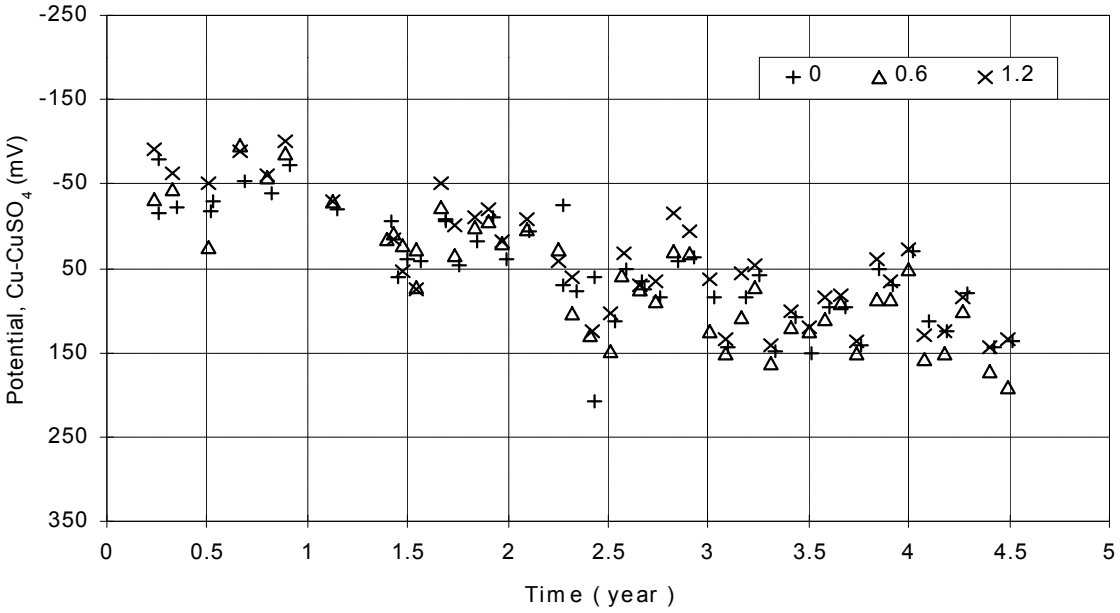

a. 0.0, 0.6, and 1.2 lb/yd^3 admixed chloride series

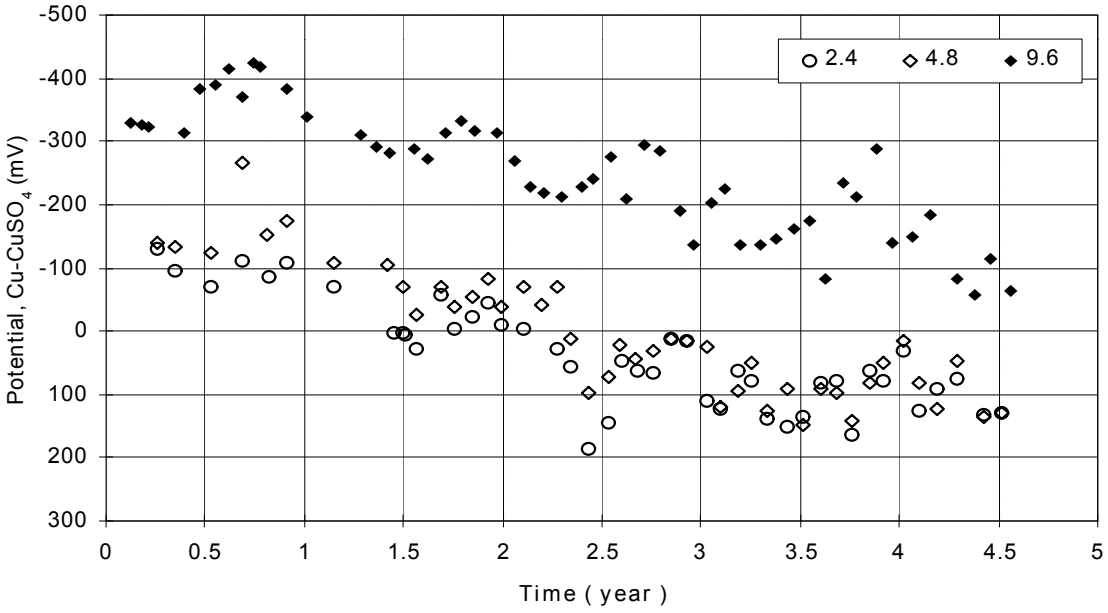

b. 2.4, 4.8, and 9.6 lb/yd^3 admixed chloride series.

Figure 5.2. Corrosion potentials versus time for different admixed chloride series, 3LP Measurements for indoor specimens.

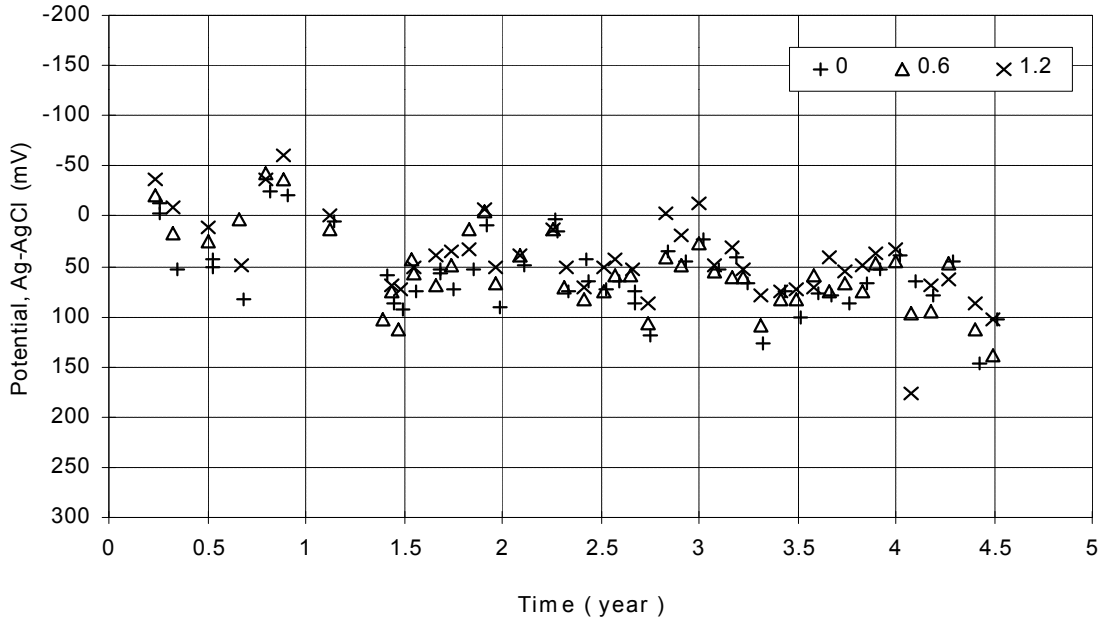

a. 0.0, 0.6, and 1.2 lb/yd^3 admixed chloride series

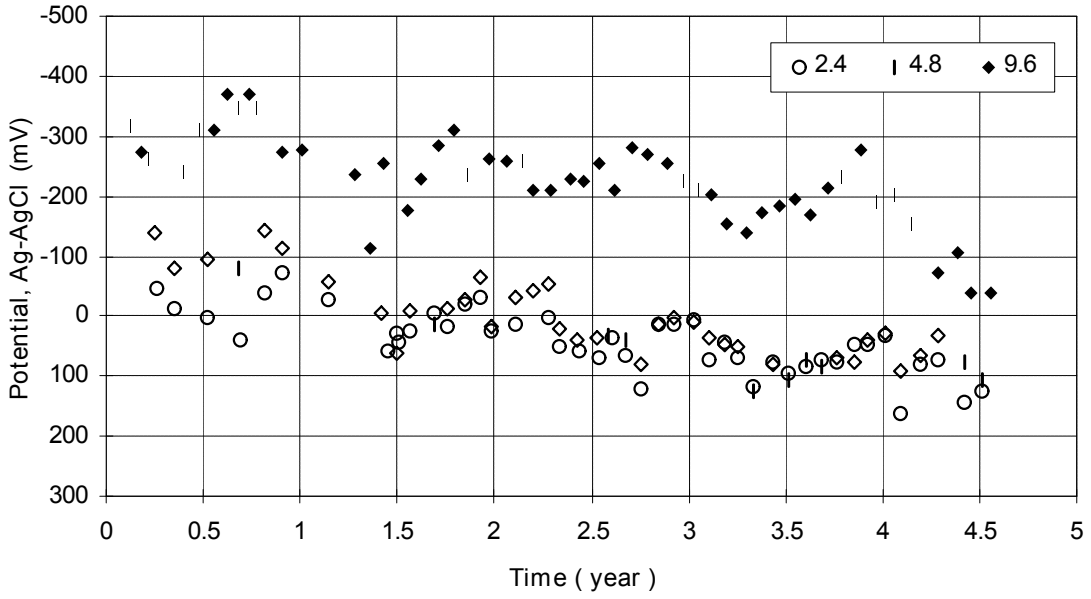

b. 2.4, 4.8, and 9.6 lb/yd^3 admixed chloride series.

Figure 5.3. Corrosion potentials versus time for different admixed chloride series, Gecor Measurements for indoor specimens.

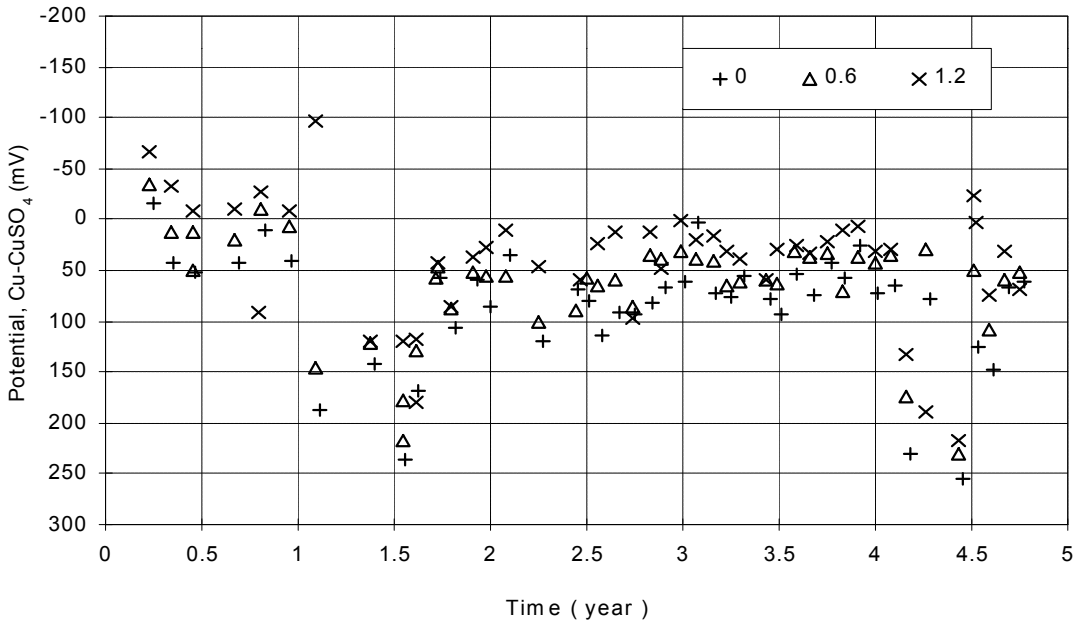

a. 0.0, 0.6, and 1.2 lb/yd³ admixed chloride series

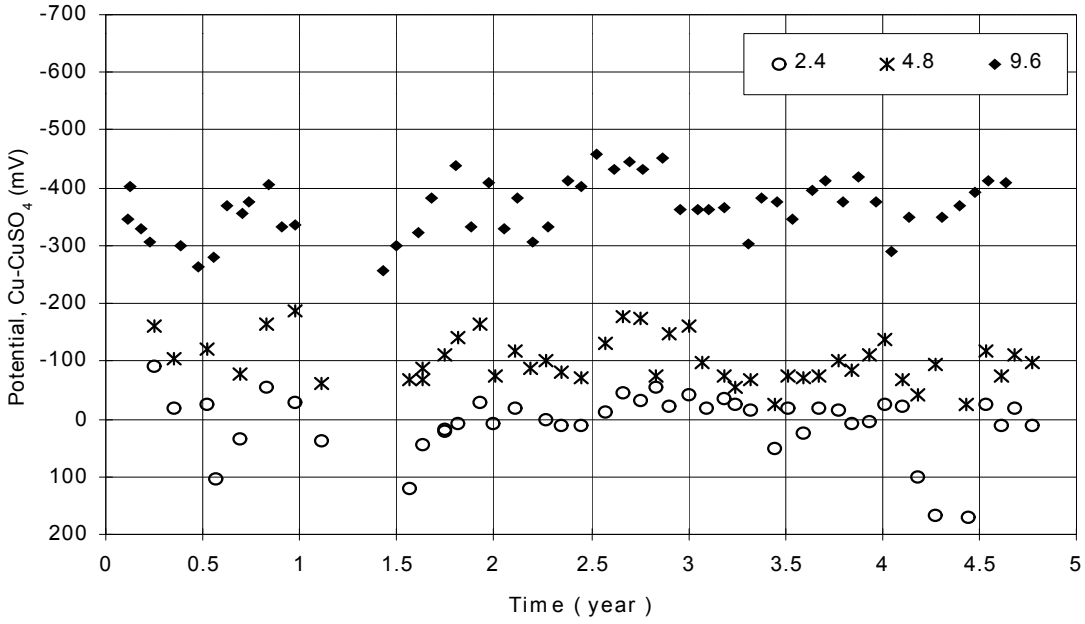

b. 2.4, 4.8, and 9.6 lb/yd³ admixed chloride series.

Figure 5.4. Corrosion potentials versus time for different admixed chloride series, 3LP Measurements for outdoor specimens, 2 in. cover depth.

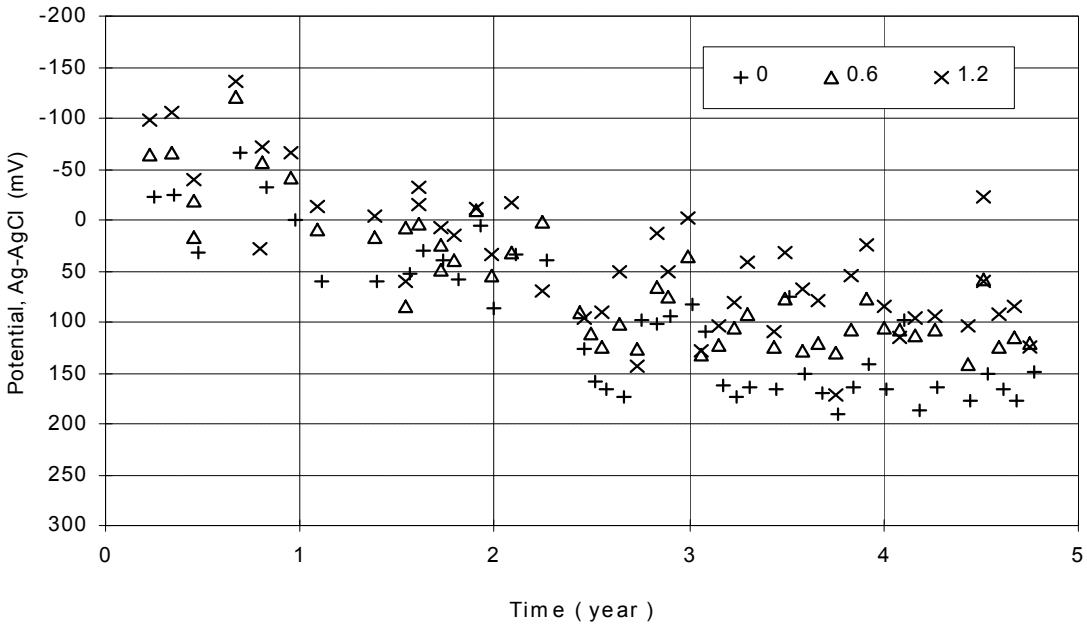

a. 0.0, 0.6, and 1.2 lb/yd^3 admixed chloride series.

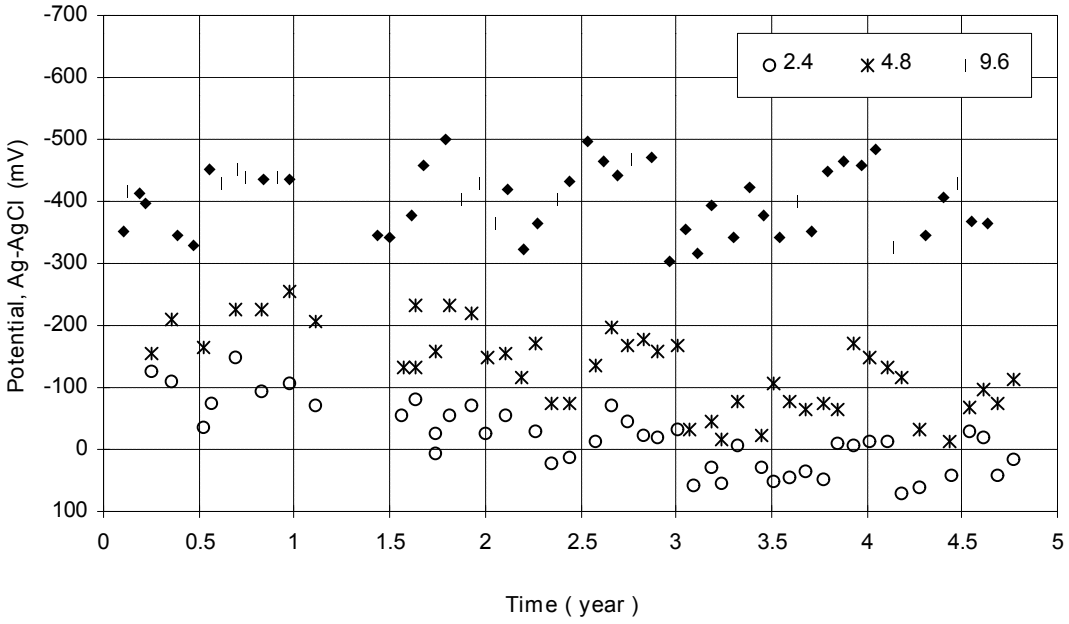

b. 2.4, 4.8, and 9.6 lb/yd^3 admixed chloride series.

Figure 5.5. Corrosion potentials versus time for different admixed chloride series, Gecor Measurements for outdoor specimens, 2 in. cover depth.

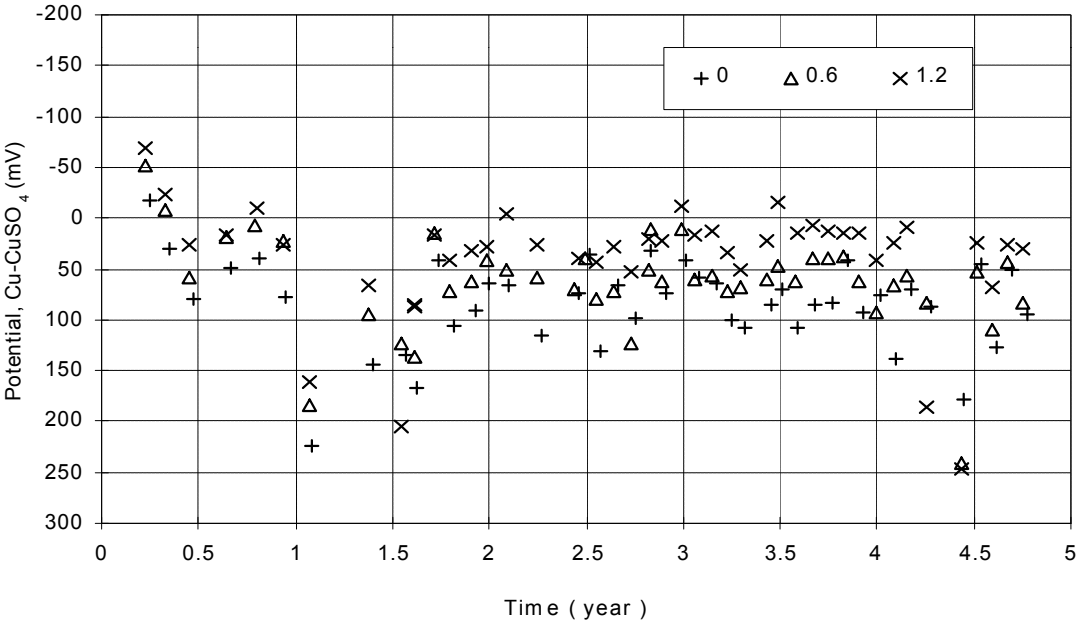

a. 0.0, 0.6, and 1.2 lb/yd^3 admixed chloride series.

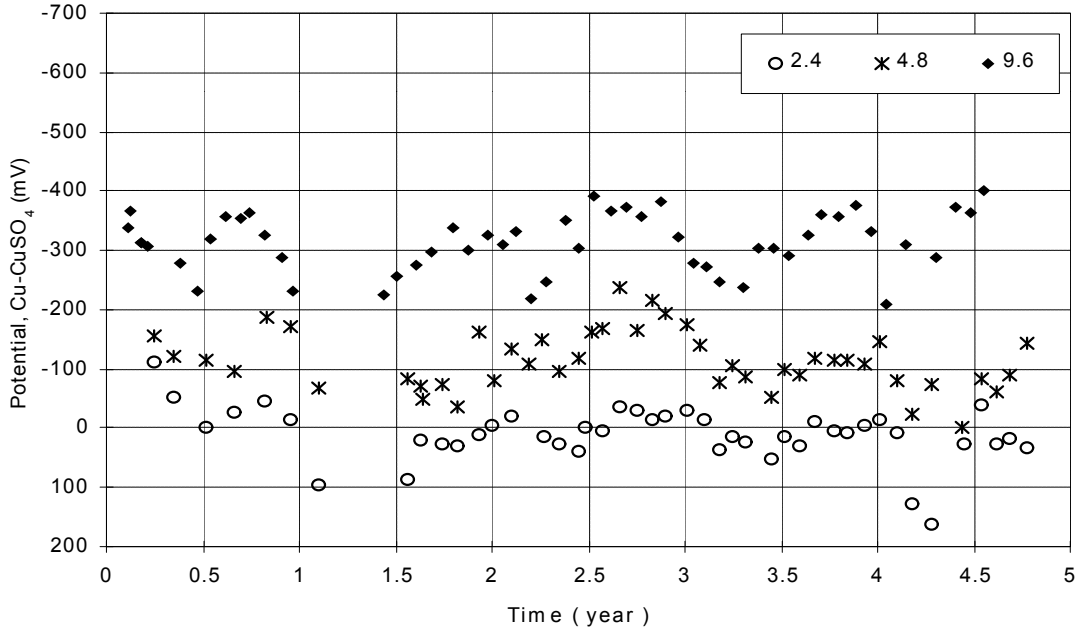

b. 2.4, 4.8, and 9.6 lb/yd^3 admixed chloride series.

Figure 5.6. Corrosion potentials versus time for different admixed chloride series, 3LP Measurements for outdoor specimens, 3 in. cover depth.

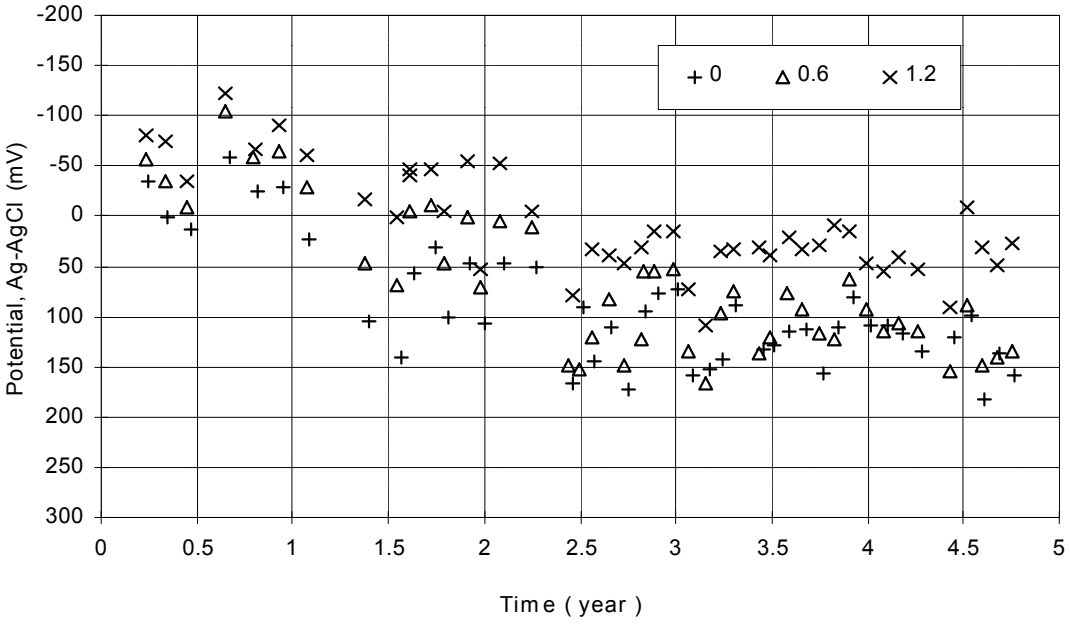

a. 0.0, 0.6, and 1.2 lb/yd^3 admixed chloride series.

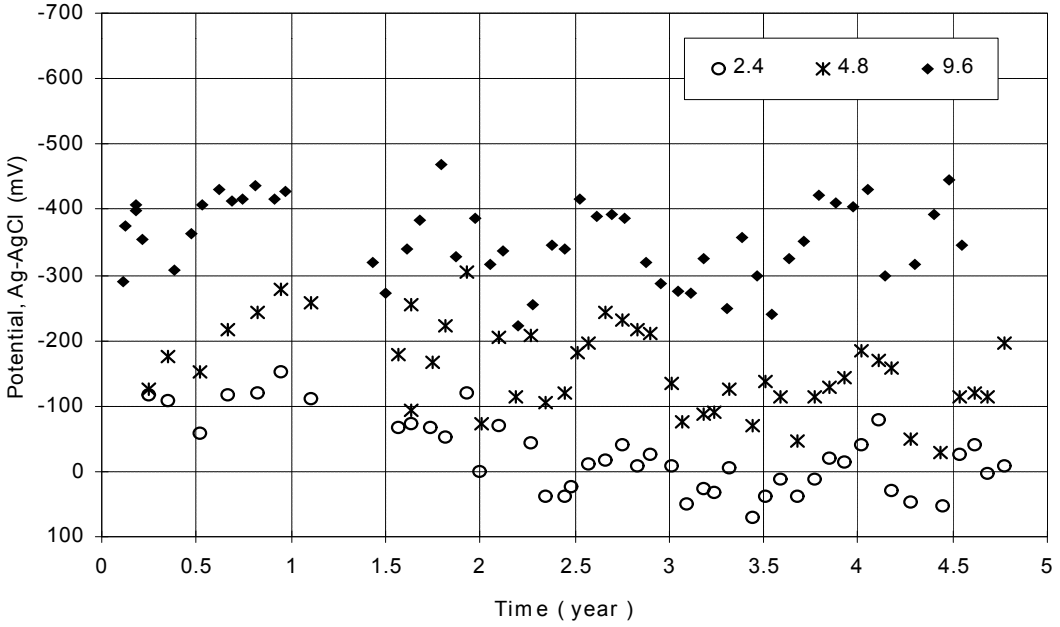

b. 2.4, 4.8, and 9.6 lb/yd^3 admixed chloride series.

Figure 5.7. Corrosion potentials versus time for different admixed chloride series, Gecor Measurements for outdoor specimens, 3 in. cover depth.

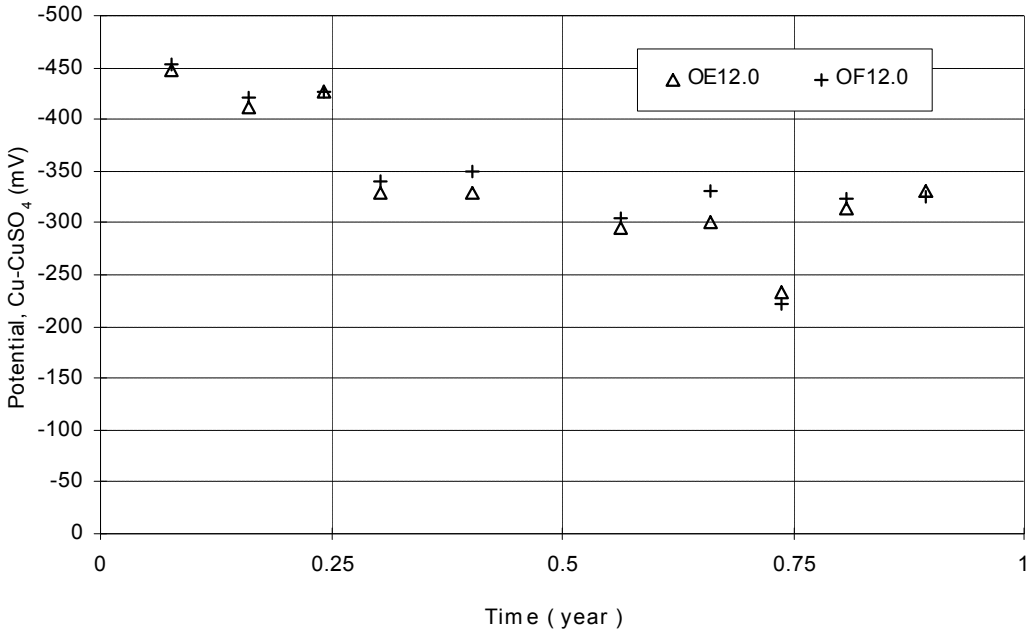

a. 3LP measurement for 12.0 lb/yd^3 admixed chloride series.

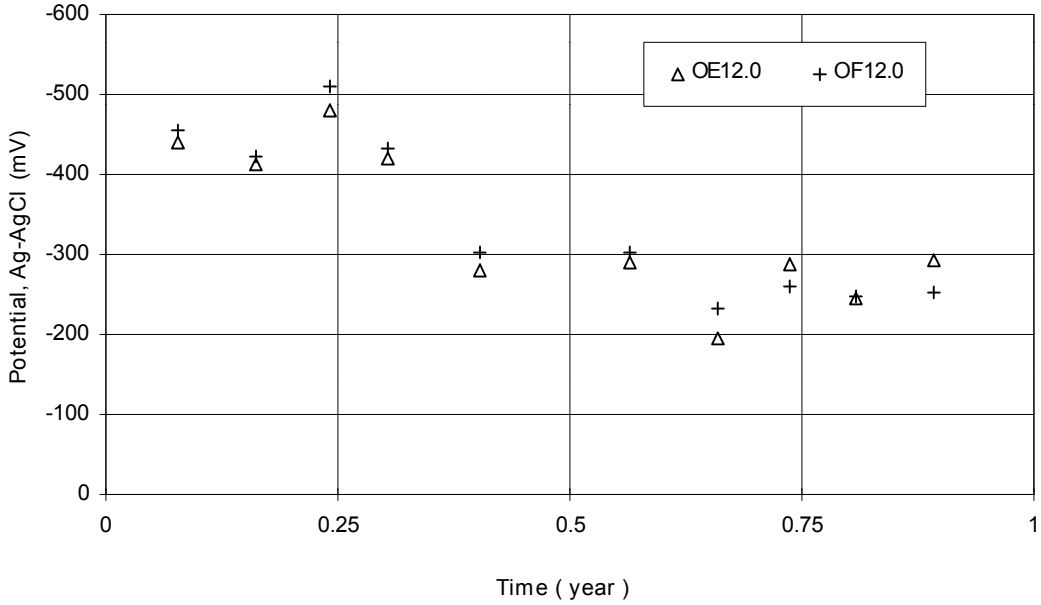

b. Gecor measurement for 12.0 lb/yd^3 admixed chloride series.

Figure 5.8. Corrosion potentials versus time for four additional slabs, outdoor specimens, 1 in. cover depth.

depth. Among the different admixed chloride series, there is a significant difference in measured corrosion potentials when the admixed chloride level is above 2.4 lb/yd^3, and the corrosion potential becomes more negative as the admixed chloride content increases; when admixed chloride content is below 1.2 lb/yd^3, there is no significant difference in measured corrosion potentials. It can also be seen that the measured corrosion potentials decrease (more positive) at the early stage (about 1.5 to 2.5 years) for the low admixed chloride levels. This is mostly due to the formation of the passive film on the steel surface. According to other researchers [107-108], it usually takes more than one year for the reinforced concrete specimens to develop a stable passive film.

For the high level admixed chloride series, there is a slight seasonal change in the measured corrosion potential due to the changes of seasonal outdoor exposure conditions.

As shown in Figure 5.8, there is no significant difference in measured corrosion potentials between slabs with isolated rebars and interconnected rebars. This may indicate that most of the corrosion in reinforced concrete structures is micro-cell corrosion.

Comparing with indoor and outdoor series, for the high admixed chloride series, the measured corrosion potentials in outdoor specimens are significantly greater (more negative) than that of indoor series; while for the low admixed chloride series, there is no significant difference in measured corrosion potentials between indoor and outdoor test series.

5.2.2 Measured Corrosion Rate Versus Times, Temperature and Concrete Ohmic Resistance

Figures 5.9 to 5.14 present the measured corrosion rates (3LP and Gecor), concrete ohmic resistances, temperatures for the six series of admixed chlorides, indoor specimens at different time, respectively. Figures 5.15 to 5.20 present the measured corrosion rates (3LP and Gecor), concrete ohmic resistances, temperatures for the six series of admixed chloride, outdoor specimens with 2 inch cover depth at different time, respectively, while Figures 5.21 to 5.26 are for specimens with 3 inch cover depth and Figure 5.27 is for the four additional specimens with 1 inch cover.

For indoor series, it can be seen from Figures 5.9 to 5.14 that the corrosion rates measured with the 3LP and Gecor devices decrease at early stage and then tend to stabilize at certain values; and the higher the admixed chlorides the greater the measured corrosion rate. The decrease of corrosion rate for the low admixed chloride series may be related to the gradual formation of the passive film; for the high admixed chlorides it may be related to the changes of area ratio of anode and cathode. The seasonal change of measured resistance of concrete is due to the changes of temperature and moisture in concrete at different measurement intervals. It is also noted that the resistance of concrete decreases as the admixed chloride content increases, because the ionic conductivity of concrete increases as the salt content increases in the pore water of concrete.

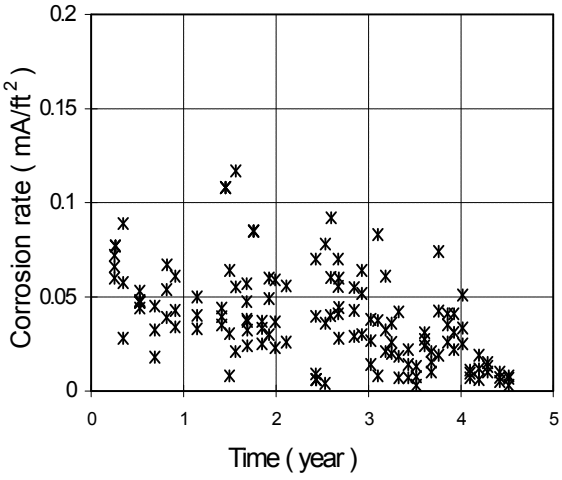

a. Corrosion rate versus time (Gecor device).

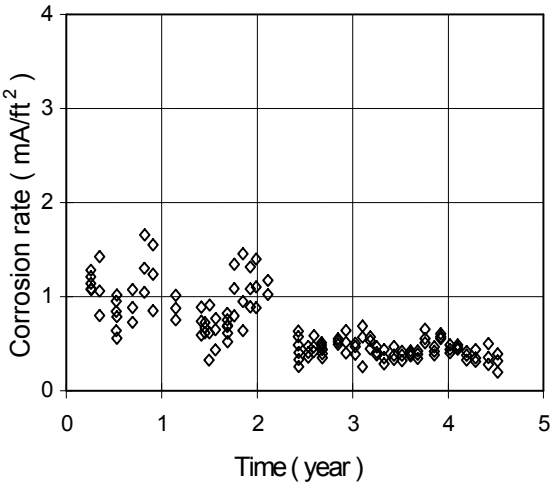

b. Corrosion rate versus time (3LP device).

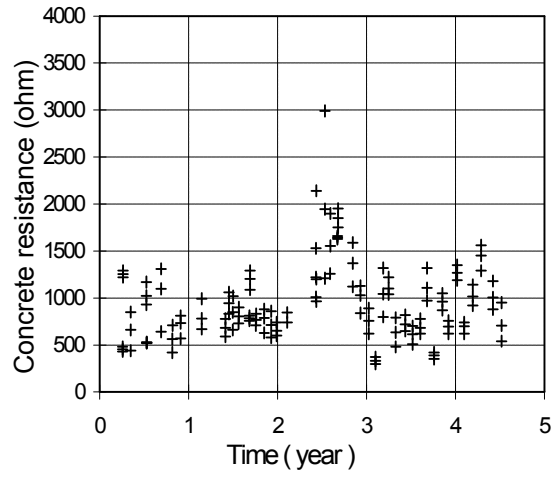

c. Concrete ohmic resistance at measurements.

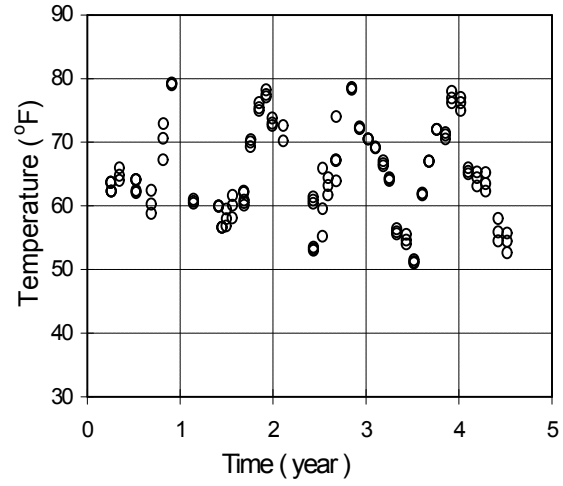

d. Temperature at depth of reinforcement.

Figure 5.9. Corrosion rate, concrete ohmic resistances and temperatures over corrosion time, 0.0 lb/yd^3 admixed chloride, indoor specimens.

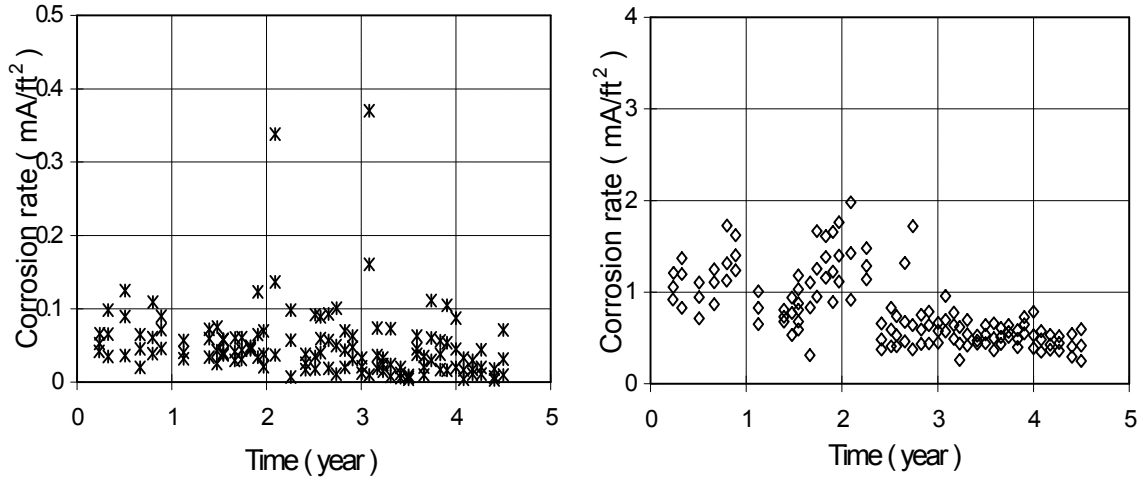

a. Corrosion rate versus time (Gecor device). b. Corrosion rate versus time (3LP device).

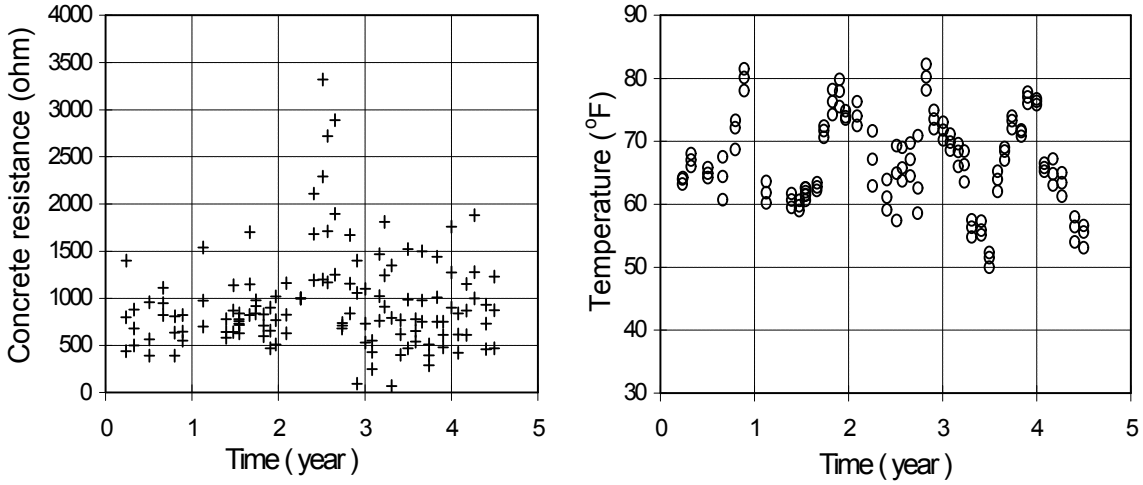

c. Concrete ohmic resistance at measurements. d. Temperature at depth of reinforcement.

Figure 5.10. Corrosion rate, concrete ohmic resistances and temperatures over corrosion time, 0.6 lb/yd^3 admixed chloride, indoor specimens.

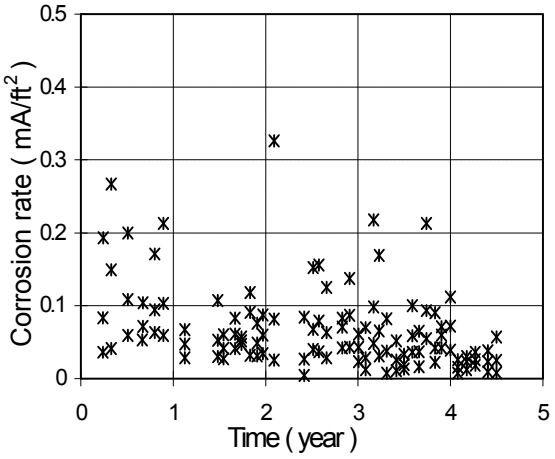

a. Corrosion rate versus time (Gecor device).

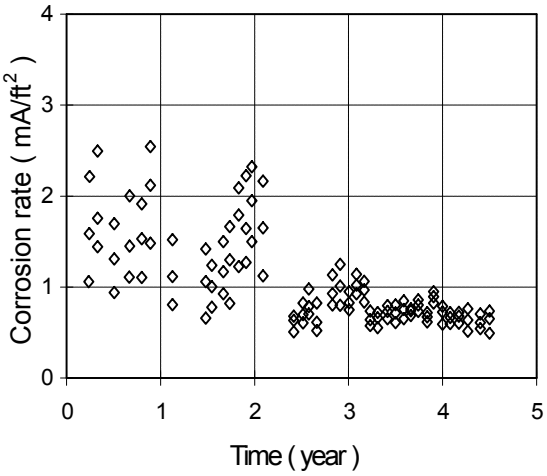

b. Corrosion rate versus time (3LP device).

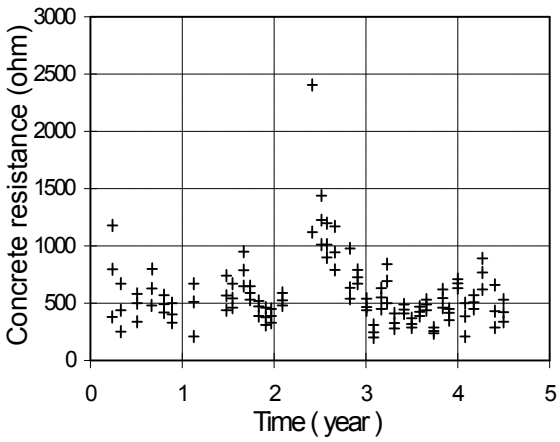

c. Concrete ohmic resistance at measurements.

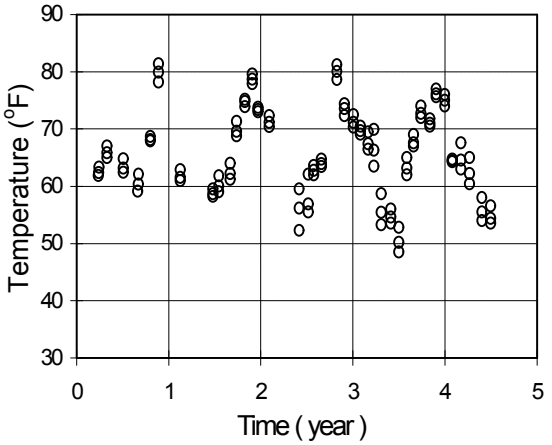

d. Temperature at depth of reinforcement.

Figure 5.11. Corrosion rate, concrete ohmic resistances and temperatures over corrosion time, 1.2 lb/yd^3 admixed chloride, indoor specimens.

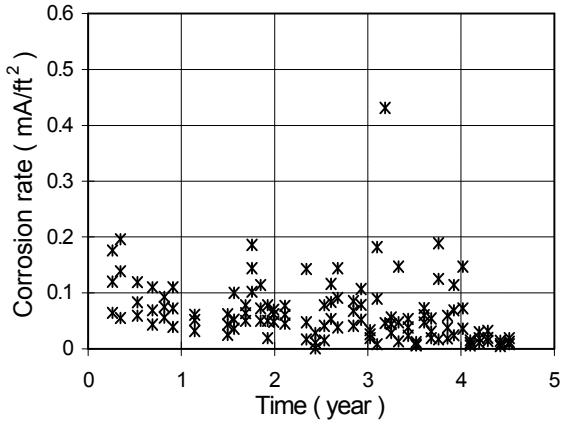

a. Corrosion rate versus time (Gecor device).

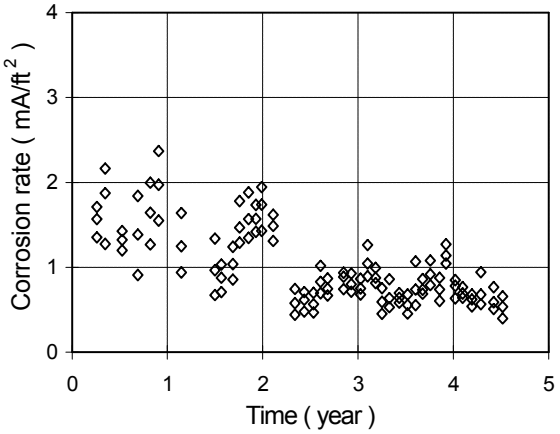

b. Corrosion rate versus time (3LP device).

a. Corrosion rate versus time (Gecor device).
b. Corrosion rate versus time (3LP device).

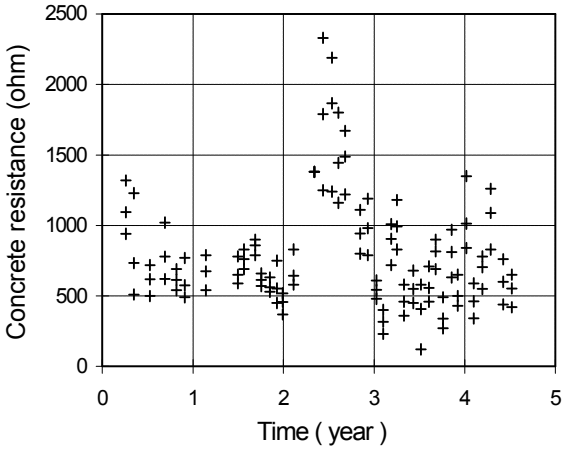

c. Concrete ohmic resistance at measurements.

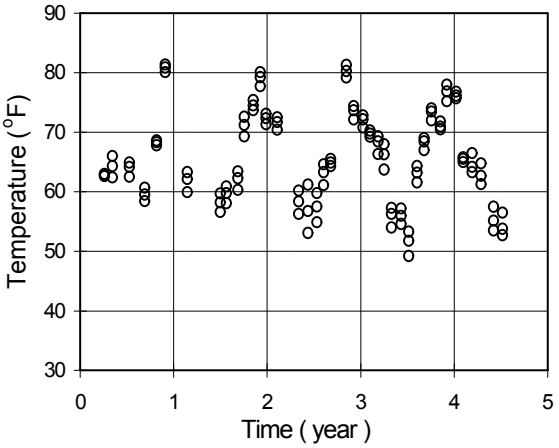

d. Temperature at depth of reinforcement.

Figure 5.12. Corrosion rate, concrete ohmic resistances and temperatures over corrosion time, 2.4 lb/yd^3 admixed chloride, indoor specimens.

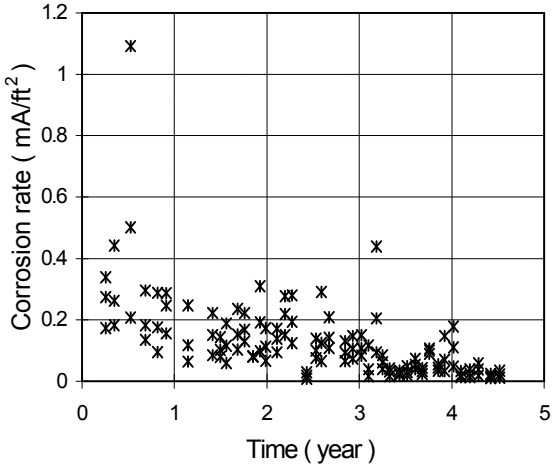

a. Corrosion rate versus time (Gecor device).

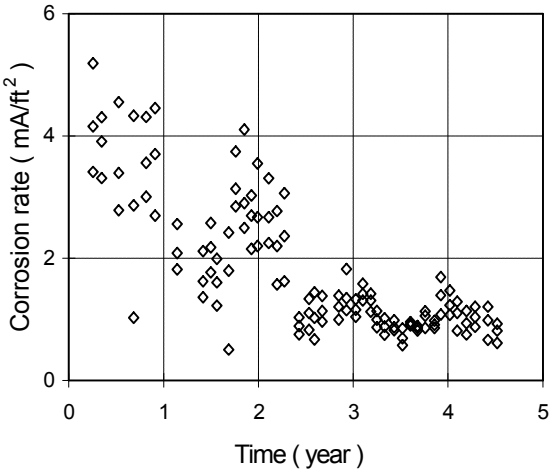

b. Corrosion rate versus time (3LP device).

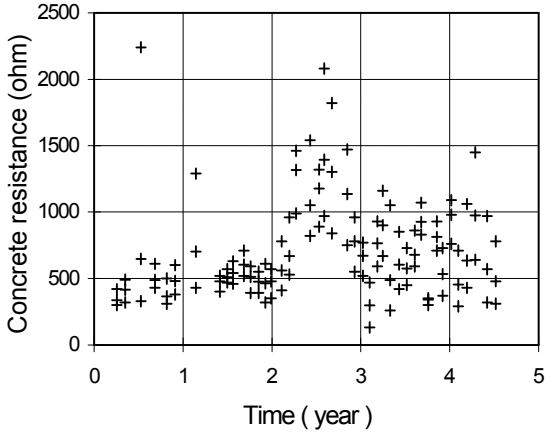

c. Concrete ohmic resistance at measurements.

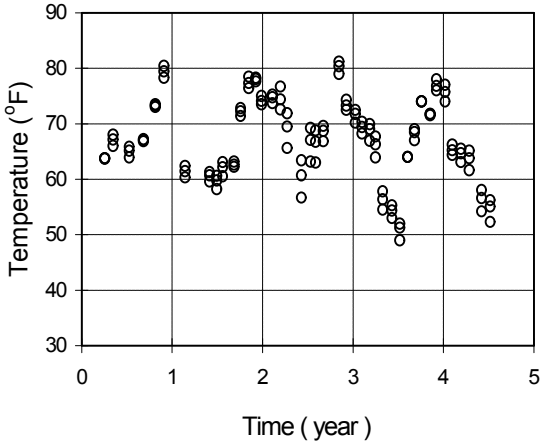

d. Temperature at depth of reinforcement.

Figure 5.13. Corrosion rate, concrete ohmic resistances and temperatures over corrosion time, 4.8 lb/yd^3 admixed chloride, indoor specimens.

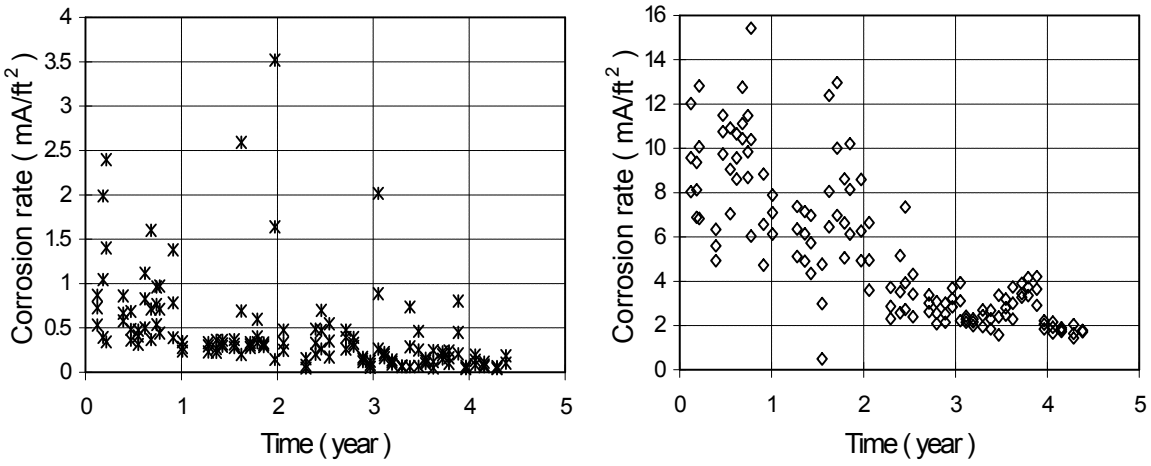

a. Corrosion rate versus time (Gecor device). b. Corrosion rate versus time (3LP device).

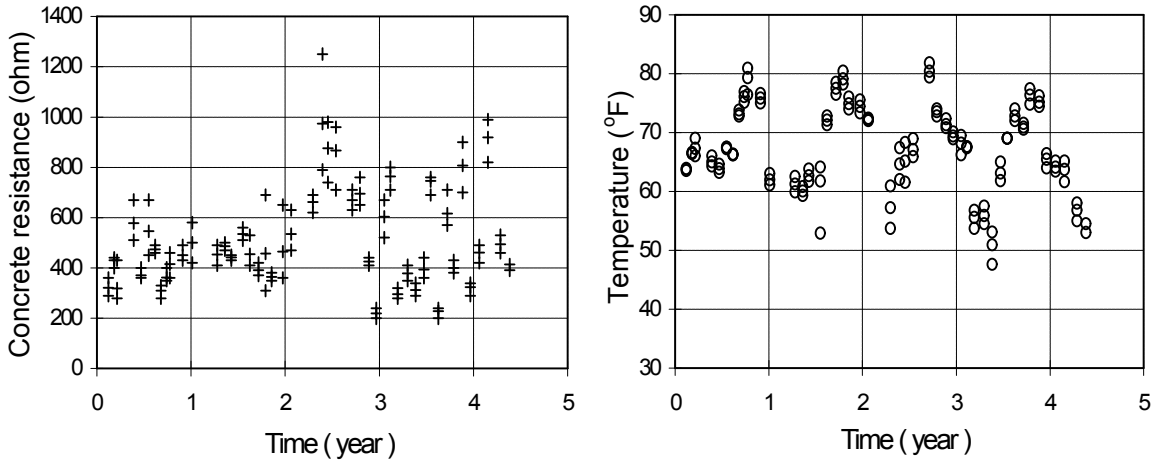

c. Concrete ohmic resistance at measurements. d. Temperature at depth of reinforcement.

Figure 5.14. Corrosion rate, concrete ohmic resistances and temperatures over corrosion time, 9.6 lb/yd^3 admixed chloride, indoor specimens.

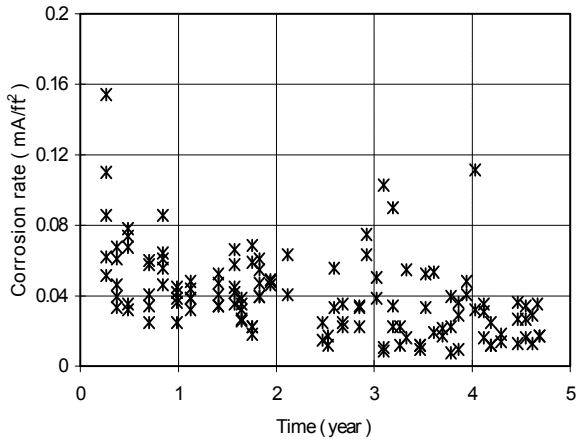

a. Corrosion rates versus time (Gecor device).

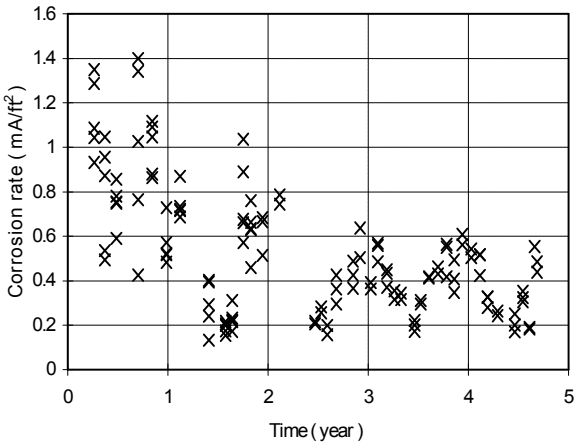

b. Corrosion rates versus time (3LP device).

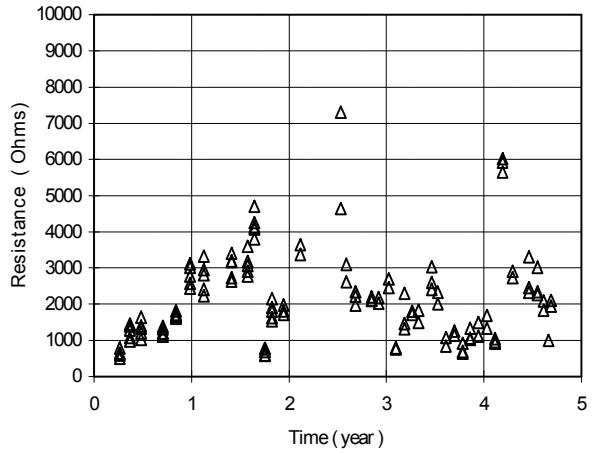

c. Concreteohmic resistance at measurements.

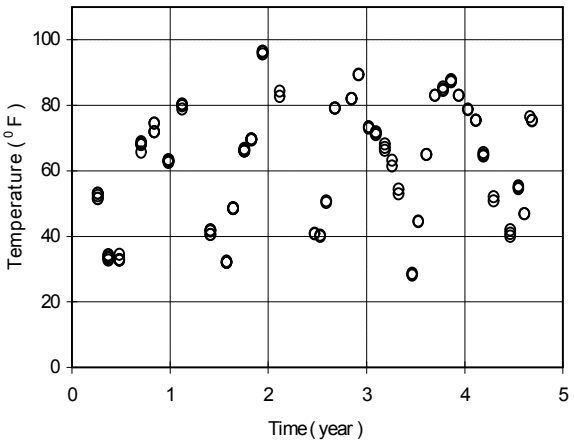

d. Temperature at depth of reinforcement.

Figure 5.15. Corrosion rates, concreteohmic resistance and temperature over corrosion time, 0.0 lb/yd³ admixed chloride, outdoor specimens, 2 in. cover.

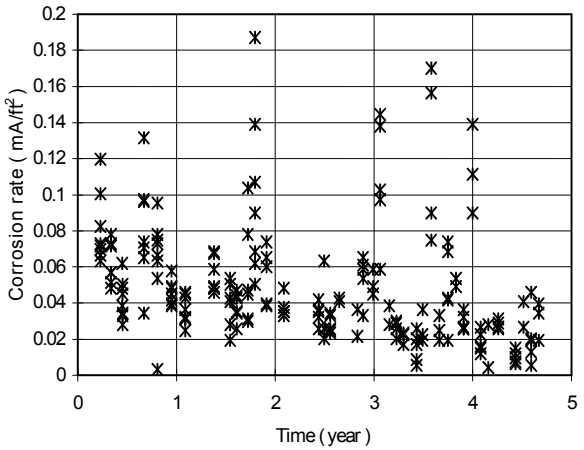

a. Corrosion rates versus time (Gecor device).

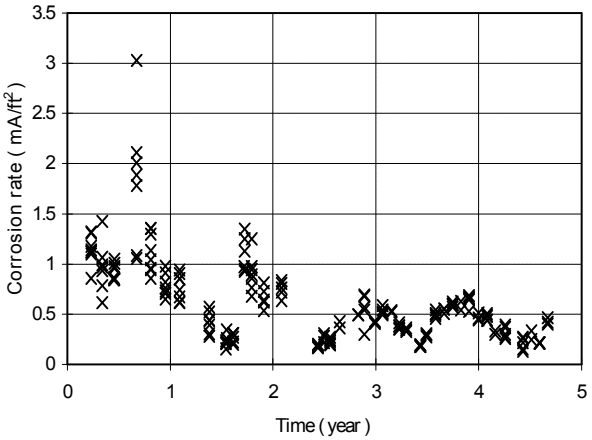

b. Corrosion rates versus time (3LP device).

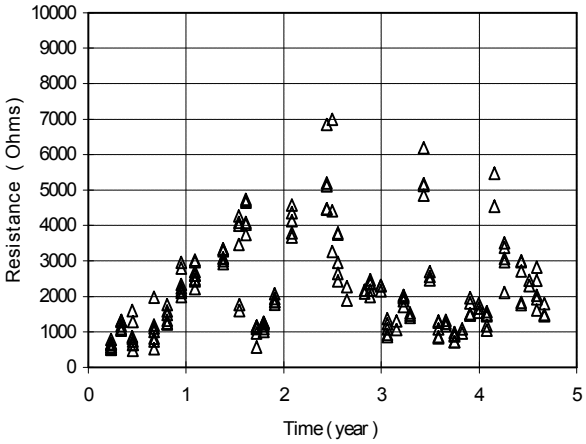

c. Concreteohmic resistance at measurements.

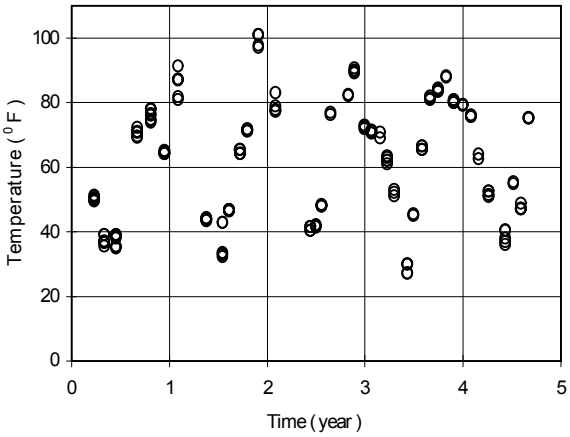

d. Temperature at depth of reinforcement.

Figure 5.16. Corrosion rates, concreteohmic resistance and temperature over corrosion time, 0.6 lb/yd^3 admixed chloride, outdoor specimens, 2 in. cover.

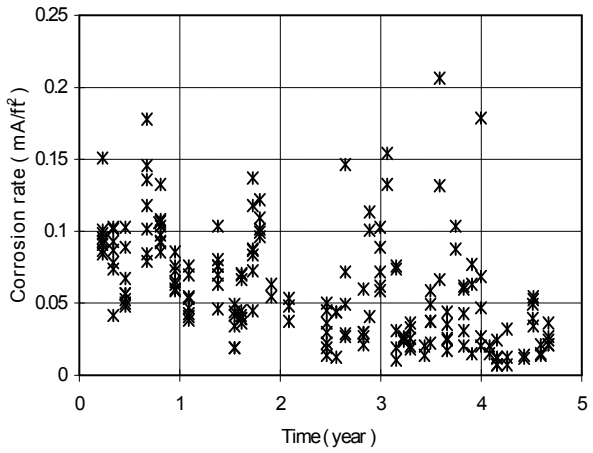

a. Corrosion rates versus time (Gecor device).

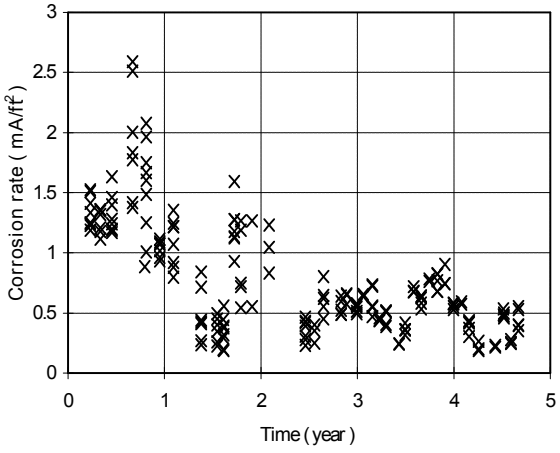

b. Corrosion rates versus time (3LP device).

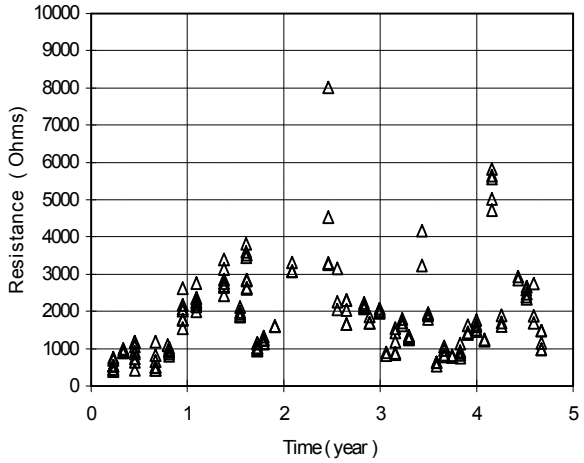

c. Concreteohmic resistance at measurements.

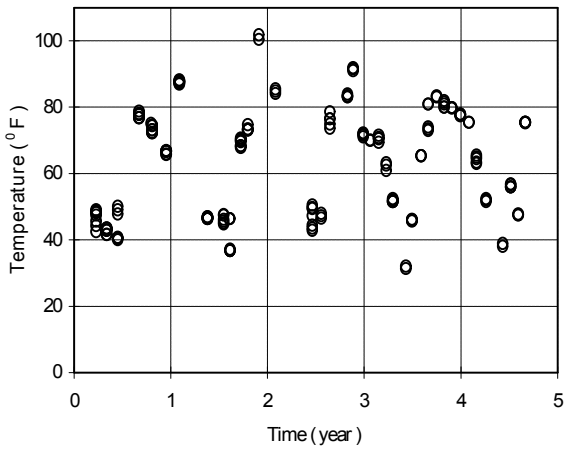

d. Temperature at depth of reinforcement.

Figure 5.17. Corrosion rates, concreteohmic resistance and temperature over corrosion time, 1.2 lb/yd^3 admixed chloride, outdoor specimens, 2 in. cover.

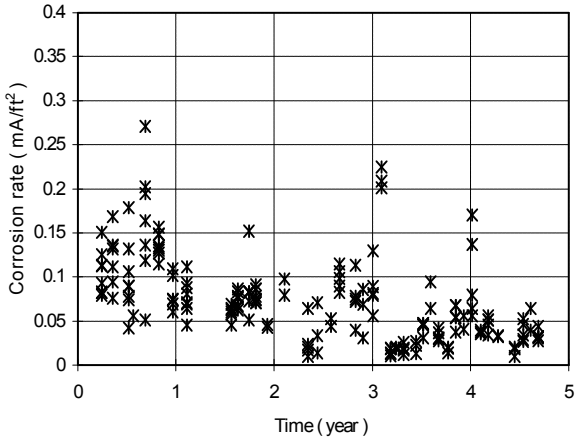

a. Corrosion rates versus time (Gecor device).

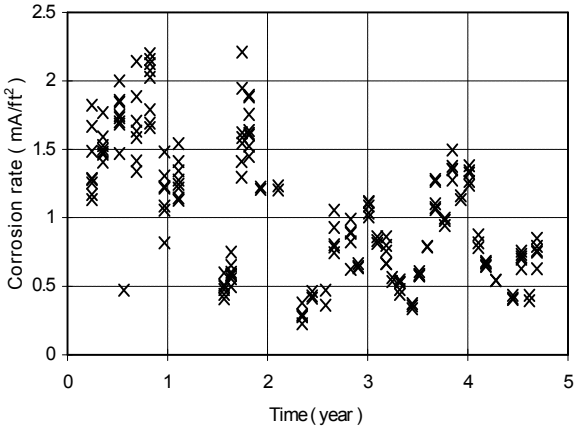

b. Corrosion rates versus time (3LP device).

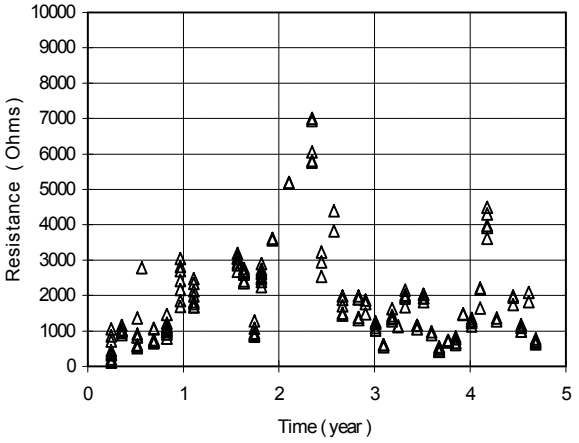

c. Concreteohmic resistance at measurements.

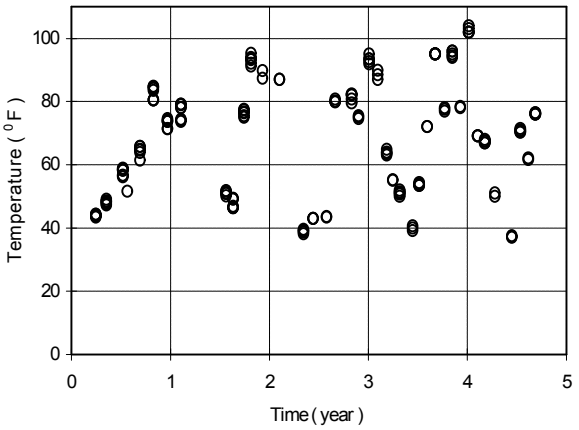

d. Temperature at depth of reinforcement.

Figure 5.18. Corrosion rates, concreteohmic resistance and temperature over corrosion time, 2.4 lb/yd^3 admixed chloride, outdoor specimens, 2 in. cover.

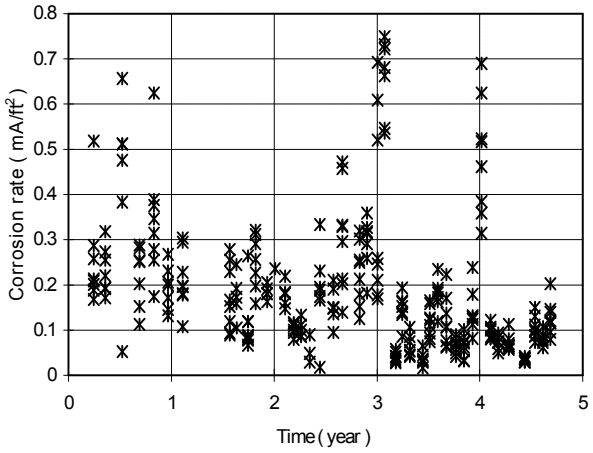

a. Corrosion rates versus time (Gecor device).

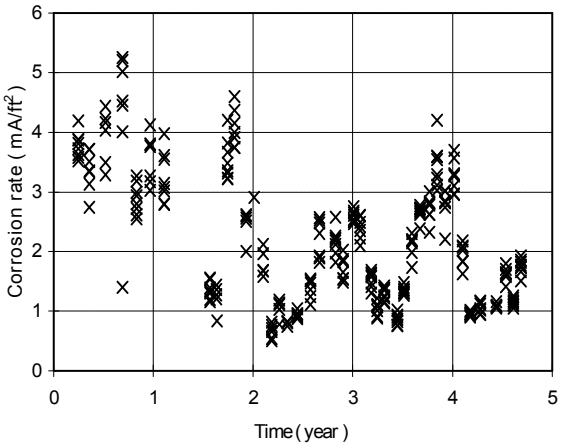

b. Corrosion rates versus time (3LP device).

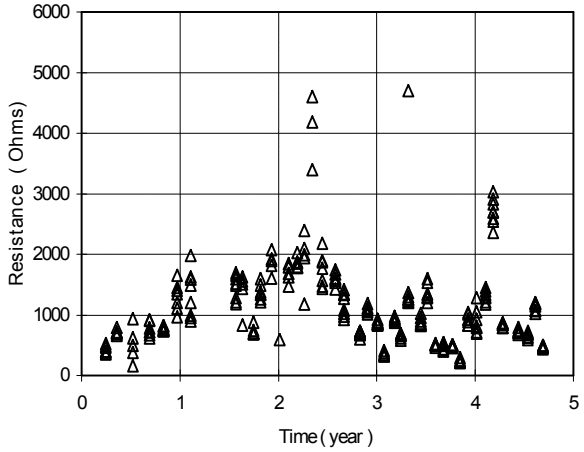

c. Concreteohmic resistance at measurements.

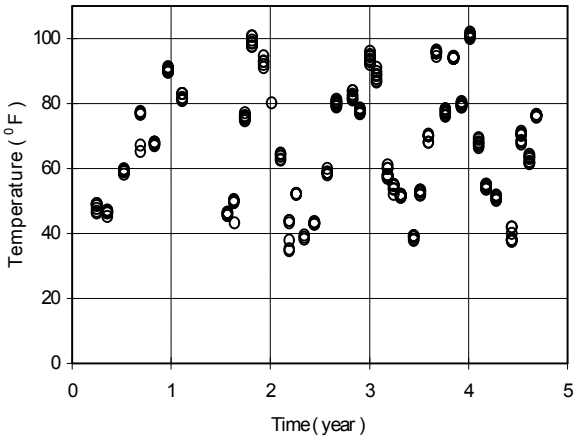

d. Temperature at depth of reinforcement.

Figure 5.19. Corrosion rates, concreteohmic resistance and temperature over corrosion time, 4.8 lb/yd^3 admixed chloride, outdoor specimens, 2 in. cover.

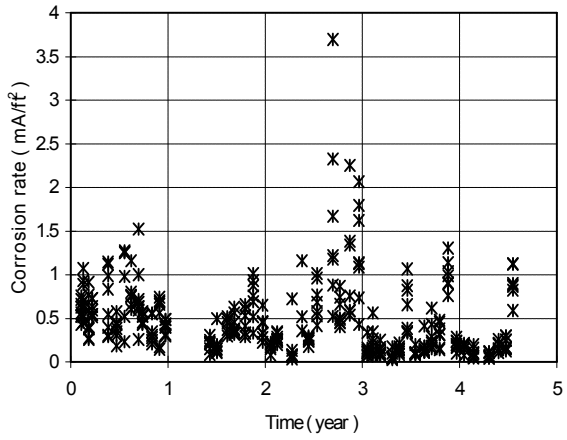

a. Corrosion rates versus time (Gecor device).

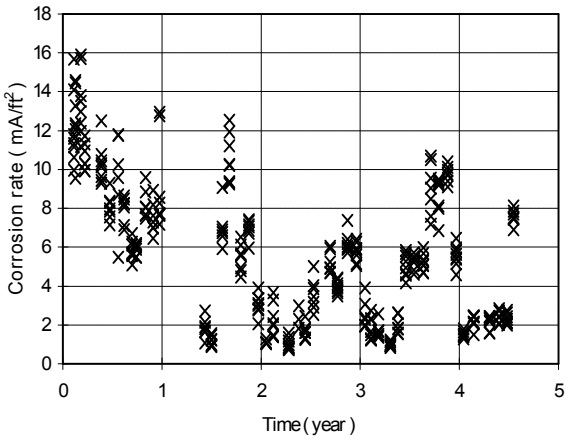

b. Corrosion rates versus time (3LP device).

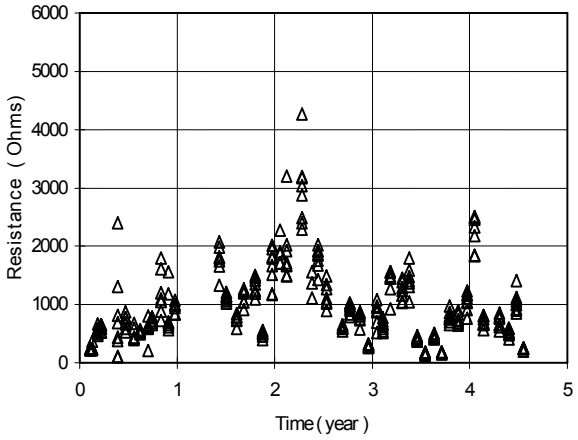

c. Concreteohmic resistance at measurements.

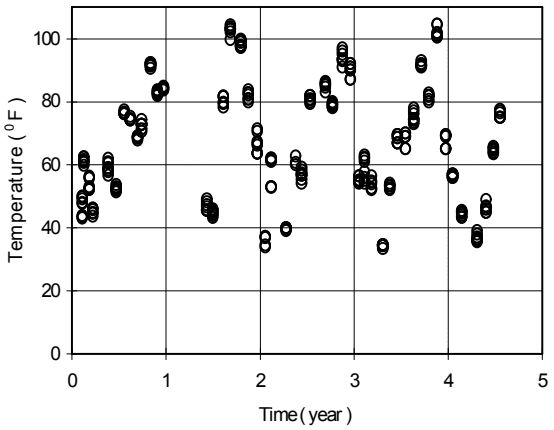

d. Temperature at depth of reinforcement.

Figure 5.20. Corrosion rates, concreteohmic resistance and temperature over corrosion time, 9.6 lb/yd^3 admixed chloride, outdoor specimens, 2 in. cover.

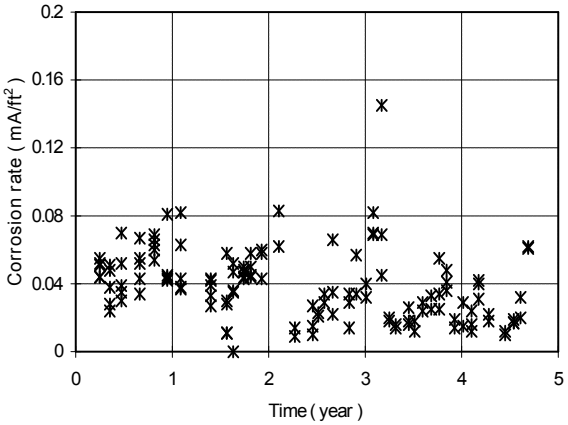

a. Corrosion rates versus time (Gecor device).

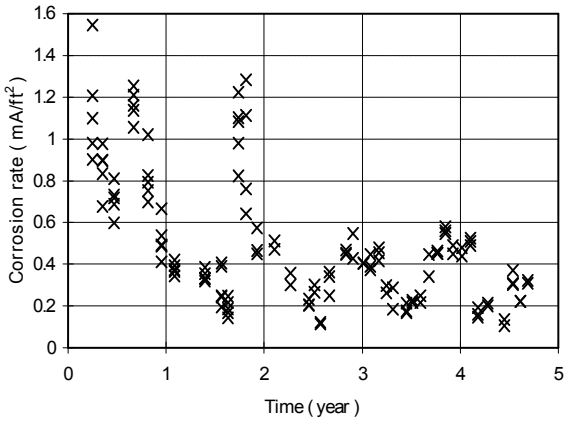

b. Corrosion rates versus time (3LP device

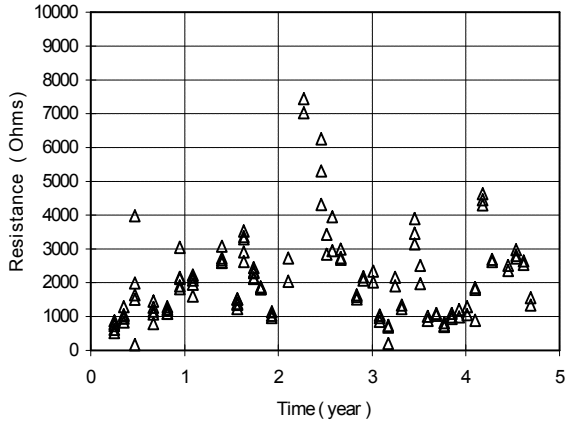

c. Concreteohmic resistances at measurements.

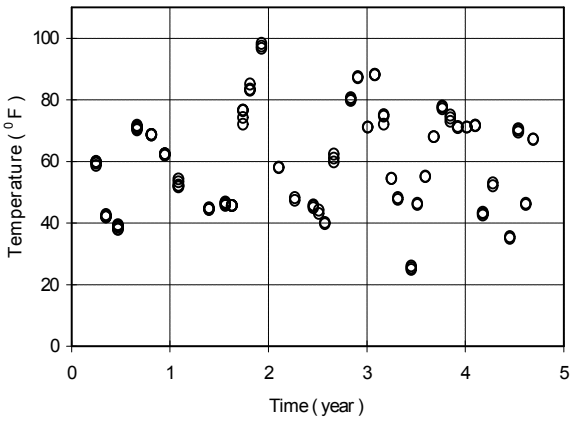

d. Temperatures at depth of reinforcement.

Figure 5.21. Corrosion rates, concreteohmic resistance and temperature over corrosion time, 0.0 lb/yd^3 admixed chloride, outdoor specimens, 3 in. cover.

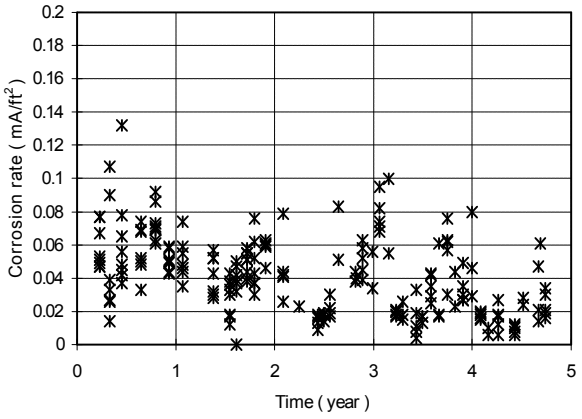

a. Corrosion rates versus time (Gecor device).

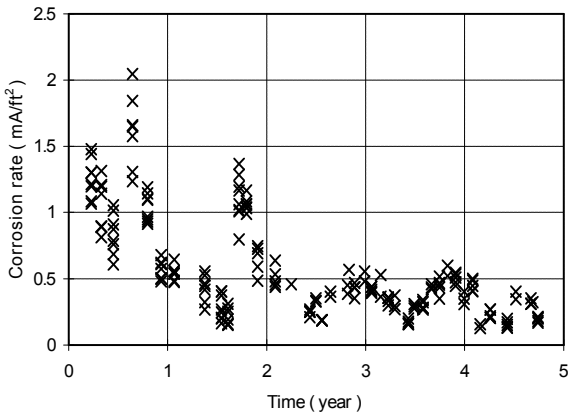

b. Corrosion rates versus time (3LP device

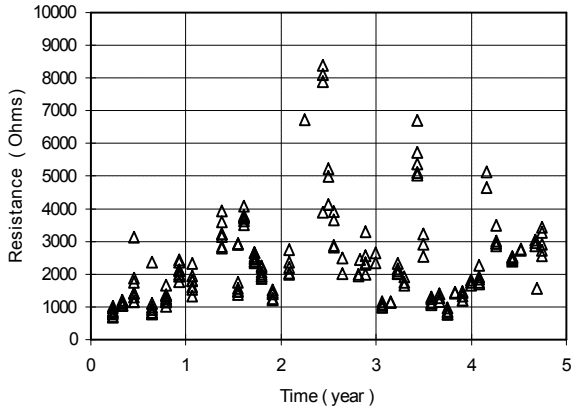

c. Concreteohmic resistances at measurements.

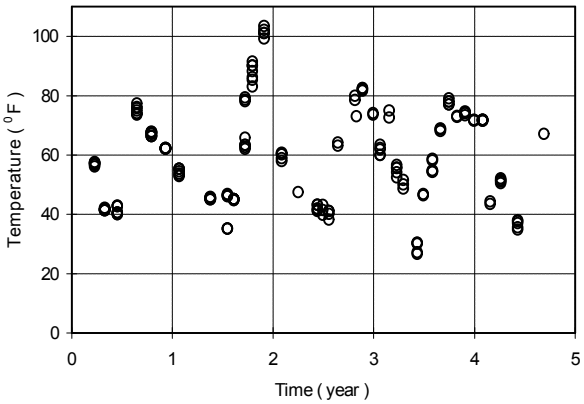

d. Temperatures at depth of reinforcement.

Figure 5.22. Corrosion rates, concreteohmic resistance and temperature over corrosion time, 0.6 lb/yd^3 admixed chloride, outdoor specimens, 3 in. cover.

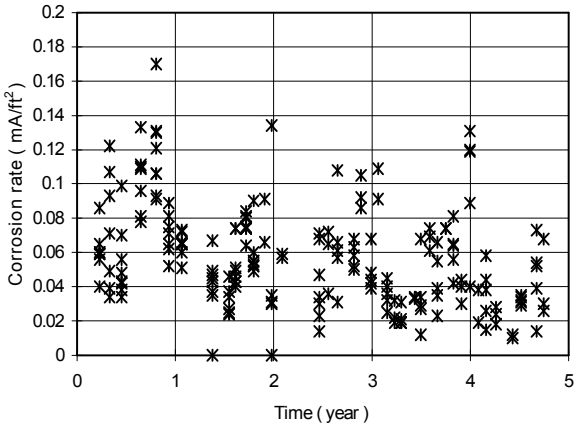

a. Corrosion rates versus time (Gecor device).

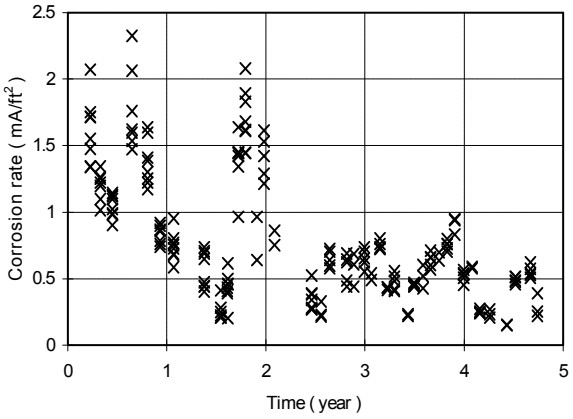

b. Corrosion rates versus time (3LP device)

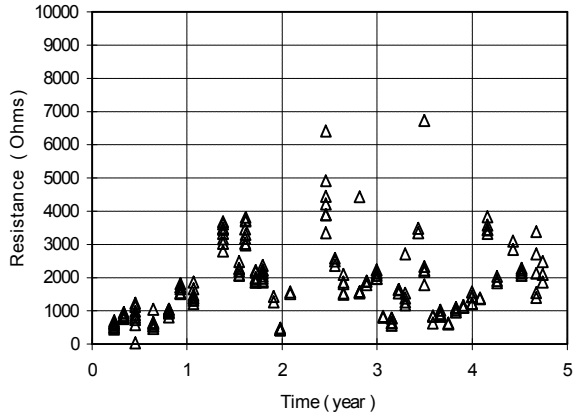

c. Concreteohmic resistances at measurements.

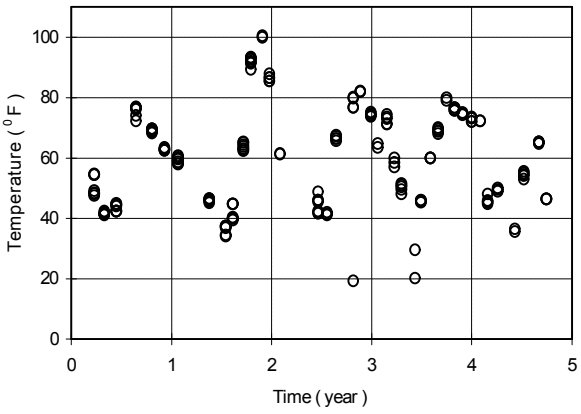

d. Temperatures at depth of reinforcement.

Figure 5.23. Corrosion rates, concreteohmic resistance and temperature over corrosion time, 1.2 lb/yd^3 admixed chloride, outdoor specimens, 3 in. cover.

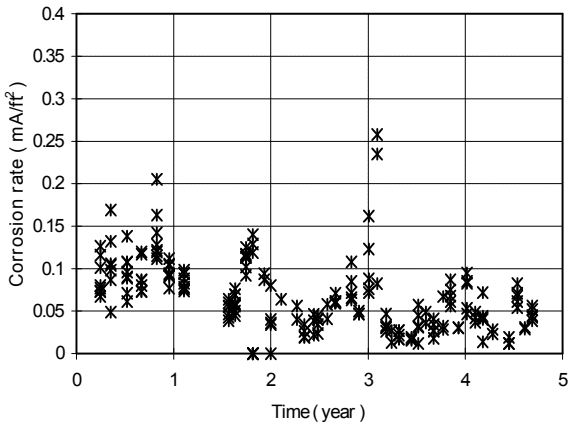

a. Corrosion rates versus time (Gecor device).

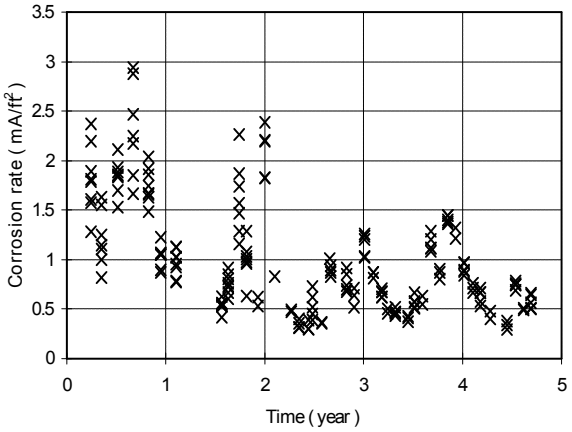

b. Corrosion rates versus time (3LP device)

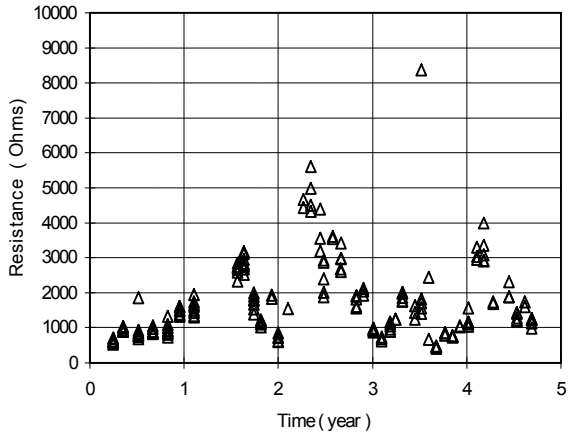

c. Concreteohmic resistances at measurements.

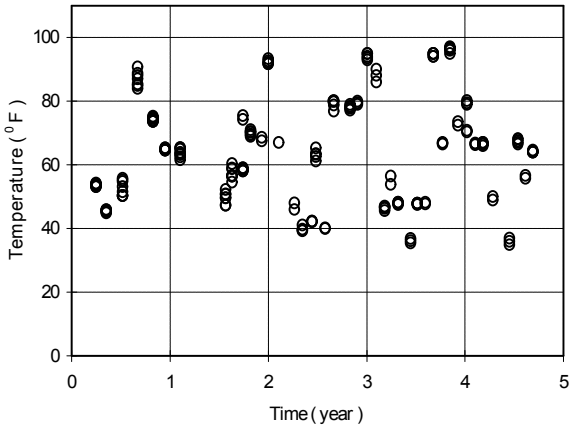

d. Temperatures at depth of reinforcement.

Figure 5.24. Corrosion rates, concreteohmic resistance and temperature over corrosion time, 2.4 lb/yd^3 admixed chloride, outdoor specimens, 3 in. cover.

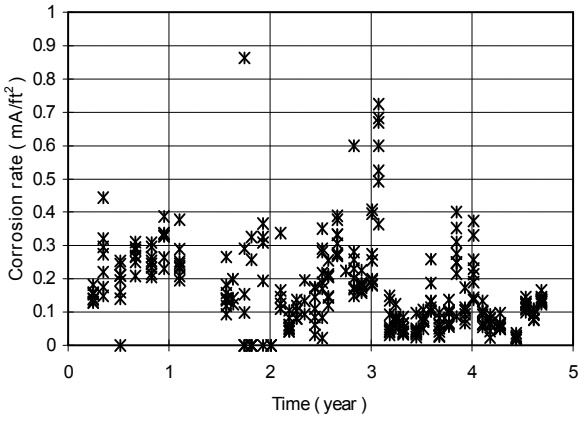

a. Corrosion rates versus time (Gecor device).

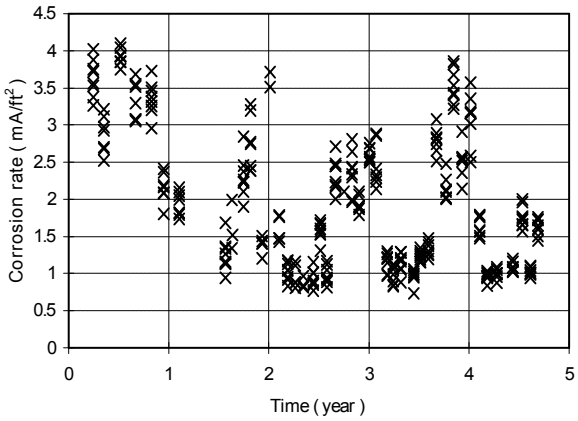

b. Corrosion rates versus time (3LP device)

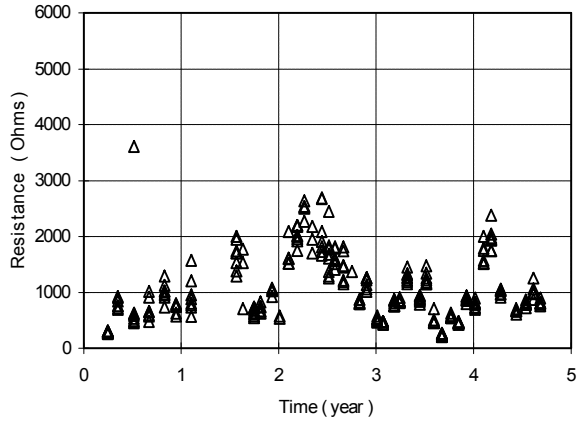

c. Concreteohmic resistances at measurements.

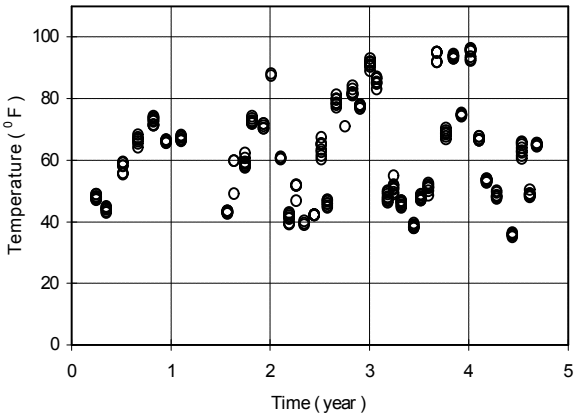

d. Temperatures at depth of reinforcement.

Figure 5.25. Corrosion rates, concreteohmic resistance and temperature over corrosion time, 4.8 lb/yd^3 admixed chloride, outdoor specimens, 3 in. cover.

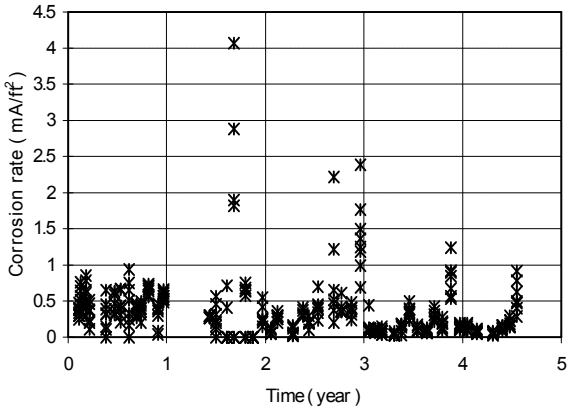

a. Corrosion rates versus time (Gecor device).

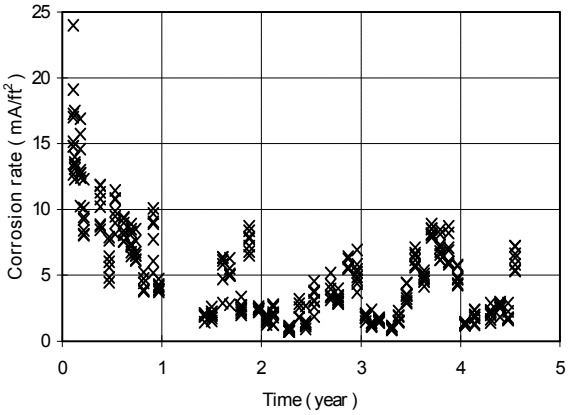

b. Corrosion rates versus time (3LP device)

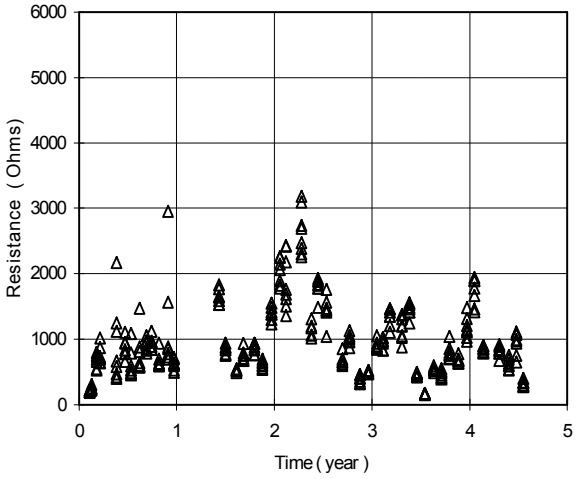

c. Concreteohmic resistances at measurements.

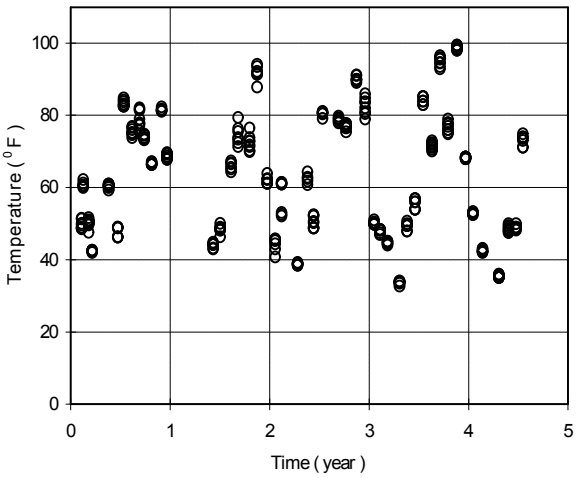

d. Temperatures at depth of reinforcement.

Figure 5.26. Corrosion rates, concreteohmic resistance and temperature over corrosion time, 9.6 lb/yd^3 admixed chloride, outdoor specimens, 3 in. cover.

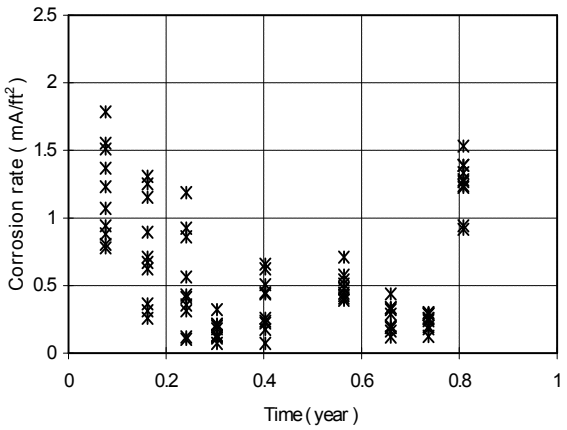

a. Corrosion rates versus time (Gecor device).

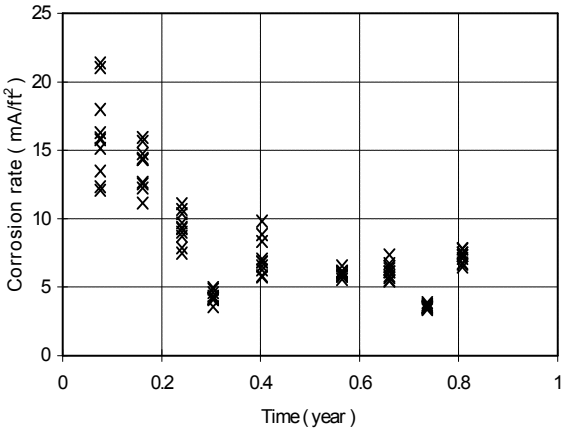

b. Corrosion rates versus time (3LP device)

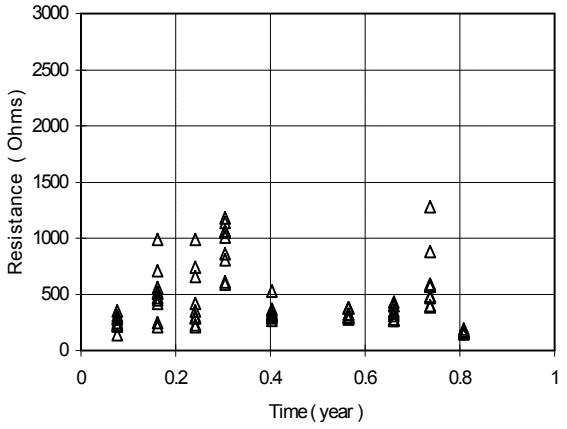

c. Concrete ohmic resistances at measurements.

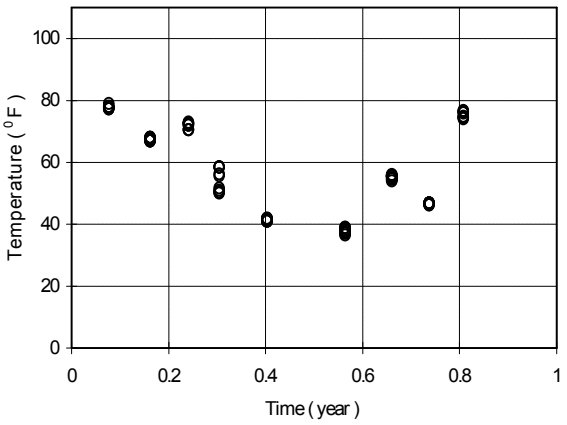

d. Temperatures at depth of reinforcement.

Figure 5.27. Corrosion rates, concrete ohmic resistance and temperature over corrosion time, 12.0 lb/yd^3 admixed chloride, outdoor specimens, 3 in. cover.

For outdoor series, it can be seen from Figures 5.15 to 5.27 that the corrosion rates measured with the 3LP and Gecor devices are strongly affected by the temperature and resistance of concrete at the measurement moment. The dynamic corrosion process is related to the changes of exposure conditions such as temperature, moisture. There is no significant difference in corrosion rates between 2 and 3 in. cover series at same admixed chloride test specimens. Among the admixed chlorides series, the measured corrosion rates increase as the chloride content increases at same time when the amount of the admixed chlorides is above 2.4 lb/yd^3 while below 1.2 lb/yd^3, there is no significant difference in measured corrosion rates. For the low admixed chlorides series, it is noted that the measured corrosion rates are relatively high at the early stage and after about two years reach a low value. This is related to the gradually formation of the passive film on the steel surface. For the high admixed chlorides series, because of high concentration of the chloride ions, the passive film is not easily developed and corrosion takes place continuously; the higher measured corrosion rates are also observed in the early stage which may be related to the change of area ratio of anode and cathode. It is also observed that the resistance of concrete decreases as the admixed chloride content increases at the same time; this is due to the increase of ionic conductivity of concrete as the salt content increases in the pore water of concrete.

Comparing the indoor and outdoor test series, the measured corrosion rates in outdoor are more strongly affected by the environmental conditions.

5.2.3 Chloride Content Analysis

Two test methods, water soluble (ASTM C1218) and acid soluble (ASTM C1152) chloride content analysis, were performed at the age of four-year exposure. The results are summarized in Table 5.2.

Table 5.2. Results of chloride content analysis after four-year outdoor exposure.

Admixed Chloride Content (lb/yd^3)	Acid Soluble Chloride Content (lb/yd^3)	Water Soluble Chloride Content (lb/yd^3)
0.0	0.53	0.28
0.6	1.06	0.50
1.2	1.33	0.74
2.4	2.43	1.73
4.8	4.15	3.54
9.6	8.34	7.15
12.0 *	10.21	9.15

* After 0.83 year outdoor exposure. (1 lb/yd^3 = 0.59 kg/m^3)

There is a good relationship between the results from these two methods, as can be seen in equation 5.1,

$$C_{water} = a\, C_{acid} - b \qquad (5.1)$$

where a and b are coefficients, which mainly depend on amount of cement, type of cement and aggregate used in concrete. From the linear regression analysis, the values of a and b equal 0.932 and 0.459, respectively, for the concrete designed in this study (R^2 = 99 % and RMSE=0.20). Figure 5.28 shows the relationship between water soluble and acid soluble chloride content. Because water soluble method is time consuming, acid method is recommended in the field test.

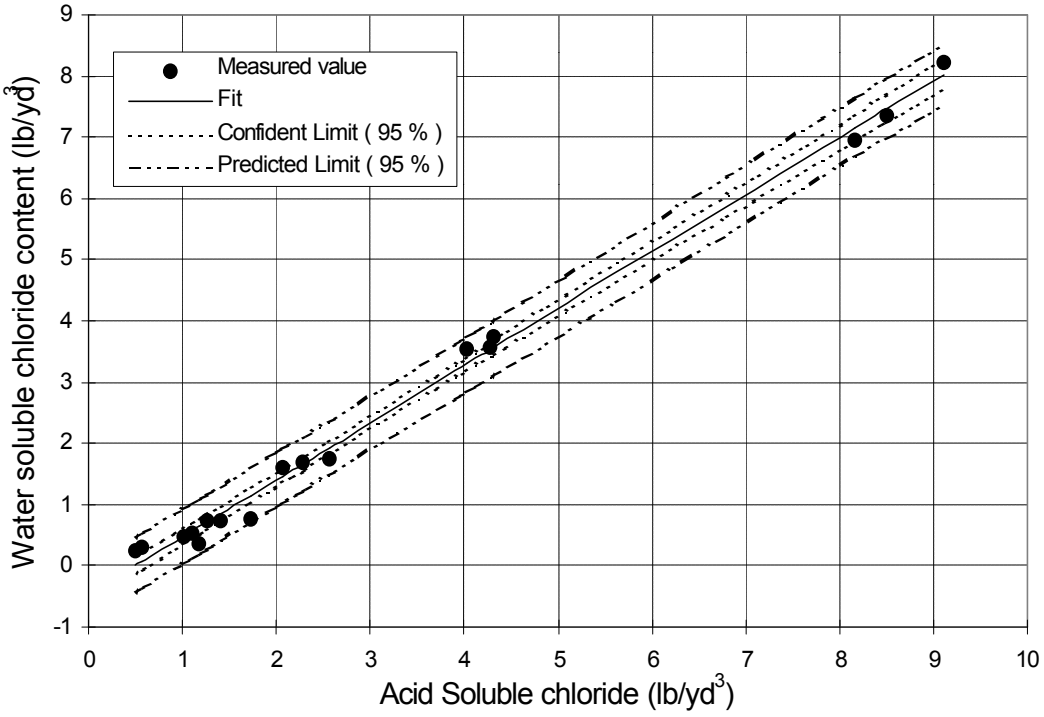

Figure 5.28. Relationships between acid soluble and water soluble chloride content analysis.

5.2.4 Ohmic Resistance of Concrete and Chloride Content

As can be seen in Figures 5.15 to 5.26, the ohmic resistance of concrete is related to the chloride content, temperature and moisture condition in the concrete. The mean of ohmic resistance of the concrete with different admixed chloride series and exposure sites up to five years are summarized in Table 5.3. It can be seen that ohmic resistance of concrete decreases as the chloride content increases from 1.2 lb/yd^3 to 9.6 lb/yd^3. Compared with outdoor series, indoor specimens have much lower ohmic resistance. This is most likely due to weekly spraying of water on the specimens which results in a high moisture content in indoor specimens. The high moisture content can also cause lack of oxygen supply in the cathode area in indoor specimens and slow down the corrosion reactions.

Table 5.3. Mean ohmic resistance of concrete up to five years at different exposure conditions.

Admixed Chloride Content lb/yd^3	Ohmic Resistance of Concrete (ohms)	
	Indoor	Outdoor
0.0	928	2193
0.6	943	2329
1.2	601	1920
2.4	779	1732
4.8	677	1072
9.6	507	935

For the same exposure conditions, the ohmic resistance of concrete is mainly determined by the chloride content. There is a good relationship between resistance of concrete and acid soluble chloride content for outdoor specimens as shown in Figure 5.29.

5.2.5 Relative Humidity in Concrete

The relative humidity in concrete differs from time to time. Figure 5.30 gives the changes of relative humidity in air and in concrete at depth of two inches during a daytime. Although relative humidity in air changes significantly, relative humidity in concrete at depth of two inches changes slightly. Figure 5.31 shows the relative humidity in concrete at depth of two inches at different ages.

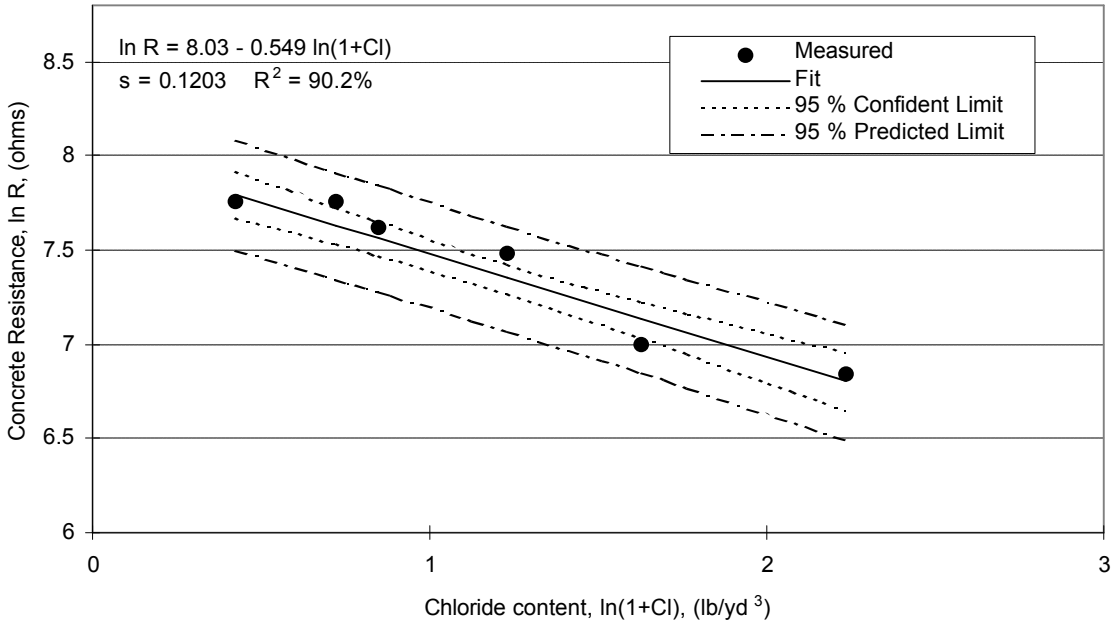

Figure 5.29. Relationship between ohmic resistance of concrete and acid soluble chloride content for outdoor specimens.

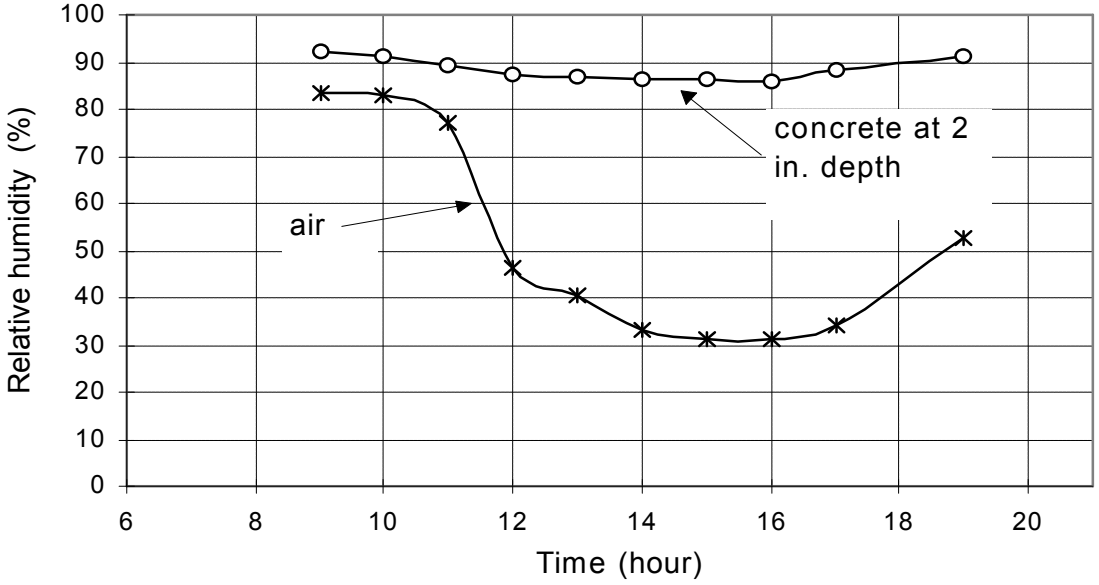

Figure 5.30. Changes of relative humidity in air and concrete at 2 inch depth during a daytime (from 9:00 am to 7:00 pm, Oct. 11, 1995).

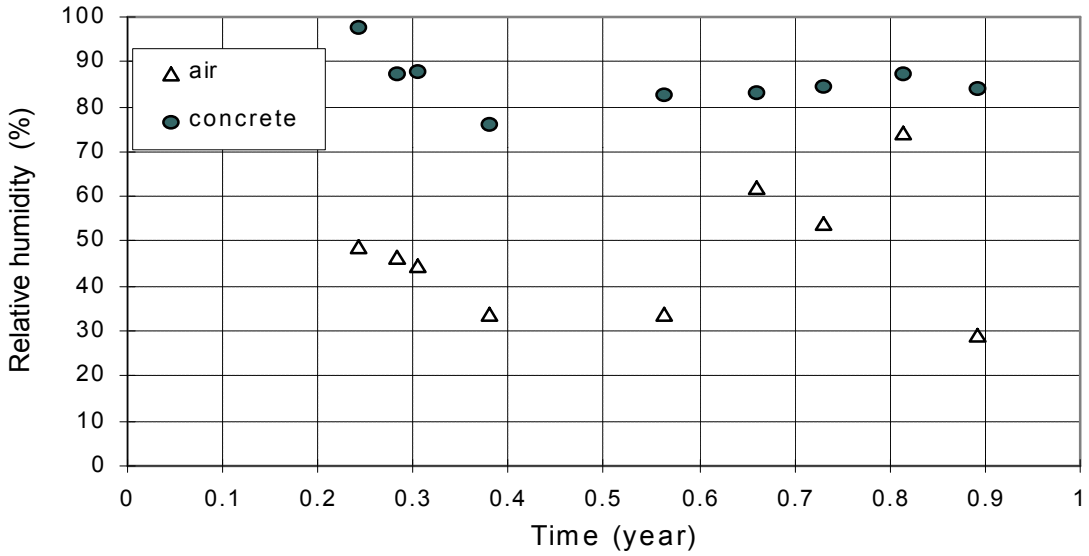

Figure 5.31. Changes of relative humidity in air and concrete at 2 in. depth over time.

5.3 Weight Loss Measurements

Three cores with 4 in. diameter and 5 in. deep were taken from each slab at the time the test specimens cracked. The steel segments were prepared, cleaned, evaluated according to ASTM G1-90, method C3.5 [89]. The calculated mean weight loss and corrosion rates from weight loss method are summarized in Table 5.4.

Table 5.4. Measured weight loss and calculated average corrosion rates over time.

Test Series	Exposure period (year)	Weight loss lb/ft^2 (mg/cm^2)	Mean corrosion rate (mA/ft^2)
OA2859.6	1.84	0.080 (39.3)	2.18
OB3859.6	3.67	0.123 (60.1)	1.67
IA2859.6*	3.67	0.048 (23.6)	0.67
OE18512.0**	0.87	0.061 (29.8)	3.50
OF18512.0**	0.87	0.061 (29.8)	3.50
Block 9.6	2.38	0.080 (39.2)	1.68

*Note: Test series IA28596 has not cracked.

**Note: OE single layer isolated reinforcing steel, OF double layers interconnected reinforcing steel.

The results show that indoor series with same high admixed chlorides has much lower corrosion rate than that of outdoor series with same test series. Due to the difference in corrosion rates, cracking has not occurred in indoor specimens with highest admixed chloride, whereas cracking has already occurred in outdoor specimens with same test series. The differences in the corrosion rates between indoor specimens and outdoor specimens may result from the different moisture contents in the concrete. The high moisture content in indoor specimens may limit the oxygen supply at cathode area and cause a low corrosion rate.

5.4 Comparison of Corrosion Rates by Linear Polarization Method and Weight Loss Method

Based on monthly corrosion measurements by the 3LP and Gecor devices, the mean corrosion rates over time can be calculated. Table 5.5 presents the results from weight loss method and linear polarization method.

Table 5.5. Corrosion rates from different test methods.

Test Series	Exposure period (year)	Mean corrosion rate (mA/ft^2)		
		Weight Loss method	3LP	Gecor
OA2859.6	1.84	2.18	7.89	0.50
OB3859.6	3.67	1.67	4.64	0.39
IA2859.6*	3.67	0.67	5.34	0.45
OE18512.0	0.87	3.50	8.02	0.62
OF18512.0	0.87	3.50	8.22	0.55
Block 9.6	2.38	1.68	6.03	0.36

*Test Series IA28596 has not cracked.

There is a significant difference, generally a factor of 10, between the results of the 3LP and Gecor method. It appears that results from 3LP overestimate the corrosion rates, whereas results from Gecor underestimate the corrosion rates. The under-estimation of the corrosion rates from the Gecor may be related to the high interfacial capacitance of steel in concrete with chloride additions [109]. Since a number of factors such as temperature and ohmic resistance of concrete could affect the results of corrosion rate measurements obtained from 3LP and Gecor devices, corrections for these factors need to be made in order to estimate an equivalent value for corrosion rate and predict the service life. For example, annual mean temperature in Blacksburg, Virginia, is about 52°F (11°C); while the measurements were taken on the outdoor specimens during daytime, and temperatures at the depth of reinforcement varied between 35 to 110°F. The mean temperature for the measurement times was definitely higher than that of annual mean temperature. This may cause an overestimate of the average corrosion rate by the 3LP method. Therefore, the instantaneous corrosion rates from linear polarization method can not be directly

used for predicting the service life of reinforced concrete structures due to corrosion. It is necessary to develop a model to characterize the corrosion rate so that the measured corrosion rate from the linear polarization method can be adjusted to an equivalent value based on annual mean temperature and resistance of concrete. The statistical model for characterizing the corrosion rate based on the obtained corrosion data is presented in section 5.5.

5.5 Modelling the Dynamic Corrosion Process

Corrosion rate is an important parameter for quantitatively predicting the time to cracking and subsequent deterioration processes. As stated in section 5.2 corrosion rate is a dynamic parameter, which varies with changes of climate conditions (such as temperature and relative humidity), exposure time and chloride content. The measured corrosion rate from the linear polarization technology such as 3LP or Gecor device is only an instantaneous value corresponding to a certain temperature and moisture at the measurement moment. Hence, the measured corrosion rate should be adjusted to an equivalent value according to the service exposure conditions, which can be used to predict the service life of reinforced concrete structures.

A non-linear multiple regression model has been proposed to predict the equivalent corrosion rate of steel in reinforced concrete based on the experimental corrosion database obtained in this research using a linear polarization method.

5.5.1 Model Development

Due to the dynamic processes of corrosion of steel in concrete, it is important to develop a time dependent model to characterize the corrosion rate. Thousands of corrosion data including corrosion rates, corrosion potentials, ohmic resistances of concrete and temperatures obtained from monthly corrosion measurements at different levels of chloride contaminated concrete specimens, makes it possible to perform a sound statistical correlation for characterizing corrosion rate data. Based on previous results [106,110], a set of non-linear models among the corrosion rate, temperature, ohmic resistance of concrete and exposure time were performed.

As stated earlier, the measured corrosion rate varies with changes of temperature, chloride content, resistance of concrete and corrosion period. In general, these variables influence the corrosion rate as shown in equations 5.2 - 5.5:

$$i_{cor} = a\, e^{\frac{-Q}{RT}} \qquad (5.2)$$

$$i_{cor} = b\,[Cl^-]^m \tag{5.3}$$

$$i_{cor} = c\,t^n \tag{5.4}$$

$$i_{cor} = d\,R_c^{\,l} \tag{5.5}$$

where i_{cor}: corrosion rate;
T: absolute temperature;
R: gas constant;
Q: thermal activation energy;
$[Cl^-]$: chloride content;
R_c: ohmic resistance of concrete;
a, b, c, d, m, n and l are constants.

The overall effects may be modeled by the collective effects of equations 5.2 to 5.5 as shown in equation 5.6,

$$i_{cor} = k\,e^{\frac{-Q}{RT}}\,[Cl^-]^m\,t^n\,R_c^{\,l} \tag{5.6}$$

One of the best models which contain temperature, concrete ohmic resistance, chloride content and exposure time versus corrosion rate was found using a multiple non-linear regression model based on corrosion data from 3LP method,

$$\ln i_{cor} = A + B \ln Cl + \frac{C}{T} + D\,R_c + E\,t^{-0.215} \tag{5.7}$$

where A, B, C, D and E are regression coefficients;
i_{cor} is the corrosion rate. (mA/ft^2);
Cl is chloride content (lb/yd^3);
T is temperature at the depth of steel surface (in degree Kelvin);
R_c is ohmic resistance of concrete (Ohms);
t is corrosion time (year).

The regression results from the corrosion database (2927 measurements from seven series of chloride contaminated specimens, up to five-year outdoor exposure conditions) are as follows:

$$\ln i = 7.98 + 0.771 \ln Cl - 3006/T - 0.000116\,R_c + 2.24\,t^{0.215} \tag{5.8}$$

where the regression coefficient r is 0.95, and the root mean square error (RMSE) is 0.33. Note that the values of chloride content used for developing this model were obtained from the acid soluble test method (ASTM C1152). However, only free chloride ions influence the corrosion processes. Thus, the following presents the regression equation for water soluble chlorides,

$$\ln i = 8.37 + 0.618 \ln Cl - 3034/T - 0.000105 R_e + 2.32 t^{-0.215} \qquad (5.9)$$

where the regression coefficient r is 0.95, and the root mean square error (RMSE) is 0.33.

The predicted values obtained from the above regression model are well fitted with the measured corrosion rates (see Figure 5.32). Figures 5.33 to 5.38 illustrate the measured corrosion rates at different times and the model predicted values for the admixed chloride 2.4, 4.8 and 9.6 lb/yd^3 outdoor specimens, respectively.

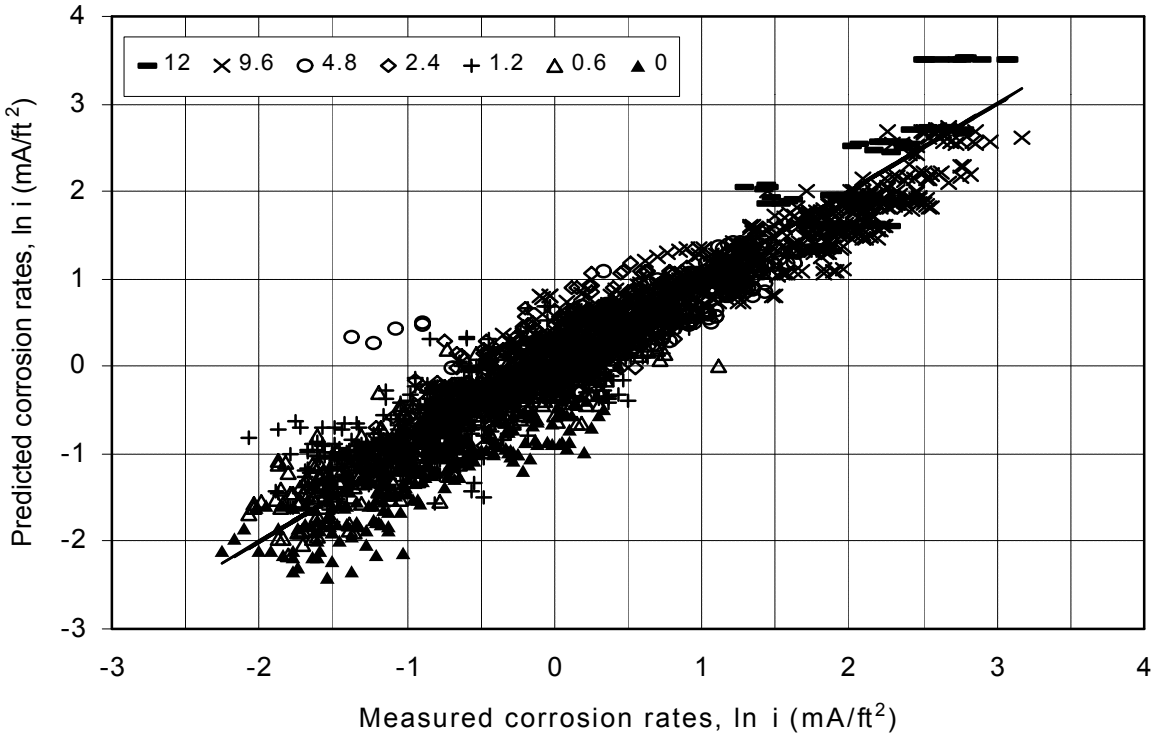

Figure 5.32. The measured corrosion rates versus model predicted values.

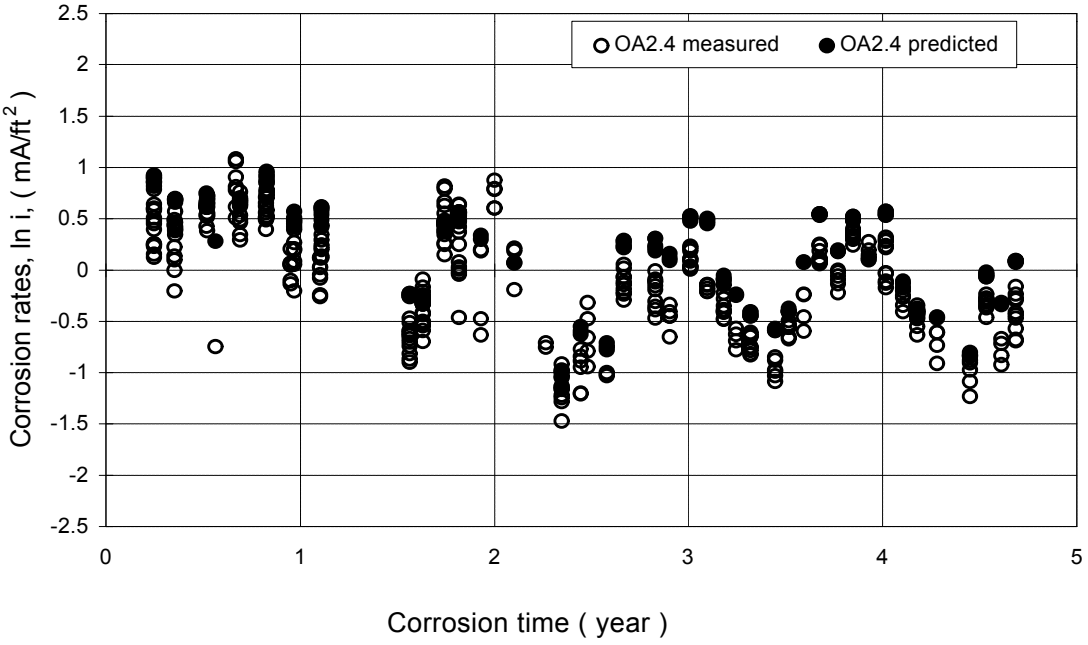

Figure 5.33. Measured corrosion rates and predicted values over time, admixed chloric 2.4 lb/yd^3, 2 in. cover depth, outdoor exposure.

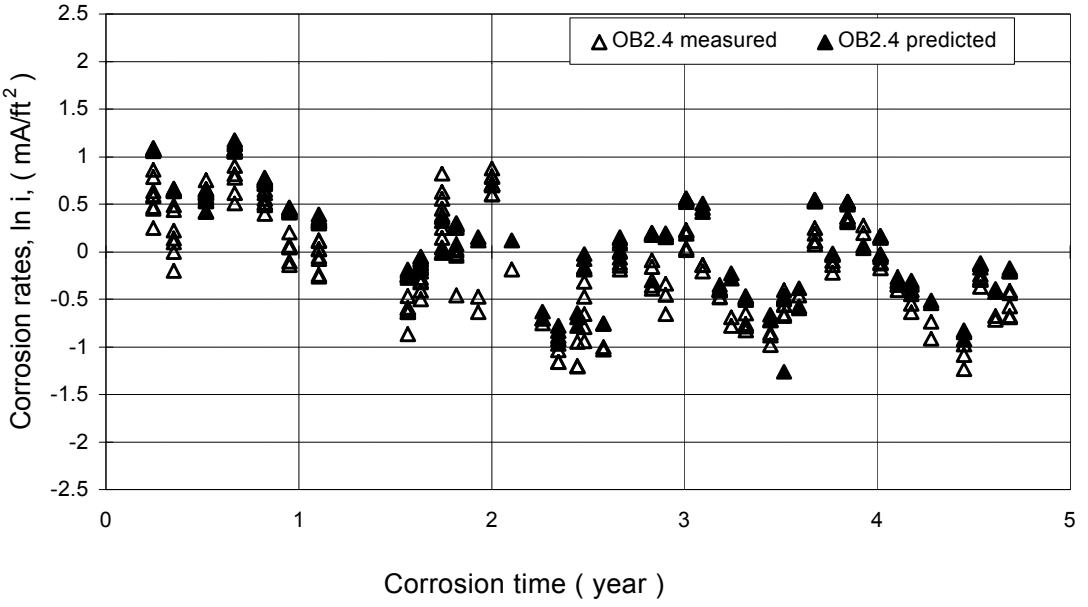

Figure 5.34. Measured corrosion rates and predicted values over time, admixed chloride 2.4 lb/yd^3, 3 in. cover depth, outdoor exposure.

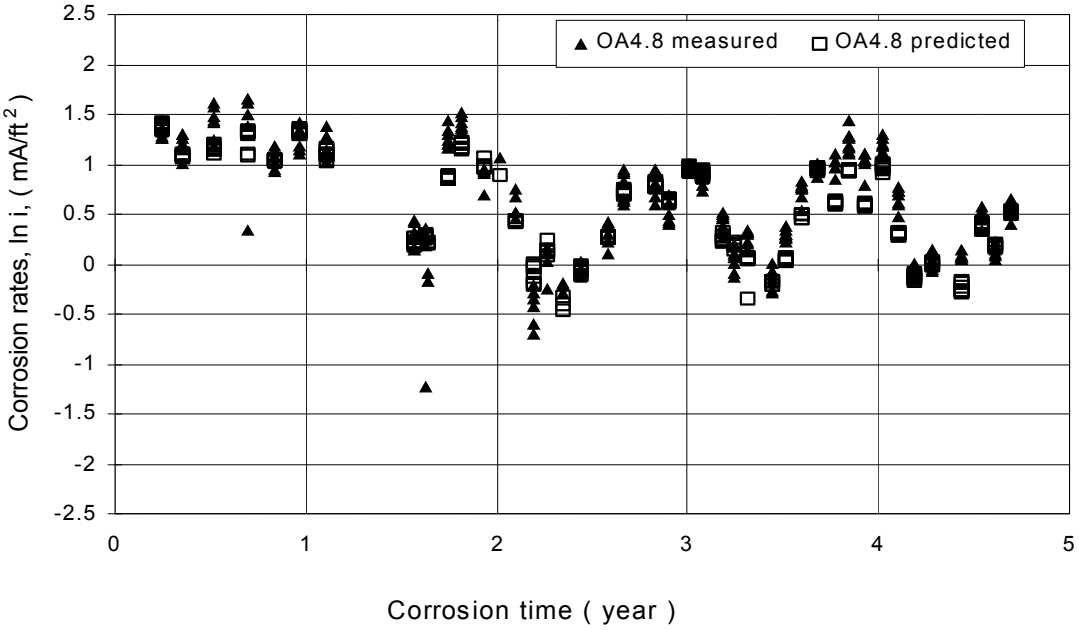

Figure 5.35. Measured corrosion rates and predicted values over time, admixed chloric 4.8 lb/yd^3, 2 in. cover depth, outdoor exposure.

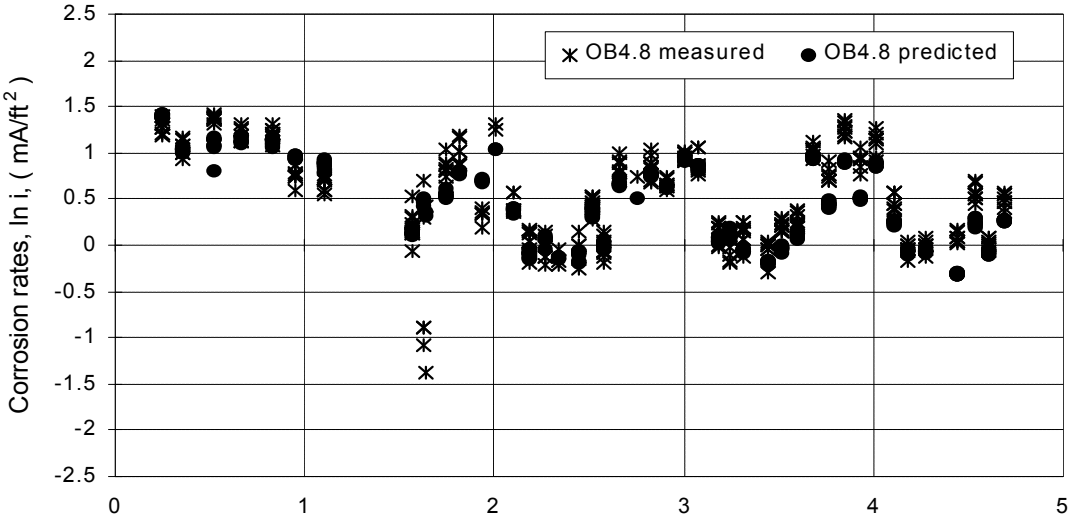

Figure 5.36. Measured corrosion rates and predicted values over time, admixed chloride 4.8 lb/yd^3, 3 in. cover depth, outdoor exposure.

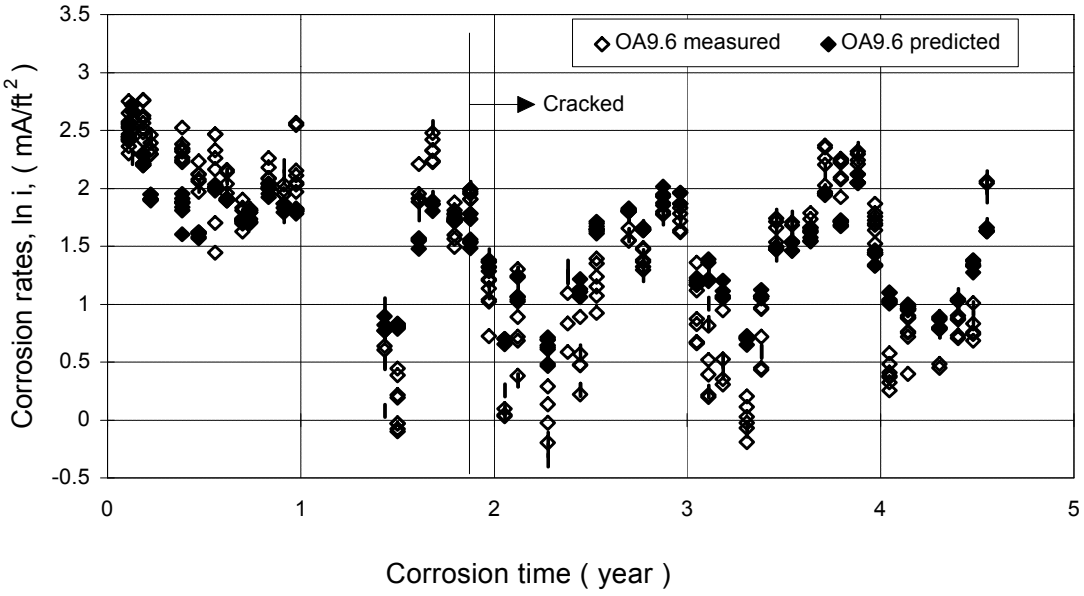

Figure 5.37. Measured corrosion rates and predicted values over time, admixed chloric 9.6 lb/yd^3, 2 in. cover depth, outdoor exposure.

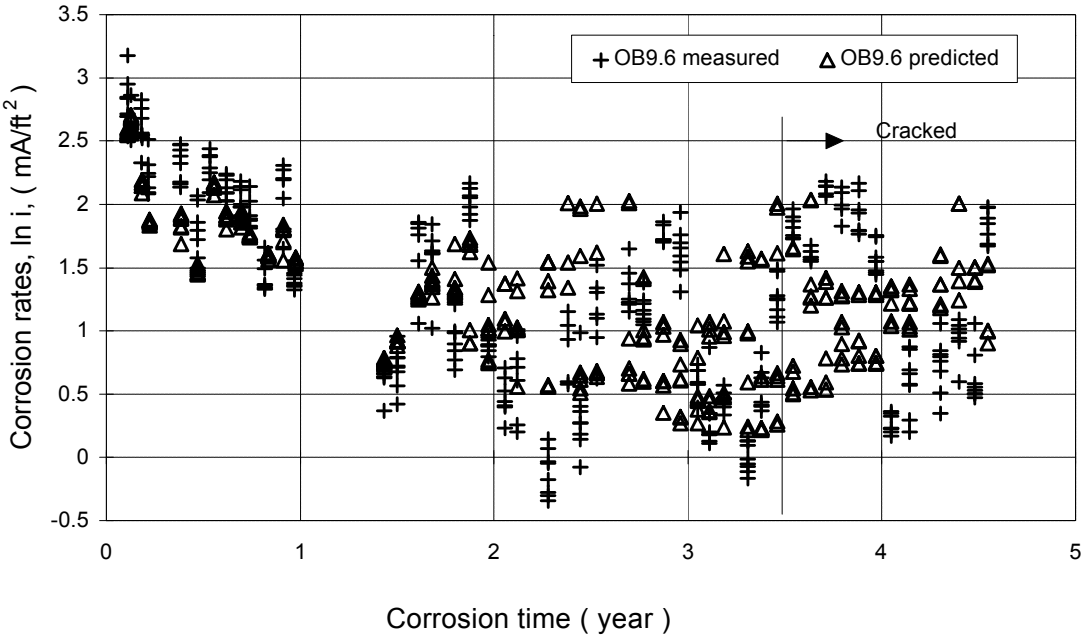

Figure 5.38. Measured corrosion rates and predicted values over time, admixed chloride 9.6 lb/yd^3, 3 in. cover depth, outdoor exposure.

Figures 5.37 and 5.38 also illustrate that predicted corrosion rates are in agreement with the measured corrosion rates before cracking. However, after cracking, the variations between the measured corrosion rates and predicted values are higher. This is most likely due to the change in the oxygen diffusion and moisture conditions after the concrete cracks.

No such correlation was found for the measured corrosion rates obtained from the Gecor device. This may be most likely due to the high variations in the measured corrosion rates within the test corrosion cells [106].

5.5.2 Model Interpretations

The effects of significant variables such as temperature, chloride content, corrosion time and resistance of concrete, which influence the corrosion rate, can be shown from equation 5.8, and will be briefly discussed in the following paragraphs.

Temperature

Temperature has a significant effect on corrosion rate of steel in concrete as described in section 2.2.4. The regression model also indicates the similar relationship of temperature and corrosion rate as shown in equation 2.26 and Clear's equation 2.27. In general, corrosion rates rise as the temperature increases. If the other parameters are held constant, the calculated corrosion rates at different temperature using this model is illustrated in Figure 5.39.

Because changes of temperature in concrete will also result in changes of other parameters such as resistance of concrete and oxygen diffusion, the overall effect of temperature on corrosion rate in concrete is very complex and controlled by interactions among other factors. In case of dry environment, the corrosion rate can be relatively small even at a high temperature due to a high resistance of concrete.

Ohmic Resistance of Concrete

Degree of saturation of concrete also has a major effect on the corrosion processes; it influences the diffusion of oxygen and ionic ohmic resistance of concrete. The ohmic resistance of concrete may change significantly from more than 10^4 ohms in a dry environment to about several hundred ohms when concrete is saturated. In fully saturated concrete or dry concrete, the corrosion rate is very slow or the corrosion process stops. As is known, corrosion of steel in concrete requires a sufficient supply of oxygen to provide the cathodic corrosion reaction as well as moisture to act as an electrolyte of low resistance. Usually, the oxygen availability at the steel surface exceeds the amount needed for corrosion for normal outdoor exposure of concrete [111].

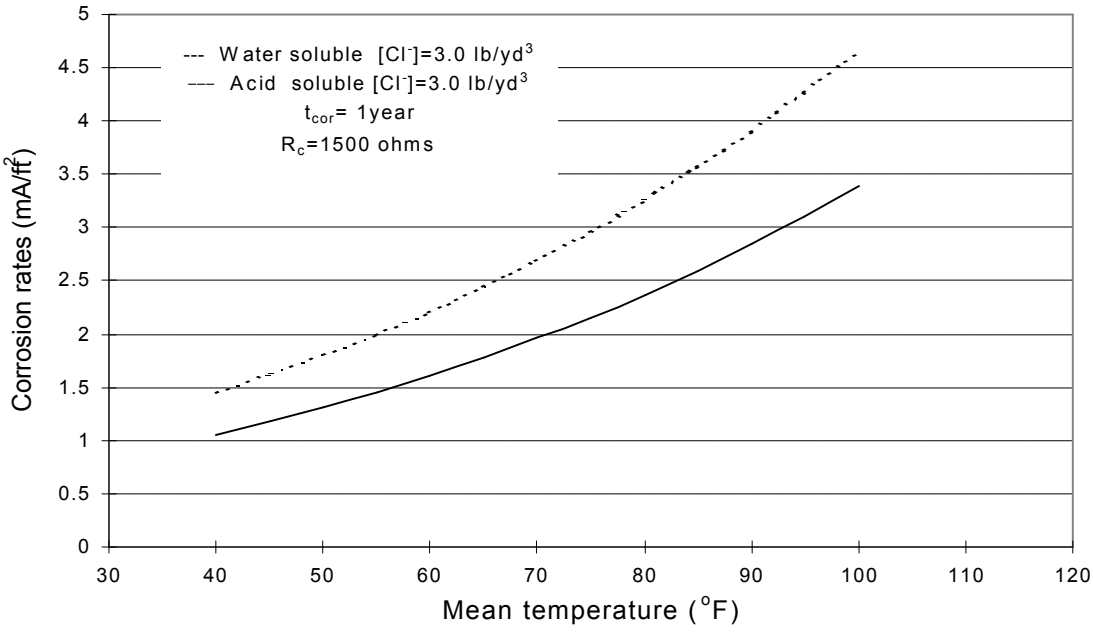

Figure 5.39. Effects of temperature on the corrosion rate.

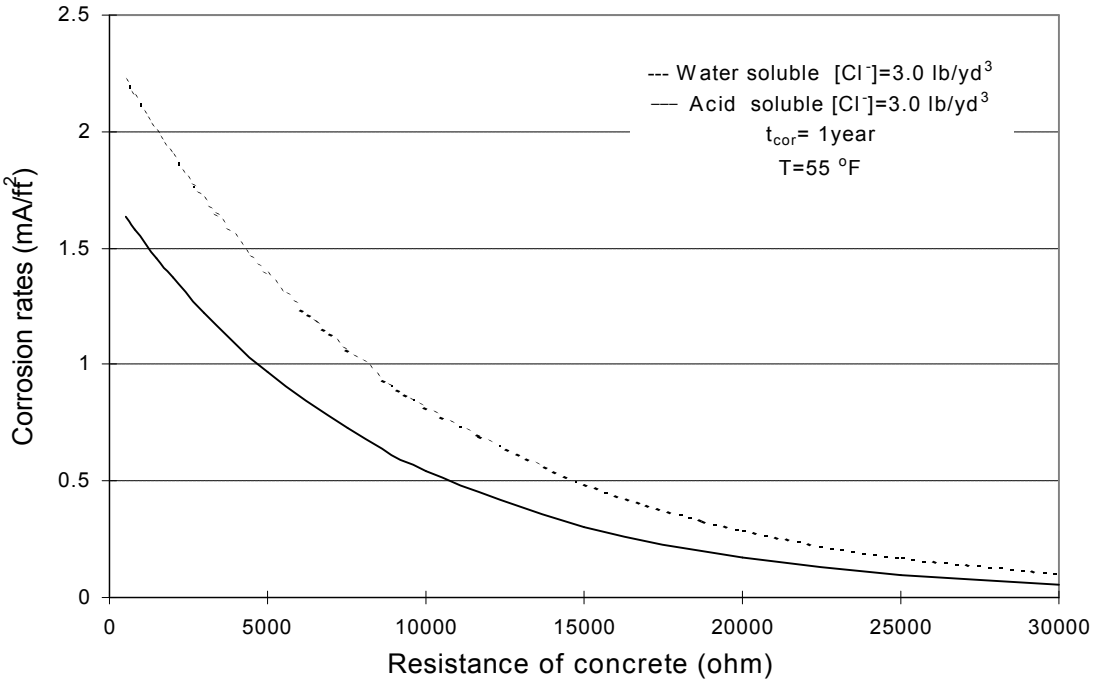

Figure 5.40. Effects ofohmic resistance of concrete on the corrosion rate.

Therefore, corrosion rate of steel in concrete increases as concrete ohmic resistance decreases in the normal outdoor exposure conditions. The regression model also shows the similar relationship between corrosion rate and ohmic resistance of the concrete. Figure 5.40 illustrates the influence of degree of saturation on corrosion rate which varies with the ohmic resistance of the concrete.

Only for the case of reinforced concrete structures totally immersed in water, the corrosion rate is controlled by the oxygen supply and corrosion takes place very slowly, although the ohmic resistance is very low. Therefore, the model can not be used for the cases where the corrosion rate is primary controlled by cathodic reaction.

Chloride Content

The regression results show that value of corrosion rate increases as the amount of chloride content increases in concrete, which indicates that corrosion rate will be higher at a high level of chloride contaminated concrete than that at a low level. This is due to the increase of conductivity of concrete as chloride ions increase, and chloride ions can also complex with ferrous ions to form a water soluble product which can also accelerate the corrosion processes. Figure 5.41 illustrates the effect of chloride content on corrosion rate.

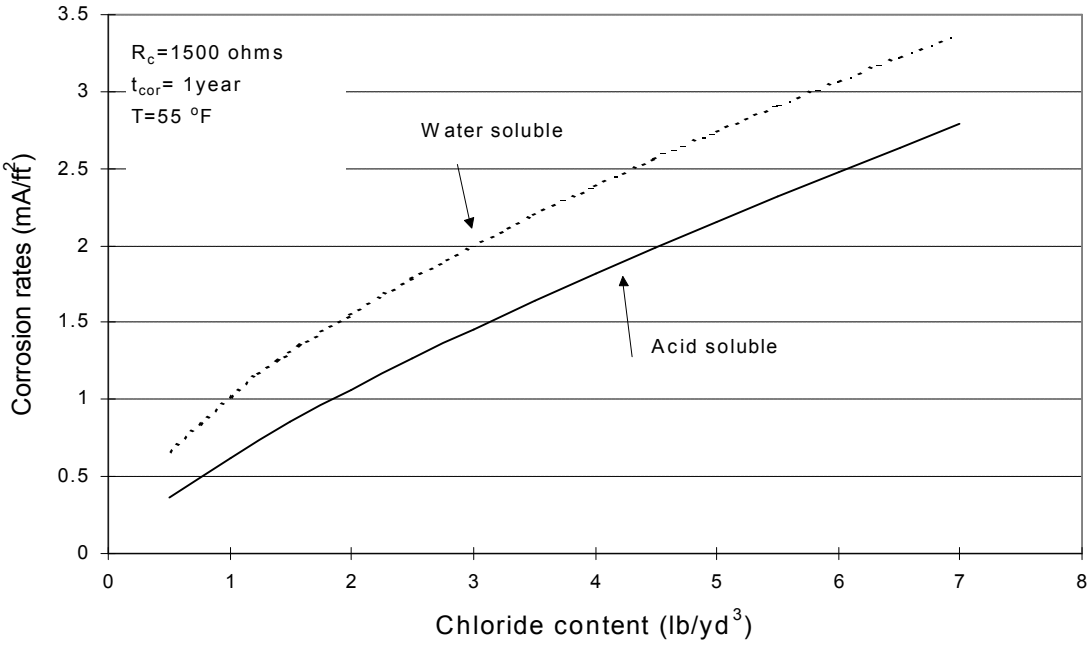

Figure 5.41. Effects of chloride content on the corrosion rate.

Exposure Time

Corrosion exposure time has a significant effect on the corrosion rate during early stages after corrosion initiation (see Figure 5.42). The corrosion rate decreases rapidly at the early stage (first year after initiation) and then tends to reach a near constant value. This is due to the changes of ratio of anode and cathode area, and also results from the formation of the rust products on the steel surface which slows down the diffusion of iron ions away from the steel surface.

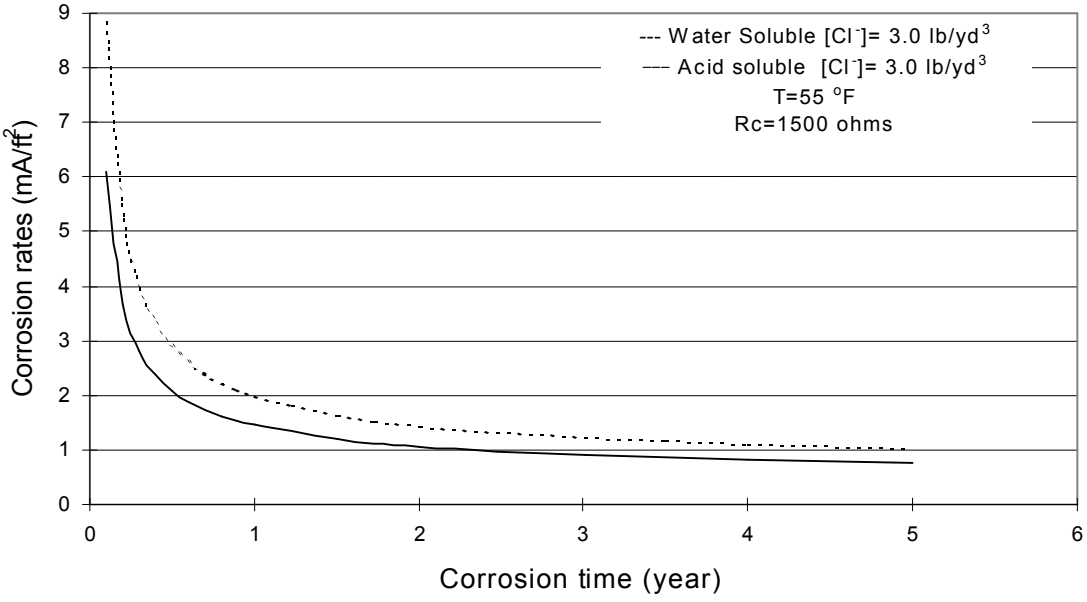

Figure 5.42. Effects of corrosion time on the corrosion rate.

Cover Depth

From the model, the corrosion rate appears not to be affected by cover depth. However, because there is a slight difference in temperature and moisture at different cover depths, these parameters may affect the corrosion rate. The experimental results showed that the corrosion rate at 2 inch cover depth was about 5 % higher than that of 3 inch cover depth because there was about 1 to 2 ^{o}F difference in the mean temperature between two cover depths. Figure 5.43 shows the changes of temperature at different cover depths due to changes of air temperature during a particular day.

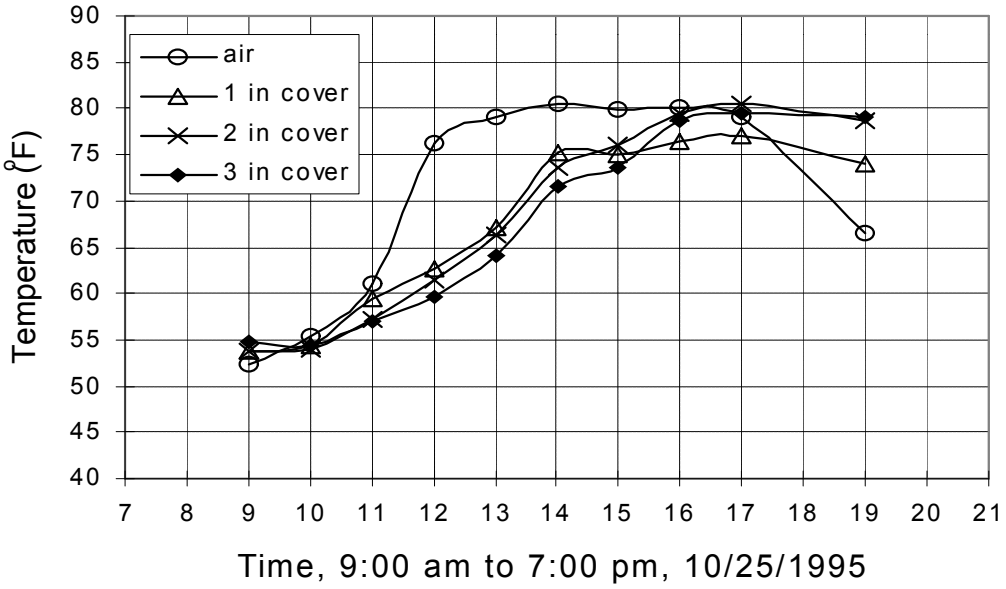

Figure 5.43. Changes of temperatures at different cover depths during daytime.

As stated above, the effects of temperature, chloride content, resistance of concrete and corrosion time on corrosion rate can be well explained by the model. Based on an annual mean of temperature, resistance of concrete and amount of chloride at depth of reinforcement, corrosion rate of steel in concrete can be estimated from the above model. The service life of chloride induced corrosion of reinforced concrete structure, which is a function of corrosion rate, can also be predicted.

5.5.3 Model Applications

The annual mean temperature in Blacksburg, Virginia, is about 52 ºF, and ohmic resistance of concrete may be taken from Table 5.3. According to equation 5.8, the adjusted corrosion rate for 3LP can be obtained. The results are summarized in Table 5.6.

As seen from the table, the adjusted corrosion rates by the model are still about 1.5 - 1.6 times higher than that from weight loss. This is due to the fact that the actual polarization area for the

3LP device is larger than the nominal polarization area. Therefore, the equivalent corrosion rate may be taken as the adjusted corrosion rate by the model divided by a factor of 1.5 to 1.6.

Table 5.6. Adjusted corrosion rates and measured corrosion rates.

Series	corrosion time	W_{loss} (mA/ft^2)	3LP (mA/ft^2)	Adjusted (mA/ft^2)
OA2859.6	1.84	2.18	7.89	3.33
OB3859.6	3.67	1.67	4.64	2.59
OE(F)18512.0	0.87	3.50	8.12	5.54
Block9.6	2.38	1.68	6.03	2.80

1 mA/ft^2 = 1.076 $\mu A/cm^2$

Because the proposed model was developed from the admixed chloride concrete, as is known, there is a significant difference in chloride concentration in the pore solution for the same amount of chloride content between admixed chloride concrete and field concrete. For the admixed chloride concrete, chloride ions may be uniformly distributed in the concrete and some of them have already combined with cement hydrates; while for the field concrete, chloride ions, which mainly come from the environment, may mainly present in the concrete around concrete pore systems. Because only the concentration of chloride ions in pore solution has a great effect on the corrosion process, further work needs to be done on determining the difference in chloride concentration in concrete pore solution between admixed chloride concrete and field concrete before using the proposed model for predicting the corrosion rate.

5.6 Modeling the Time to Cracking

The existing models for predicting the time to cracking, as presented in section 3.2 and 3.3, underestimate the time to cracking of corrosion of steel in concrete and need to be modified. Based on observed times to cracking and measured corrosion rates, a corrosion-cracking model has been suggested and time to cracking has been modelled using the critical amount of corrosion products.

5.6.1 Corrosion-Cracking Model

It is well recognized that mechanism of corrosion damage of reinforced concrete is due to the formation of rust products on the steel surface which has about 4 to 6 times higher volume than that of steel to induce expansive stress and cause cracking and spalling of the cover concrete. Although, corrosion takes place in concrete as pitting corrosion and thus non-uniformly, it is

assumed that uniform corrosion products are formed around the steel surface to simplify the analysis. The uniform corrosion products result in a uniform expansive stress applied to the surrounding concrete. Not all of corrosion products are responsible for the expansive pressure, some of them may fill the voids around the steel/concrete interface or migrate away from the steel/concrete interface. Due to the complexity of the problem, corrosion cracking is only restricted to the stresses resulting from the expansion of corrosion products. Other effects such as dynamic loading, freezing and thawing are not considered at this time, although they may influence the processes of corrosion damage. Figure 5.44 shows a schematic diagram of the basic model for the corrosion-cracking processes.

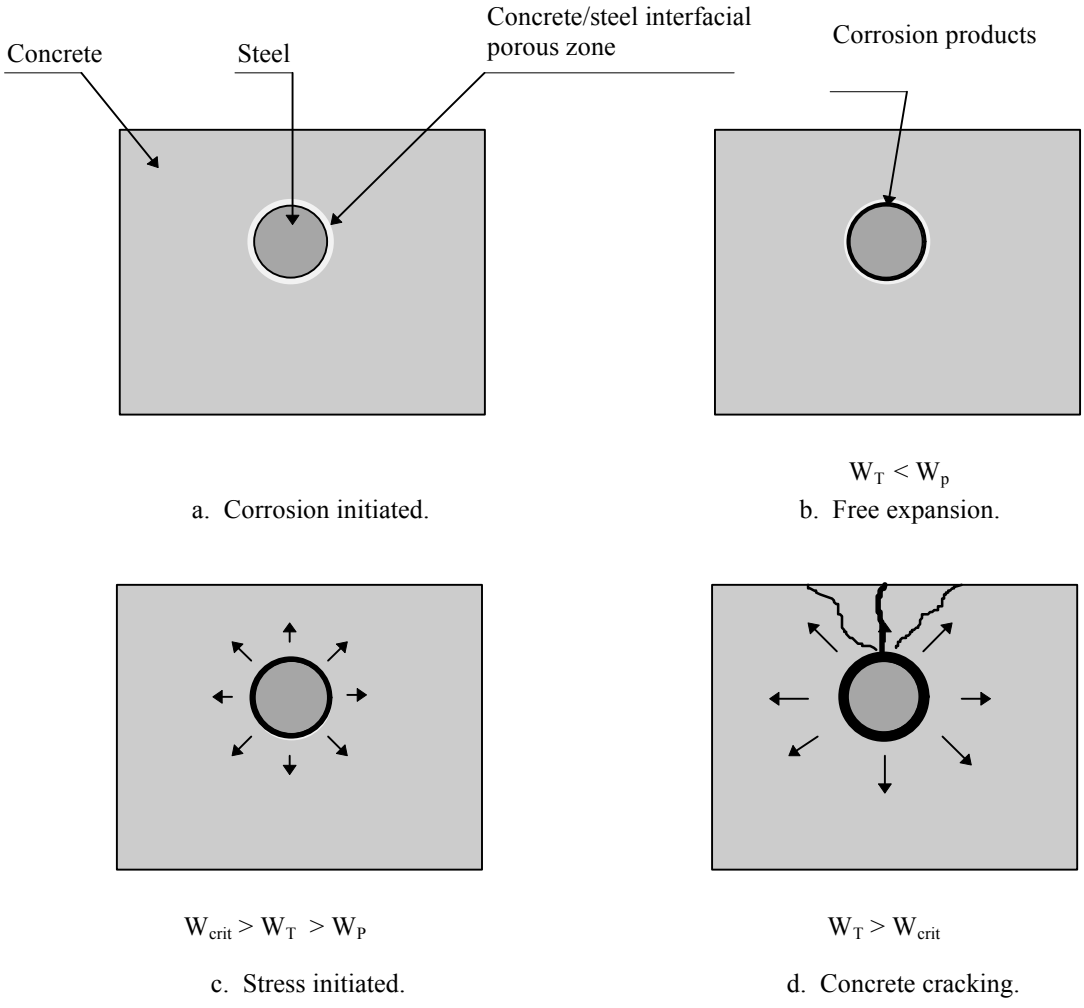

Figure 5.44. A schematic diagram of the corrosion-cracking processes.

There are three stages considered in the proposed model and are briefly explained as follows:

a. Free Expansion. As the passive film is broken by chloride ions, the metallic Fe at the anode is oxidized to form ferrous ions, which can react with hydroxyl ions to produce ferrous hydroxide and then can be further converted to hydrated ferric oxide. In the present model, it has been assumed that there exists a porous zone around the steel/concrete interface caused by the transition from cement paste to steel, entrapped / entrained air voids and corrosion products diffusing into the cement paste capillary voids. The volume of this porous zone is directly related to the surface area of reinforcement, W/C ratio, degree of hydration and degree of consolidation. As the corrosion takes place on the surface of the steel, the porous zone will gradually fill with the corrosion products. When the total amount of corrosion products, W_T, is less than the amount of corrosion products required to fill the porous zone around the steel/concrete interface, W_P, the formation of corrosion products at this stage will not create any stress on the surrounding concrete.

b. Stress Initiation. As the total amount of corrosion products, W_T, exceeds the amount of corrosion products needed to fill the porous zone around the steel/concrete interface, W_P, the formation of corrosion products starts to create expansive pressure on the surrounding concrete, and this pressure increases with an increase in corrosion products.

c. Cracking. When the total amount of corrosion products, W_T, reaches the critical amount of corrosion products, W_{crit} (the limiting amount of the corrosion products needed to induce cracking of the cover concrete), the internal stress from the volume increase of rust products will exceed the tensile strength of concrete and crack the cover concrete. It is obvious that W_{crit} is mainly dependent on quality of concrete and cover depth. The value of W_{crit} should be relatively high in high strength concrete with a thick cover depth, while it is small in low strength concrete with a thin cover depth.

There are two important concepts, W_P and W_{crit}, in this suggested model, and time to cracking can be predicted based on these values. Some assumptions are necessary to estimate W_P and W_{crit}, and are discussed in detail in the following paragraphs.

Estimation of W_P

The amount of the corrosion products needed to fill the porous zone around the steel/concrete interface is difficult to measure. Further work needs to be conducted on quantitatively estimating the total volume of these interconnect pores around the steel/concrete interface.

Considering the steel/concrete interface is somewhat like the transition zone between cement paste and aggregate and influenced by the water/cement ratio, degree of consolidation and hydration, aggregate sizes and steel reinforcement, the value of W_P may be expressed as,

$$W_P = r_{rust} V_P \quad (5.10)$$

where r_{rust} is the density of corrosion products and V_P is the total volume of interconnected pores around the steel/concrete interface.

Let d_0 denote the thickness of porous zone around the steel/concrete interface, which depends on the total volume of interconnected pores around the steel/concrete interface. A steel bar having originally diameter D will increase its diameter to $D+2d_0$, when the amount of corrosion products reaches W_P. For a unit length of steel bar, since $d_0 << D$, W_P can be estimated from equation 5.11,

$$W_P = \pi \rho_{rust} d_0 D \quad (5.11)$$

It can be seen that W_P is related to the size of the reinforcement, density of rust products and property of steel/concrete interface.

Estimation of W_{crit}

The critical amount of rust products consists of two parts, W_P, the amount of corrosion products to fill the total interconnected porous around the steel/concrete interface, and W_S, the amount of corrosion products that generate the critical tensile stresses. As $d_s << D$, for a unit length of steel bar, the value of W_S can be estimated from equation 5.12,

$$W_S = \rho_{rust} \left(\pi (D + 2d_0) d_s + \frac{W_{st}}{\rho_{st}} \right) \quad (5.12)$$

where r_{rust}: the density of corrosion products;
r_{st}: the density of steel;
d_0 : the thickness of pore band around the steel/concrete interface;
d_s : the thickness of corrosion products to generate the tensile stresses.
D: the diameter of steel reinforcement;
W_{st}: mass of steel corroded.

Based on equations 5.11 and 5.12, the critical amount of corrosion products may be re-written as following:

$$W_{crit} = \rho_{rust} \left(\pi (d_s + d_0) D + \frac{W_{st}}{\rho_{st}} \right) \quad (5.13)$$

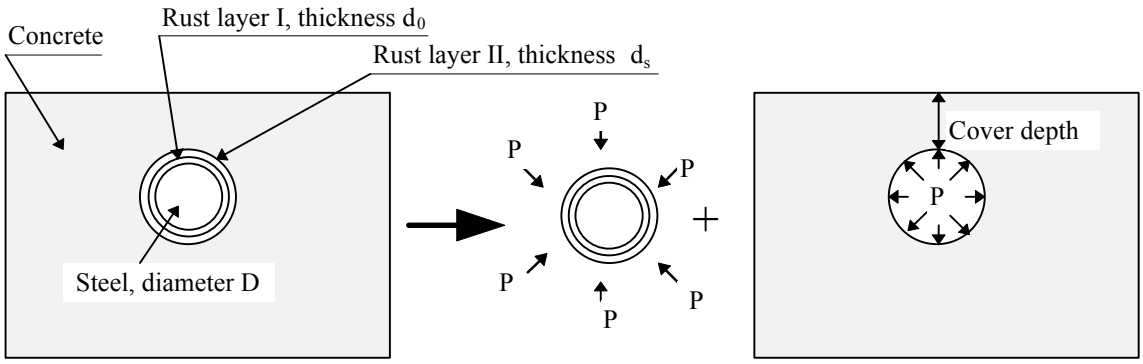

Figure 5.45. Expansive pressure on surrounding concrete due to formation of rust products.

Note that W_{st}, the amount of steel corroded equals αW_{crit}, in which α is the molecular weight of steel divided by the molecular weight of corrosion products. Value α depends on the kind of corrosion products, for example, α equals 0.523 when corrosion products are considered as $Fe(OH)_3$ and 0.622 for $Fe(OH)_2$.

The thickness of corrosion products, d_s, needed to generate the critical tensile stress which induces cracking of the cover concrete, can be routinely solved by the finite element method [12,112-113]. Figure 5.45 gives the diagram of interactions of reinforcing steel, rust products layer and surrounding concrete. Considering concrete to be a homogeneous elastic material and a thick-wall concrete cylinder with inner radium $a = (D+2d_0)/2$, and outer radium $b = C + (D+2d_0)/2$, in which C is cover depth, then the pressure P at concrete/rust products interface can be expressed as [114],

$$P = \frac{2E_{ef}d_s}{(D+2d_0)\left(\frac{b^2+a^2}{b^2-a^2}+\nu_c\right)} \qquad (5.14)$$

where ν_c is Poisson's ratio of the concrete, E_{ef} is an effective elastic modulus of the concrete which $E_{ef} = E_c/(1+\phi_{cr})$, E_c is elastic modulus of the concrete and ϕ_{cr} is the creep coefficient of the concrete. d_s is the radical displacement of the concrete under pressure P, in this particular case, because elastic modulus of steel is about seven times more than that of concrete, it is considered that the radical displacement of the concrete under pressure P is the thickness of corrosion products generating the pressure on the concrete.

If, at failure, considering that cracking occurs just over the reinforcement (the observed corrosion cracks in reinforced concrete structures are mostly located above the steel rebars, as shown in Figure 5.1), the minimum stress required to cause cracking of the cover concrete equals the tensile strength of concrete,

$$P = \frac{2Cf_t'}{D + 2d_0} \tag{5.15}$$

where C is the cover depth of concrete and f_t' is the tensile strength of concrete.

From equations 5.14 and 5.15, d_s may be expressed as,

$$d_s = \frac{Cf_t'}{E_{ef}} \left(\frac{a^2 + b^2}{b^2 - a^2} + \nu_c\right) \tag{5.16}$$

Therefore, the critical amount of corrosion products needed to induce cracking of the cover concrete can be estimated from equations 5.13 and 5.16,

$$W_{crit} = \rho_{rust} \left(\pi \left[\frac{Cf_t}{E_{ef}} \left(\frac{a^2 + b^2}{b^2 - a^2} + \upsilon_c\right) + d_0 \right] D + \frac{W_{st}}{\rho_{st}} \right) \tag{5.17}$$

It can be seen that the critical amount of corrosion products needed to induce cracking of the cover concrete is mainly dependent on the tensile strength of concrete, cover depth , elastic modulus of concrete and properties of steel/concrete interface.

5.6.2 Growth of Rust Products

As the rust layer grows thicker, the ionic diffusion distance increases, and the rate of rust production decreases because the diffusion is inversely proportional to the oxide thickness. The rate of rust production can be written as follows,

$$dW_{rust} / dt = k_p / W_{rust} \tag{5.18}$$

where W_{rust} is amount of rust products (lb/ft), t is corrosion time (year) and k_p is the rate of rust production. k_p is related to the rate of metal loss, which may be expressed in terms of corrosion rate,

$$k_p = 2.59 \times 10^{-6} (1/a)\, p D\, i_{cor} \qquad (5.19)$$

in which a is related to types of rust products, D is the steel diameter (in.) and i_{cor} is the annual mean corrosion rate (mA/ft^2).

Integrating equation 5.18, the growth of rust products can be obtained,

$$W_{rust}^2 = 2 \int_0^t k_p \, d\, t \qquad (5.20)$$

By knowing the corrosion rate, the amount of rust products for a certain period of corrosion can be estimated.

5.6.3 Time to Cracking

As stated earlier, when the total amount of corrosion products reaches the critical amount of rust products, the internal expansion stress will exceed the tensile strength of concrete and cause the cracking of the cover concrete. According to equation 5.20, for a constant corrosion rate, the time to cracking, t_{cr} can be given as follows:

$$t_{cr} = \frac{W_{crit}^2}{2\, k_p} \qquad (5.21)$$

where W_{crit} is the critical amount of corrosion products. Since corrosion rate is a function of corrosion time as presented in equation 5.8, using the numerical method, the time to cracking can be also calculated from equation 5.20.

Figures 5.46 and 5.47 present the analysis results by the model for the time to corrosion cracking of the cover concrete at different conditions. As can be seen from the figures, the time to corrosion cracking of the cover concrete is mainly influenced by the corrosion rate, tensile strength of concrete, concrete cover depth and type of corrosion products.

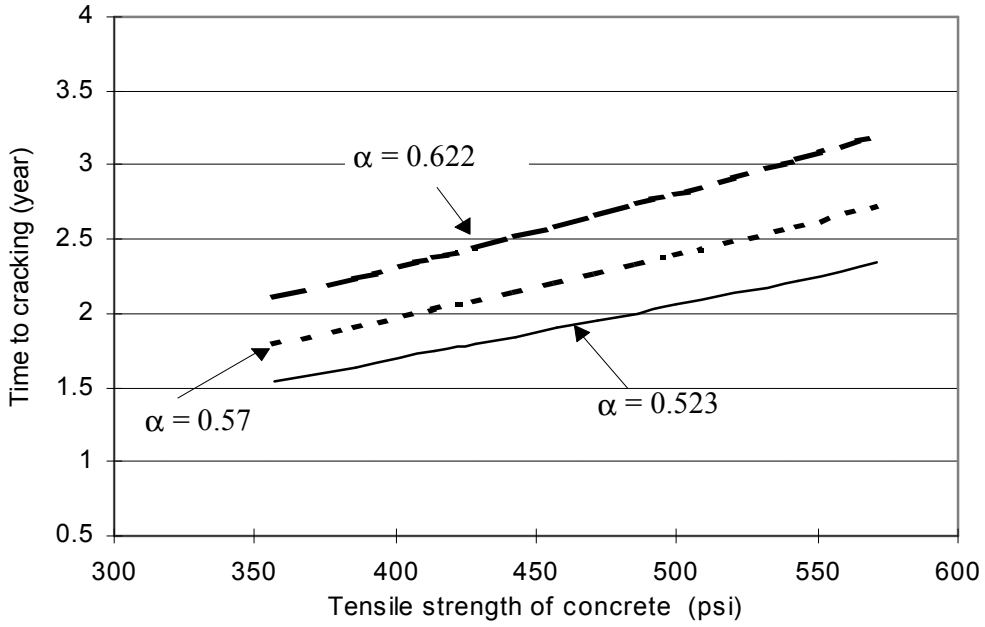

Figure 5.46. Effects of tensile strength of concrete and type of corrosion products time to cracking (2 in. cover depth and corrosion rate 2 mA/ft^2)

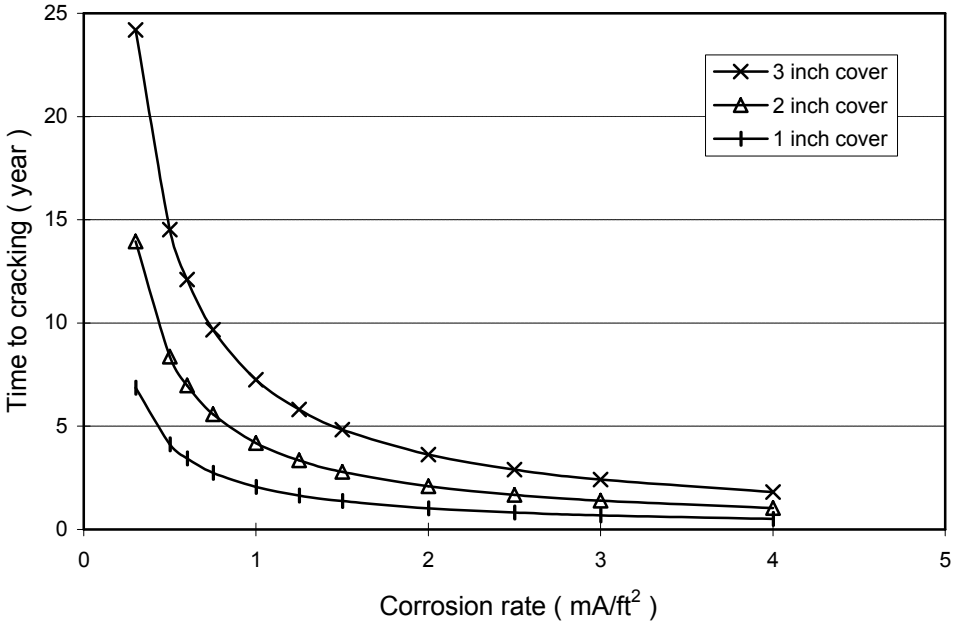

Figure 5.47. Effects of corrosion rates and cover depths on the time to cracking. (f'_t = 472 psi, E_c = 3,900,000 psi and α =0.57)

5.6.4 Applications of the Proposed Models

For outdoor specimens, f'_c = 4500 psi (31.5 MPa), let us take tensile strength, f'_t=472 psi (3.3 MPa); elastic modulus of concrete, E_c = 3,900,000 psi (27 GPa) and creep coefficient φ_{cr} = 2.0; Poisson ratio, ν_c = 0.18; density of rust products, ρ_{rust} = 225 lb/ft^3 (3600 kg/m^3); assume that the composition of rust products is between $Fe(OH)_3$ and $Fe(OH)_2$, α varies from 0.523 to 0.622; and also assume that the thickness of porous zone equals 4.9 mils (12.5 μm). According to equation 5.17, the calculated critical amounts of rust products for OA2859.6, OB3859.6, and OE(F)18512.0 are plotted in Figure 5.48. It can be seen that the predicted critical mass of rust products is well in agreement with the experimental results.

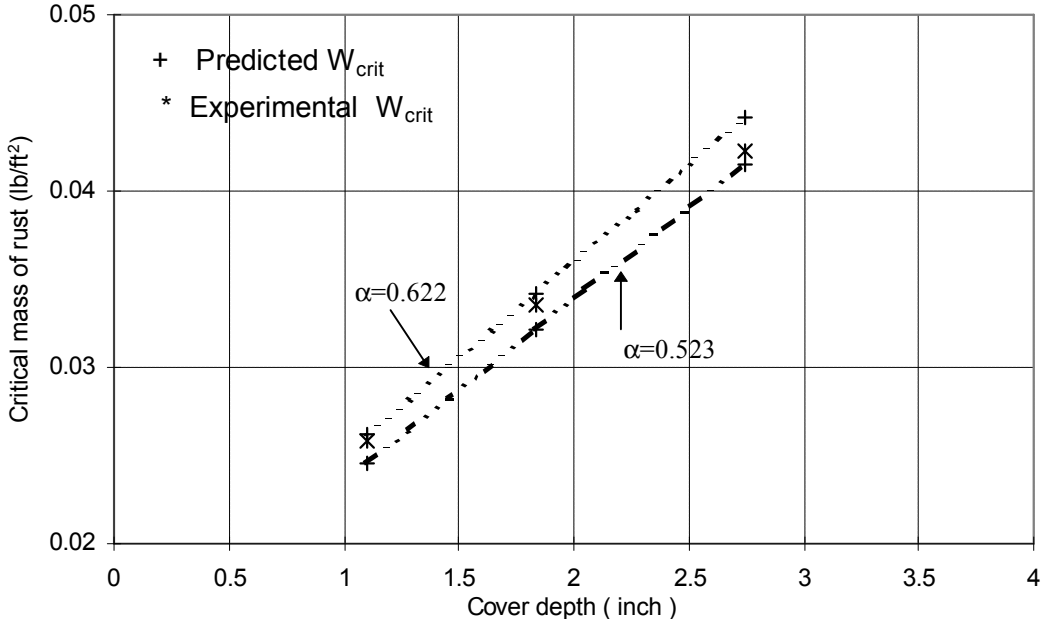

Figure 5.48. Critical mass of rust products versus concrete cover depth.

Based on calculated critical amount of rust products and measured corrosion rates, the times to cracking can be obtained from equation 5.21. The results are summarized in Table 5.7. As it can be seen from the table, the observed times to cracking are within the predicted values by the model.

Table 5.7. Model predicted times to cracking and observed times to cracking.

Series	Steel diameter (in.)	Cover depth (in.)	Measured corrosion rate (mA/ft^2)	Model predicted t_{cr} (year)	Observed t_{cr} (year)
OA2859.6	0.63	1.87	2.18	1.53 to 2.06	1.84
OB3859.6	0.63	2.74	1.67	3.34 to 4.49	3.54
OE(F)18512.0	0.63	1.07	3.50	0.56 to 0.75	0.72
Block9.6	0.50	2.05	1.68	1.79 to 2.40	2.38

Note: The predicted times to cracking were calculated taking α value of 0.523 ($Fe(OH)_3$) and 0.622 ($Fe(OH)_2$), respectively. The higher α, the longer time to cracking, because the density of $Fe(OH)_3$ is much lower than that of $Fe(OH)_2$.

According to the proposed time-to-corrosion cracking and corrosion rate models, the predicted times to corrosion cracking for two other series of specimens can be calculated. Table 5.8 presents the estimated corrosion rates and times-to-corrosion cracking for 2.4 and 4.8 lb/yd^3 admixed chloride series with 2 and 3 inches cover depth. The next cracking will occur soon for specimens with 4.8 lb/yd^3 admixed chloride series and 2 inches cover depth. Because only two series specimens have cracked, the proposed model needs to be validated or modified based on the observed times to cracking of other series specimens.

Table 5.8. Model predicted times to cracking for other two series specimens.

Series	steel diameter (in.)	Cover depth (in.)	Estimated corrosion rate (mA/ft^2)	Model predicted t_{cr} (year)
OA2854.8	0.63	2.0	0.79	4.8 to 6.3
OB3854.8	0.63	3.0	0.79	6.7 to 9.1
OA2852.4	0.63	2.0	0.43	8.9 to 12.1
OB2852.4	0.63	3.0	0.43	12.9 to 17.5

6.0 Conclusions

The following conclusions can be made from this study:

1. For outdoor exposure condition, the measured corrosion rates varied with corrosion time; and measured values were strongly dependent on environmental exposure conditions such as temperature, moisture for the same admixed chloride series. When amount of admixed chloride exceeded 2.4 lb/yd^3, the measured corrosion rates increased significantly with an increase in the amount of admixed chloride.

2. Comparing indoor and outdoor exposure, cracking has already occurred in outdoor specimens with admixed chloride of 9.6 lb/yd^3, whereas no cracking has been observed in indoor specimens with the same test series. The metal loss measurements show that the corrosion rate in outdoor specimens with admixed chloride of 9.6 lb/yd^3 was about three times higher than that of indoors with same test series. The low corrosion rate in indoor specimens is most likely due to the higher moisture content in indoor specimens from weekly water spraying on the specimens which limits the supply of oxygen.

3. Compared with the measured corrosion rates from weight loss tests, results from 3LP were overestimated corrosion rates due to the difference in the actual polarization area and the nominal polarization area; whereas results from Gecor were underestimated corrosion rates.

4. The measured corrosion rate from current commercial linear polarization devices, such as 3LP and Gecor, only represents the instantaneous value which may vary with the corrosion time and environmental exposure condition. Therefore, the measured corrosion rate at one time should be adjusted to an equivalent value used for predicting service life corresponding with the service exposure conditions such as temperature, moisture and chloride content.

5. Ohmic resistance of concrete varies with the chloride content and exposure conditions. For the same exposure conditions, ohmic resistance of concrete decreases as the chloride content increases.

6. An interaction model was developed based on the experimental corrosion database. The proposed model shows that corrosion rate is a function of the temperature, ohmic resistance of concrete, chloride content and corrosion time related to the service conditions of concrete structure. Based on annual mean temperature, ohmic resistance of concrete and chloride content for the reinforced concrete, the corrosion rate can be predicted by the model.

7. The corrosion-cracking conceptual model proposed here shows that the critical mass of the corrosion products (W_{crit}) to induce cracking of the cover concrete has two parts, the amount of corrosion products to fill the total interconnected pores around the steel/concrete interface

(W_p) and the amount of corrosion products to generate the critical tensile stress (W_s). The critical mass of the rust production is mainly influenced by the type of the corrosion products, concrete cover depth, rebar size, and properties of the concrete and steel/concrete interface.

8. The time to corrosion cracking model developed here shows that the time to corrosion cracking of the cover concrete in a chloride contaminated concrete structure is a function of corrosion rate and critical mass of the corrosion products. The times to cracking predicted by the model are in good agreement with the observed times to cracking based on this study.

7.0 Recommendations for Further Studies

1. Only the highest admixed chloride series has cracked. Continued research is still needed to verify or modify the proposed models based on the times when other series of test specimens crack.

2. The laboratory work done on this research focused on the different series of admixed chlorides to simulate different corrosion rates. In the field situation, the chloride content at the depth of reinforcing steel in bridge decks is a variable value which usually increases with time due to the annual application of the de-icing salts. The effects of constant chloride content on corrosion activities may differ from that of varied chloride content. Further work is needed on the effects of varied chloride content on the corrosion activities in concrete.

3. The difference of chloride concentration in pore solution between the admixed chloride concrete and field concrete needs to be further investigated.

4. The proposed corrosion-cracking model for predicting time to cracking is limited to the corrosion damage caused by the volume increase from the formation of rust. In the field situation, other factors such as traffic load, freezing-thawing may act simultaneously with the corrosion which may accelerate the cracking process. Much work is required on the corrosion cracking under the dynamic loading.

References

1. Page, C. L., and Treadaway K.W.J. (1982). "Aspects of Electrochemistry of Steel in Concrete," Nature, vol. 297, pp. 109-115.
2. Townsend, H. E., Cleary H. J., Allegra L. (1981). "Breakdown of Oxide films in Steel Exposure to Chloride Solutions," Corrosion - NACE, vol. 37, pp. 384-391.
3. Verbeck G. J. (1975). "Mechanism of Corrosion in Concrete," Corrosion of Metals in Concrete, ACI SP-49.
4. Mehta, P. K. (1993). Concrete Structure, Properties and Materials, Prentice-Hall, Inc..
5. Baboian, R. (1992). "Synergistic Effects of Acid Deposition and Road Salts on Corrosion," Corrosion Forms and Control for Infrastructures, ASTM STP 1137, pp. 17-29.
6. Fasullo, E. J. (1992). "Infrastructure: The Battlefield of Corrosion," Corrosion Forms and Control for Infrastructures, ASTM STP 1137, pp. 1-16.
7. Tuutti, K. (1982). Corrosion of Steel in Concrete, Swedish Cement and Concrete Research Institute, Stochkolm.
8. Cady, P. D., and Weyers R. E. (1983). "Chloride Penetration and the Deterioration of Concrete Bridge Decks," Cement, Concrete & Aggregate, vol. 5, No. 2, pp. 81-87.
9. Crank, J. (1956). The Mathematics of Diffusion, The Clarendon Press, Oxford.
10. Cady, P.D., and Weyers R.E. (1984). "Deterioration Rates of Concrete Bridge Decks," Journal of Transportation Engineering vol. 110, No. 1, January, pp. 34-45.
11. Bazant Z. P. (1979). "Physical Model for Steel Corrosion in Sea Structures-Theory," Journal of the Structural Division, June, pp. 1137-1153.
12. Bazant Z. P. (1979). "Physical Model for Steel Corrosion in Sea Structures-Applications," Journal of the Structural Division, June, pp. 1155-1166.
13. Kenneth C. Clear, Inc. (1990). Test Procedures, Data Analysis, and General Information, K.C.C. Inc. 3-LP Package, Sterling, VA.
14. Kenneth C. Clear. (1992). "Measuring Rate of Corrosion of Steel in Field Concrete Structure," Transportation Research Record, No. 1211, pp. 28-38.
15. Geocisa, Geotecnia Y Cimientos, S.A. (1991). Instructions Manual for Gecor Corrosion-Rate-Meter, Geocisa, Madrid, Spain.
16. Broomfield, J. P., Rodriguez J., Ortega L. M. and Garcia A. M. (1993). "Corrosion Rate Measurements in Concrete Bridges by Means of the Linear Polarization Technique Implemented in a Field Device," Paper presented at ACI Fall Convention, Minneapolis, Minnesota, USA, November.
17. Peterson, J. E. (1993). A Time to Cracking Model for Critically Contaminated Reinforced Concrete Structures, Masters of Science Thesis, Virginia Polytechnic Institute and State University, Blacksburg, December, VA.
18. Newhouse, C. D. (1993). Corrosion Rates and the Time to Cracking Model for Critically Contaminated Reinforced Concrete Structures, Masters of Science

Thesis, Virginia Polytechnic Institute and State University, Blacksburg, VA, December.
19. Fontana, M. G. (1971). Corrosion, 27, 127.
20. Uhlig, H. H. (1971). Corrosion and Corrosion Control, Wiley, New York.
21. Uhlig, H. H. (1948). The Corrosion Handbook, Wiley, New York.
22. Pourbaix, M. (1976). Atlas of Electrochemical Equilibrium in Aqueous Solutions, Pergamon, London.
23. Evans, U. R. (1960). The Corrosion and Oxidation of Metals, Arnold & Co., London.
24. Kortiim, G. (1965). Treatise on Electrochemistry, Elsevier, New York, pp. 444-453.
25. Glasstone, S. (1942). Principles of Electrochemistry, Var Noftrand, New York, p. 448.
26. Tafel, J. Z. (1904). Physik. Chem, 50, 641.
27. Stearn, M., and Geary A. L. (1957). "Electrochemical Polarization No. 1: Theoretical Analysis of the Shape of Polarization Curve," Journal of Electrochemical Society, Vol. 104, pp. 56-63.
28. Speller, F. (1951). Corrosion, McGraw - Hill, London.
29. Shreir, L. L. (1976). Corrosion: Metal/Environment Reactions, Volume 1, pp. 2:15.
30. Tomoshov, N. D. (1966). Theory of Corrosion and Protection of Metals, Mcmillan Co., New York.
31. Barneyback, R. S., and Diamand S. (1981). "Expression and Analysis of Pore Fluids from Harden Cement Pastes and Mortars," Cement Concrete Research, vol. 11, pp. 279-285.
32. Page, C. L. (1979). "The Corrosion of Reinforcing Steel in Concrete: Its Cause and Control," Bulletin, 77, Institution of Corrosion Science and Technology (U. K.), Nov..
33. Hausmann, D. A. (1967). "Steel Corrosion in Concrete: How Does It Occur," Materials Protection, vol. 6, pp. 19-23.
34. Sagoe-Grentsil, K. K. and Glasser, T. P. (1989). "Steel in Concrete: Part 1: A Review of the Electrochemical and Thermodynamic Aspects," Mag. Concr. Res, vol. 41, pp. 205 - 212.
35. Cabrera, J. G. (1996). "Deterioration of Concrete Due to Reinforcement Steel Corrosion," Cement Concrete Composites, vol. 18, pp. 47-59.
36. Byfors, K., Hansson C. M., and Tritthart J. (1986). "Pore Solution Expression as a Method to Determine the Influence of Mineral Additives on Chloride Binding," Cem. Concr. Res, vol. 16, pp. 760-770.
37. Page, C. L., and Vennesland Ø. (1983). "Pore Solution Composition and Chloride Capacity of Silica-Fume Cement Pastes," Materiaux Construct, vol 16, pp 19-25.
38. Hansson, M. C., Markussen J. B., and Frølund T. (1985). "The Effect of Chloride Cation Type on the Corrosion of Steel in Concrete by Chloride Salts," Cem. Concr. Res., vol. 15, pp. 65-73.

39. Mehta, P. K., and Manmohan D. (1980). Pro. 7th Int. Congr. on Chemistry of Cement, Paris.
40. Nielsen A. (1985). Durability, pp. 200-243 in Beton Bogen, Aalborg Cement Company, Aalborg, Portland.
41. Parrott, L. J. (1987). A Review of Carbonation in Reinforced Concrete, BRE/C&CA Report C/1-0987, July, 369 pages.
42. González, J. A., Algaba S., and Andrade C. (1980). "Corrosion of Reinforcing Bars in Carbonated Concrete," Br. Corr. J., 3, pp. 135-139.
43. Venuat, M. (1977). "Relationship Between Concrete Carbonation and the Corrosion of Reinforcement," Recentres CEFRA COR-77, JTBTP, October.
44. Stratfull, R. F., Jurkovich W. J., and Spellman D. L. (1975). "Corrosion Testing of Bridge Decks," Transportation Research Board, No. 539, pp. 50-59.
45. Browne, R. D. (1980). "Mechanism of Corrosion of Steel in Concrete in Relation to Design, Inspection, and Repair of Offshore and Coastal Structures," Performance of Concrete in Marine Environments, ACI SP-65, American Concrete Institute, Detroit, pp. 169-204.
46. Kilareski, W. P. (1980). "Corrosion Induced Deterioration of Reinforced Concrete - An Overview," Materials Performance, March, p. 49.
47. Slater, J. E. (1978). "Corrosion of Reinforced Steel in Concrete: Magnitude of the Problem," Paper 70, present at CORROSION/78, NACE, Chicago.
48. Tuutti, K. (1977). "Corrosion of Steel in Concrete," presented at 6th European Congress on Metallic Corrosion, London.
49. Mehta, P. K. (1977). "Effect of Cement Composition on Corrosion of Reinforcing Steel in Concrete," Chloride Corrosion of Steel in Concrete, ASTM STP 629, DE Tonono and SW Dean Jr., Eds., American Society for Testing and Materials, pp. 12-19.
50. Page, C. L. (1988). "Basic Principles of Corrosion," Corrosion of Steel in Concrete, RILEM Report 60-csc. New York: Chapman and Hall.
51. Slater, J. E. (1983). "Corrosion of Metals in Association with Concrete," American Society for Testing and Materials STP 818, American Society for Testing and Materials, Philadelphia.
52. Foley, R. T. (1970). "Role of the Chloride Ion in Iron Corrosion," Corrosion, Vol. 26, p. 58.
53. Cook, H. K., and McCoy W. J. (1977). "Influence of Chloride in Reinforced Concrete," ASTM STP 629, American Society for Testing and Materials, pp. 20-29.
54. Fraczek J. (1987). "A Review of Electrochemical Principles as Applied to Corrosion on Steel in a Concrete or Grout Environment," Corrosion, Concrete, and Chloride, SP-102, ACI, Detroit, pp. 13-24.
55. Erlin, B., and Verbeck G. J. (1978). ACI SP-49, pp. 39-46.
56. Fontana, M. G., and Greene N. D. (1967). Corrosion Engineering McGraw-Hill, Inc..

57. Sageo-Crentsil, K. K., and Glasser F. P. (1990). "Analysis of the Steel: Concrete Interface," Corrosion of Reinforcement in Concrete, C. L. Page, K.W.J., Threadaway, P.B. Bamforth eds, SCI, Society of Chemical Industry, Elsevier Applied Science, London, pp. 59-64.
58. Schiessl, P., and M. Raupach. (1990). "Influence of Concrete Composition and Microclimate on the Critical Chloride Content in Concrete," Corrosion of Reinforcement in Concrete, C. L. Page, K. W. J.,Threadaway, P. B.Bamforth eds, SCI, Society of Chemical Industry, Elsevier Applied Science, London, pp. 49-58.
59. Hansson, C.M., and Sørensen B. (1990). "Threshold Concentration of Chloride in Concrete for the Initiation of Reinforcement Corrosion," Corrosion Rates of Steel in Concrete, ASTM STP 1065, N. S. Berke, V. Chaker, and D. Whiting Eds., American Society for Testing and Materials, Philadelphia, Pa., pp. 3-16.
60. Berman, H. A. (1975). "Sodium Chloride, Corrosion of Reinforcing Steel, and the pH of Calcium Hydroxides Solution," ACI Journal, Oct., pp. 587-598.
61. Clear, K.C. (1983). "Chloride at the Threshold" Report of Kenneth C. Clear Inc., March, pp. 1011.
62. (1985). "Draft CEB Guide to Durable Concrete Structures" Bulletin d'Information, No.166, Comité Euro-International d'Beton, May.
63. (1987). RILEM Committee 60-CSG, Corrosion of Steel in Concrete, State of Art Report, Edited by P. Schiessl, Chapman and Hall, London.
64. Monfore, G. E. (1968). "Electrical Resistivity of Concrete," J. PCA (Portland Cement Association) Res. Develop. Lab., 10, No. 2, pp. 35-48.
65. Gjorv, O. E., Vennesland O., and El-Busaidy A. H. S. (1977). Proc-Annu. Offshore Technol. Conf, vol 9, No. 1, pp. 581-588.
66. Alonso, C., Andrade C., and González J. A. (1988). "Relation Between Concrete Resistivity and Corrosion Rate of the Reinforcements in Carbonated Mortar Made with Several Cement Types," Cem. Concr. Res, vol. 18, pp. 687-698.
67. López, W., and González J. A. (1993). "Influence of the Degree of Pore Saturation on the Resistivity of Concrete and the Corrosion Rate of Steel Reinforcement," Cem. Concr. Res, vol. 23, pp. 368-376.
68. Kobayashi, K., and Shuttoh K. (1991). "Oxygen Diffusion of Various Cementitious Materials," Cem. Concr. Res, vol. 21, pp. 273-284.
69. Collepordi, M., Marcialis A., and Tuniziani R. (1972). "Penetration of Chloride Ions into Cement Pastes and Concretes," Journal of the American Ceramic Society, vol. 55, pp. 534-535.
70. Page, C. L., Short M. R, and Tarras El A. (1981). "Diffusion of Chloride Ions in Hardened Cement Paste," Cem. Concr. Res, vol. 11, No.3, pp. 395-406.
71. López, W., González J. A., and Andrade C. (1993). "Influence of Temperature on the Service Life of Rebars ," Cem. Concr. Res., vol. 23, pp. 1130-1140.
72. Thompson, N.G., Islam, Lankard, D.A., and Virmani Y. P. (1995). "Environmental Factors in the Deterioration of Reinforced Concrete," Materials Performance, vol. 34, pp. 43-47.

73. Virmani, Y. P., Clear K. C., etc. (1983). "Time-To-Corrosion of Reinforcing Steel in Concrete," vol.5, FHWA/RD - 83/012.
74. "Standard Test Method for Half Cell Potentials of Reinforcing Steel in Concrete," ASTM C 876-91, Annual Book of ASTM Standards, Volume 04.02,
75. Arup, H. (1979). Danish Corrosion Centre - Newsletter, No. 2.
76. Spellman, D. L., and Stratfull R. F. (1973). "Concrete Variables and Corrosion Testing," Highway Research Record 423
77. Stratfull, R.F. (1973). "Half Cell Potentials and the Corrosion of Steel in Concrete," Highway Research Record 433
78. Elsener, B., and Böhni H. (1991). "Electrochemical Methods for the Inspection of Reinforcement Corrosion in Concrete Structures-Field Experience," Electrochemical Methods in Corrosion Research, Proceedings of 4th International Symposium, Espoo, Finland, July, pp. 635-646.
79. Sykes, J.M. (1994). "Electrochemical Studies on Steel in Concrete," Electrochemical Methods in Corrosion Research, Proceedings of 5th International Symposium, Sosimbra, Portugal, Sept., pp. 833-842.
80. Berkeley, K.G.C., and Pathmanaban S. (1987). "Practical Potentials Monitoring in Concrete," UK CORROSION'87, Brighton, UK, Oct., pp. 115-131,
81. Stearn, M., and Geary A.L. (1958). Electrochemical Society, Vol. 105, p. 638.
82. Andrade, C., Castelo V., Alonso C., and González J. A. (1981). "The Determination of the Corrosion Rate of Steel Embedded in Concrete by the Polarization Resistance and AC Impedance Methods," ASTM STP 906, pp. 43- 63.
83. Hope, B. B. , A. K Ip, and Manning D. (1985). "Corrosion and Electrical Impedance in Concrete," Cem. Concr. Res., vol. 15, pp. 525-534.
84. Feliú, S., González J. A., Andrade C., and Feliú V. (1988). "Determination Polarization Resistance in Reinforced Concrete Slabs," Corrosion, vol. 44, No. 10, pp. 761-765.
85. Feliú, S., González J. A., Feliú S. Jr., and Andrade C. (1990). "Confinement of Electric Signal for in Situ Measurement of Polarization Resistance in Reinforced Concrete," ACI Materials Journal, vol. 87, pp. 457-460.
86. Carassiti, F., Proverbio E., and Valente T. (1991). "Corrosion State Evaluation of Steel in Concrete by Resistivity and Polarization Resistance Measurement," Electrochemical Methods in Corrosion Research, Proceedings of 4th International Symposium, Espoo, Finland, July, pp. 647-658.
87. John, D.G., Coote A.T., Treadaway K.W.J., and Dawson J.L. (1983). "The Repair of Concrete, A Laboratory and Exposure Site Investigation," Corrosion of Reinforcement in Concrete Construction, Society of Chemical Industry, London, June, pp. 263-286.
88. Andrade, C., Soler L., and Nóvoa X. R. (1994). "Advances in Electrochemical Impedance Measurements in Reinforced Concrete," Electrochemical Methods in Corrosion Research, Proceedings of 5th International Symposium, Sosimbra, Portugal, Sept., pp. 843-856.

89. (1990). "Standard Practice for Preparing, Cleaning, and Evaluating Corrosion Test Specimens," ASTM G-1-90, Annual Book of ASTM Standards, Vol. 01.05, American Society for Testing and Materials, Philadelphia, PA.
90. (1988). "Standard Test Methods for Chemical Analysis of Hydraulic Cement," ASTM C 114 - 88, Annual Book of ASTM Standards, American Society for Testing Materials, Philadelphia, PA.
91. (1984). "Standard Method of Sampling and Testing for Total Chloride Ion in Concrete and Concrete Raw Materials," Standard Specifications for Transportation Materials and Methods of Sampling and Testing, AASHTO T 260-84, American Association of State Highway and Transportation Officials, Washington, D.C.,
92. (1992). "Standard Test Method for Water-Soluble Chloride in Mortar and Concrete," ASTM C 1218, Annual Book of ASTM Standards, American Society for Testing and Materials, Philadelphia, PA.
93. (1992). "Standard Test Method for Acid-Soluble Chloride in Mortar and Concrete," ASTM C 1152, Annual Book of ASTM Standards, American Society for Testing and Materials, Philadelphia, PA.
94. Henry. M. (1992). Rapid Analysis of Chloride Content of Contaminated Concrete, Masters of Science Thesis, Virginia Polytechnic Institute and State University, Blacksburg, VA, pp. 160.
95. Morinagn, S. (1989). "Prediction of Service Lives of Reinforced Concrete Buildings Based on Rate of Corrosion of Reinforcing Steel," Special Report of the Institute of Technology, Skimiza Corporation, Japan.
96. Andrade, C., Alonso C., and González J. A. (1989). "Approach to the Calculation of the Residual Life in According to Concrete Reinforcements Based on Corrosion Intensity Value," 9th European Congress on Corrosion, Utrecht, The Netherlands, October.
97. Clifton, J. R. (1991). "Predicting the Remaining Service Life of Concrete," NISTIR 4712, National Institute of Standards and Technology.
98. Allan, M. L. (1995). "Probability of Corrosion Induced Cracking in Reinforced Concrete," Cem. Concr. Res, vol. 25, No. 6, pp. 1179-1190.
99. Chatterji, S. (1994). "Transport of Ions Through Cement Based Materials. Part 1: Fundamental Equations and Basic Measurement Techniques," Cem. Concr. Res, vol. 24, No. 5, pp. 907-912.
100. Weyers, R. E.,Prowell B., Al-Qadi I. L., Sprinkel M. and Vorster M. (1993). Concrete Bridge Protection, Repair and Rehabilitation: Relative to Reinforcement Corrosion, SHRP-S-360, Strategic Highway Research Program, National Research Council.
101. Hji, K., Matsuoka Y. and Maruya T. (1990). "Formulation of an Equation for Surface Chloride Content of Concrete Due to Permeation of Chloride," Corrosion of Reinforcement in Concrete, C. L. Page, K.W.J., Threadaway, P.B. Bamforth eds, SCI, Society of Chemical Industry, Elsevier Applied Science, London, pp. 49-58.
102. Spellman, D.L., and Stratfull R.F. "Chlorides and Bridge Deck Deterioration," State of California Department of Public Works, Division of Highways, Materials

and Research Department, Paper Sponsored by Committee on Effect of Ice Control and Presented at 49th Annul Meeting.
103. Clementa, G. G., Jackson D. R., and Crawford G. C. "Use of Rebar Corrosion Rates in Condition Surveys of Concrete Bridge Decks," an unpublished paper.
104. Hladky, K. et al. (1989). "Development in Rate of Corrosion Measurements for Reinforced Concrete Structures," Corrosion 89, No. 169, NACE, Houston, TX.
105. Suda, K., Misra S., and Motohashi K. (1993). "Corrosion Products of Reinforcing Bars Embedded in Concrete," Corrosion Science, vol. 35, pp. 1543-1549.
106. Liu, Y., and Weyers R. E. (1996). "Time to Cracking for Chloride-Induced Corrosion in Reinforced Concrete," Corrosion of Reinforcement in Concrete Construction, C. L. Page, P. B. Bamforth and J. W. Figg eds, SCI, The Royal Society of Chemistry, Cambridge, UK, pp. 88-104.
107. Khan, M. S. (1991). "Corrosion State of Reinforcing Steel in Concrete at Early Ages," ACI Materials J, vol. 88, No. 1, pp. 37-40.
108. Moreno, E. I., Sagüés A. A., and Powers R. G. (1996). "Performance of Plain and Galvanized Reinforcing Steel During the Initiation Stage of Corrosion in Concrete with Pozzolanic Additions," Paper presented at Corrosion 96, NACE, Houston, TX.
109. Videm, K., Roar Myrdal and Rescon AS. (1996). "The Electrochemical Behavior of Steel in Concrete and How to Evaluate the Corrosion," Paper presented at Corrosion 96, NACE, Houston, TX.
110. Liu, Y., and Weyers R. E. (1997). "Predicting the Corrosion Rate of Steel in Chloride Contaminated Concrete," Paper for Fourth Canmet/ACI International Conference on Durability of Concrete, Sydney, Australia.
111. Andrade, C., Alonso C., Rz-Maribona I., and Garcia M. (1989). "Suitability of the Measurement Technique of Oxygen Permeability in Order to Predict Corrosion Rates of ConcreteRebar," Paul Klieger Conference, ACI, San Diego.
112. Dagher, H. J., and Kulendran S. (1993). "Finite Element Modeling of Corrosion Damage in Concrete," ACI Structure J., vol. 89, pp. 669-708.
113. Molina F. J., Alonso C., and Andrade C. (1993). "Cover Cracking As a Function of Rebar Corrosion, Part 2–Numerical Model," Materials and Structures, vol. 26, pp. 532-548.
114. Ugural, A. C. (1986). Advanced Strength and Applied Elasticity, Elsevier.

Appendix A. Conversion of the corrosion rate

Corrosion rate can be measured in terms of weight loss (given as mass per area per time, mass/area ·time) or depth of penetration (givens as depth of penetration per unit time). The most common unit of weight loss has been milligrams per square decimeter per day (mdd) or in SI system of unit, grams per square meter per day ($g/m^2 \cdot d$). For the depth of penetration, the most common unit is mils per year (mpy, where 1000 mils = 1 in.), and the SI system unit is millimeters per year (mm/y). Conversion factors to change from traditional units to SI units are given in Table A-1.

Table A-1. Conversion of traditional units to SI units

To convert from	To	Multiple by*
mpy	mm/y	0.0254
mpy	$g/m^2 \cdot d$	0.0695d
ipy	mm/y	25.4
ipy	$g/m^2 \cdot d$	69.5d
mdd	mm/y	0.0365/d
mdd	$g/m^2 \cdot d$	0.100

* Note: d = metal density in grams per cubic decimeter (g/cm^3)

From the linear polarization devices, the corrosion rate usually measured in terms of corrosion current density. The units of corrosion current density from 3LP device and Gecor are mA/ft^2 and $\mu A/cm^2$. The conversion of corrosion current density to corrosion rate can be easily done according to the Faraday's law,

$$\text{corrosion rate} = i_{cor}/nF$$

where i_{cor} is the corrosion current density in amperes per square meter (A/m^2), F is Faraday's constant (96494 C/mol ·ë) and n is in moles of electrons per mole of metal corroded. For steel, n equals 2.

If iron corrodes at a corrosion current density of 1 mA/ft^2, the

$$\text{corrosion rate} = i_{cor}/nF = \frac{1\times10^{-3}\ \text{A}\,(55.85\text{g/mol Fe})(86400\ \text{s/d})}{(12\times0.0254)^2\ \text{m}^2\ \frac{2\ \text{mol e}^-}{\text{mol Fe}}\,(96494\ \text{A}\cdot\text{s/mol e}^-)} = 0.27\ \text{g/m}^2\cdot\text{d}$$

and also can convert the weight loss to depth of penetration, divided by the metal density, which for Fe is 7.86 g/cm^3.

corrosion rate = (0.27 $g/m^2 \cdot d$) (1 $m^3/7.86\times10^6$ g of Fe) (365 d/y) = 0.0126 mm/y

Appendix B. Climate Data, Blacksburg, Virginia, USA

The monthly average mean temperature and total precipitation in Blackburg, Virginia, USA from 1991 to 1995 are summarized in Table B-1 and B-2 respectively.

Table B-1. The monthly average mean temperature in Blackburg, Virginia, USA (1991-1995).

YEAR	JAN.	FEB.	MAR.	APRIL	MAY	JUNE	JULY	AUG.	SEP.	OCT.	NOV.	DEC.	ANNUAL MEAN
1991	34.4	37.8	44.1	53.2	64.8	68.3	N/A	70.7	65.2	55.6	43.9	39.0	51.7
1992	35.4	38.9	42.4	51.6	57.4	64.8	73.4	68.0	64.9	51.4	43.9	33.6	52.1
1993	36.4	32.5	37.8	49.8	62.2	68	75.9	71.8	65.3	51.7	43.7	33.4	52.4
1994	28.2	36.6	42.1	55.9	56.6	71.2	73.7	70.5	63.2	N/A	N/A	N/A	N/A
1995	N/A	N/A	N/A	N/A	N/A	N/A	N/A	72.8	62.5	53.7	38.6	29.0	N/A
Record mean	31.9	32.4	41.8	50.5	59.2	66.8	71.0	70.1	63.8	52.5	42.2	33.8	51.4

Table B-2. The Total precipitation in Blackburg, Virginia, USA (1991-1995).

YEAR	JAN.	FEB.	MAR.	APRIL	MAY	JUNE	JULY	AUG.	SEP.	OCT.	NOV.	DEC.	ANNUAL TOTAL
1991	2.96	2.15	5.86	2.78	4.66	1.27	2.99	2.69	0.49	0.26	2.99	5.5	34.6
1992	2.94	3.47	3.26	5.43	4.25	6.20	9.35	4.27	1.72	2.15	3.78	2.35	49.17
1993	3.32	3.24	6.94	3.37	4.36	3.58	3.30	3.27	5.27	1.74	4.01	5.23	47.63
1994	4.42	5.77	5.85	3.93	1.41	1.69	5.99	4.20	0.97	N/A	N/A	N/A	N/A
1995	N/A	N/A	N/A	N/A	N/A	N/A	N/A	2.00	1.69	2.90	3.06	2.06	N/A
Record total	2.95	2.94	3.90	3.55	3.62	3.61	4.01	3.77	3.51	3.63	2.89	2.82	40.91

Vita

In Dec., 1966, Youping Liu, was born in Fenghua, a small town in the east of Zhejiang Province, China. He attended Southeast University (former name is Nanjing Institute of Technology), Nanjing, in September, 1984, where he majored in Civil Engineering. He graduated with a B.S. degree in July, 1988. Soon after graduation, he started his graduate studies in Tsinghua University, Beijing. He did research on areas of mineral concrete admixture, low weight silicate materials and glazed cement materials during his graduate studies, and got two patents in glazed cement materials and mineral concrete admixtures. In April, 1991, he obtained his M.S. degree in Civil Engineering. After that, he became an Assistant Professor in Shanghai Institute of Building Materials, Shanghai, where he taught undergraduate courses in Concrete Admixtures, Construction Materials and Industrial Management of Construction Materials, and did research on utilizing industrial waste materials as construction materials. He came to Virginia Polytechnic Institute & State University, Blacksburg, to pursue a Ph.D degree in Civil Engineering in Fall, 1993. Working with his advisor, Dr. Richard E. Weyers, he did research on corrosion of steel in chloride contaminated concrete structures during his graduate study. His Ph.D degree in Civil Engineering is expected in Fall, 1996.